UNCLASSIFIED

AD NUMBER
ADB004062
LIMITATION CHANGES

TO:

Approved for public release; distribution is unlimited.

FROM:

Distribution authorized to U.S. Gov't. agencies only; Test and Evaluation; MAY 1975. Other requests shall be referred to Aeronautical Systems Div., Wright-Patterson AFB, OH 45433.

AUTHORITY

ASD ltr dtd 16 Aug 1977

THIS PAGE IS UNCLASSIFIED

AEDC-TR-75-57

cy. 1

ARCHIVE COPY
DO NOT LOAN

RESULTS OF 0.2-SCALE B-1 PRODUCTION INLET
DEVELOPMENT AND VERIFICATION TESTS AT
SUBSONIC AND SUPERSONIC MACH NUMBERS

R. F. Lauer, Jr.
ARO, Inc.

PROPULSION WIND TUNNEL FACILITY
ARNOLD ENGINEERING DEVELOPMENT CENTER
AIR FORCE SYSTEMS COMMAND
ARNOLD AIR FORCE STATION, TENNESSEE 37389

May 1975

Final Report for Period July 8 — December 17, 1975

Property of U. S. Air Force
AEDC LIBRARY
F40600-75-C-0001

Prepared for

AERONAUTICAL SYSTEMS DIVISION (ASD/YHT)
and
AIR FORCE FLIGHT DYNAMICS LABORATORY (AFFDL/FXM)
WRIGHT-PATTERSON AFB, OH 45433

APPROVAL STATEMENT

This technical report has been reviewed and is approved for publication.

FOR THE COMMANDER

LAMAR R. KISSLING
Lt Colonel, USAF
Chief Air Force Test Director, PWT
Directorate of Test

FRANK J. PASSARELLO
Colonel, USAF
Director of Test

UNCLASSIFIED

REPORT DOCUMENTATION PAGE		READ INSTRUCTIONS BEFORE COMPLETING FORM
1. REPORT NUMBER AEDC-TR-75-57	2. GOVT ACCESSION NO.	3 RECIPIENT'S CATALOG NUMBER
4. TITLE (and Subtitle) RESULTS OF 0.2-SCALE B-1 PRODUCTION INLET DEVELOPMENT AND VERIFICATION TESTS AT SUBSONIC AND SUPERSONIC MACH NUMBERS		5 TYPE OF REPORT & PERIOD COVERED Final Report, July 8 - December 17, 1974
		6. PERFORMING ORG. REPORT NUMBER
7 AUTHOR(s) R. F. Lauer, Jr., ARO, Inc.		8. CONTRACT OR GRANT NUMBER(s)
9 PERFORMING ORGANIZATION NAME AND ADDRESS Arnold Engineering Development Center (XO), Arnold Air Force Station, TN 37389		10. PROGRAM ELEMENT, PROJECT, TASK AREA & WORK UNIT NUMBERS 64215F-139A-01 63202F-668A-02
11. CONTROLLING OFFICE NAME AND ADDRESS Aeronautical Systems Division (ASD/YHT) Wright-Patterson AFB, OH 45433		12. REPORT DATE May 1975
		13. NUMBER OF PAGES 148
14 MONITORING AGENCY NAME & ADDRESS(if different from Controlling Office)		15. SECURITY CLASS. (of this report) UNCLASSIFIED
		15a. DECLASSIFICATION/DOWNGRADING SCHEDULE N/A

16. DISTRIBUTION STATEMENT (of this Report)

Distribution limited to U.S. Government agencies only; this report contains information on test and evaluation of military hardware; May 1975; other requests for this document must be referred to Aeronautical Systems Division (ASD/YHT), Wright-Patterson AFB, OH 45433.

17. DISTRIBUTION STATEMENT (of the abstract entered in Block 20, if different from Report)

1. Airplanes -- B-1
2 Air inlets -- flow distortion

18 SUPPLEMENTARY NOTES 3 "   "   -- Performance

Available in DDC.

19 KEY WORDS (Continue on reverse side if necessary and identify by block number)

B-1 aircraft	scale model
jet engine inlets	inlets
wind tunnels	distortion
tests	performance

20 ABSTRACT (Continue on reverse side if necessary and identify by block number)

Results are presented for a wind tunnel investigation of the 0.2-scale B-1 aircraft inlet/forebody model during which a production version of the inlet configuration was defined and the performance characteristics verified. The test was conducted at Mach numbers from 0 to 2.3, at angles of attack from -2 to 13 deg, and at yaw angles from -6 to 6 deg. Performance data are presented primarily in the form of engine-face total-pressure

DD FORM 1473 1 JAN 73 EDITION OF 1 NOV 65 IS OBSOLETE

UNCLASSIFIED

20, Continued

recovery, turbulence index, and various distortion indices as a
function of engine-face mass-flow ratio. For the development
test phase, results are given that show the effects of reducing
the inlet diffuser ramp length, varying the inlet cowl lip
contours, changing the inlet bleed porosities, and reducing
the inlet bleed discharge area. The performance characteristics
of the selected inlet configuration are documented over the Mach
number range with inlet geometry as controlled by the individual
inlet control sensor schedules as well as by a free-stream
Mach number schedule. The effects of control system errors
and the aircraft takeoff inlet performance characteristics are
also presented.

AFSC
Arnold AFS Tenn

PREFACE

The work reported herein was conducted by the Arnold Engineering Development Center (AEDC), Air Force Systems Command (AFSC), at the request of the Aeronautical Systems Division (ASD/YHT) and the Air Force Flight Dynamics Laboratory (AFFDL), under Program Elements 64215F and 63202F, Systems 139A and 668A, respectively. The test results presented were obtained by ARO, Inc. (a subsidiary of Sverdrup & Parcel and Associates, Inc.), contract operator of AEDC, AFSC, Arnold Air Force Station, Tennessee. The work was done under ARO Project Nos. P41T-63A and -95A, and the data reduction was completed on January 15, 1975. The manuscript (ARO Control No. ARO-PWT-TR-75-30) was submitted for publication on March 12, 1975.

CONTENTS

ILLUSTRATIONS

Figure

TABLE

APPENDIXES

1.0 INTRODUCTION

At the request of the Aeronautical Systems Division (ASD), Air Force Systems Command (AFSC), a series of inlet development and verification tests was performed in the 16-ft Propulsion Wind Tunnels (16T, Transonic, and 16S, Supersonic) for the Rockwell International Corporation (RI) on a 0.2-scale model representing the forebody and left-hand nacelle of the B-1 Air Vehicle (A/V). The primary objective of the first test series, in Tunnel 16S, was to develop an inlet configuration for the production B-1 A/V that would maintain the performance and stability characteristics of the prototype configuration as reported in Ref. 1 but would be lighter in weight and have reduced drag. The second test series was devoted to verifying and documenting the inlet performance and stability characteristics of the production inlet configuration that resulted from the first test series.

Data were obtained at Mach numbers from 0 to 1.5 in the 16T tests and at M0 = 0 and from 1.8 to 2.3 in the 16S tests. Typical data obtained during the developmental test phase are presented herein showing the effects of shortening the inlet fourth ramp, changing the inlet bleed porosities, altering the cowl lip contours, and reducing the BLC bleed exit areas. From the production inlet verification test phase, results are presented which show the inlet control system schedules, the scheduled inlet performance characteristics, off-schedule performance characteristics, interference effects of opened weapons bay doors and electro-optical visual systems (EVS) pods, and the takeoff inlet performance characteristics. Representative data are generally presented in the form of engine-face total-pressure recovery, various total-pressure distortion indices, and turbulence index as a function of engine-face mass-flow ratio, corrected airflow rate, or other applicable parameters.

In addition to the tests described above, a test was conducted in Tunnel 16T at the request of the Air Force Flight Dynamics Laboratory (AFFDL), AFSC, using the same model as above configured to represent the prototype B-1 A/V. Pressure data were obtained at Mach numbers from 0.70 to 1.40 to determine the inlet drag characteristics of the 0.2-scale model inlet system. The primary objective of this test was to obtain data that will later be compared with flight test data and used to develop wind tunnel/flight test correlations in the AFFDL Airframe Propulsion Subsystem Integration (APSI) program.

2.0 APPARATUS

2.1 TEST FACILITIES

Tunnels 16T and 16S are closed-circuit, continuous flow tunnels with Mach number capabilities from 0.2 to 1.6 and from 1.5 to 2.3, respectively. A complete description of the facilities, including operating characteristics, is presented in Ref. 2.

2.2 TEST ARTICLE

The test article was a 0.2-scale model of the Rockwell International Corporation B-1 Air Vehicle. The location of the model and support system is shown in Figs. 1a and b for Tunnels 16T and S, respectively. Photographs of the installations are given in Fig. 2.

The model simulated the A/V fuselage forebody with fixed-position structural mode control vanes, various sweep angle left-hand stub wings, and the dual inlet, left-hand engine nacelle. The nacelle external lines simulated the A/V lines, with minor exceptions, to within approximately 4 in. of the engine-face station. Both the inboard and outboard inlets simulated A/V internal surfaces to the engine-face station as described below.

The variable ramp system for both inlets consisted of a fixed ramp (RA) and three movable ramps (see Figs. 3a and b). The second ramp (RB) and the ramp train, consisting of the third and fourth ramps (RC and RD), were remotely controlled using servo loop hydraulic systems for each inlet. The first three ramps (RA, RB, and RC) simulated prototype A/V geometry, but the fourth ramp (RD) tested was 16 and then 32 in. (full-scale dimensions) shortened from the prototype configuration (Ref. 1). The effects of these fourth ramp changes on the diffuser duct area distribution may be seen in Fig. 4.

Boundary-layer control for both inlets was provided by porous surfaces on the third and fourth ramps and on the sideplates as shown in Fig. 5. The sideplate porosity was eliminated during the course of the test program (solid sideplates were used), and the ramp porosity was varied slightly (the 11-percent porosity areas were briefly changed to 12.5-percent porosities) but finally remained as shown. Bleed air from the third ramp and side plates went into the bleed zone I (BLCI) compartment. Initially the BLCI air discharged through fixed area doors with a total area of 1.92 in.^{2} per inlet on the bottom of the nacelle; however, during the course of the program the discharge area was varied and the forward two doors eliminated so that the final model configuration had a total BLCI discharge area of 1.2 in.^{2} per inlet (Fig. 6). Bleed air from the fourth ramp went into the bleed zone II (BLCII) compartment and discharged through the remotely operable BLCII doors (Fig. 6). The position (and consequently the discharge area) of these

four doors was varied from the simulated prototype value of 13 deg (3.36 in.^{2} for the four doors) during the early test period. Later the fourth door was sealed and the door positions adjusted so that the final total exit area was 2 in.^{2} with the doors in the open position.

During the first test period, the effects of cowl leading-edge contours were investigated. The cowl shapes tested are shown in Fig. 7. Also during that test period at M0 = 0 and during portions of the Tunnel 16T testing, the simulated takeoff (T/O) cowl was installed on the model. The T/O cowl lip contours simulated that of the prototype A/V.

During the M0 = 0 portion of the July 1974 test period, the effects of crosswinds 90 deg relative to the model centerline were determined. The crosswinds were simulated at velocities of 20, 30, and 40 knots by an AEDC-designed, fabricated, and calibrated crosswind generator which was supplied with high-pressure air at flow rates up to 40 lbs/sec. A photograph of the crosswind-generator/model installation may be seen in Fig. 8.

Inlet/engine airflow matching was provided for each inlet by means of a remotely variable bypass door controlled by a servo-loop hydraulic actuator. The difference between the bypass doors tested and the prototype configuration doors may be seen in Fig. 9. The bypass doors were closed and sealed for all testing except those where the effects of bypass flow were investigated and during the scheduled performance portions of the testing in the second 16S entry.

Both inlets had an environmental control system (ECS) air duct subinlet in the subsonic diffuser (Fig. 3a). Air from each subinlet was ducted to a flow-measuring section with one remotely variable plug valve used to simulate aircraft airflow demand from both inlets.

Simulated engine airflow was controlled with flow-throttling, remotely operable vanes located downstream of the engine-face station to provide a choke point at the vanes so that the acoustic properties of the engine could be approximated. Downstream of the vanes, a transition section with flow-straightening screens led to an ASME-type airflow-metering section. At M0 = 0 testing in Tunnel 16S and during all 16T testing, the discharge of the airflow-metering duct was connected to a suction system to ensure choked flow at the vanes.

In Tunnel 16T, the effects of electro-optical visual system (EVS) pods (Fig. 10) and opened weapons bay doors were determined, and the left-hand stub wing was manually positioned at sweep angles of 15, 25, and 67.5 deg to ensure adequate simulation of the inlet flow field.

During a portion of the latter Tunnel 16S test period, a flat plate with full-scale and 0.2-scale local Mach number pitot-static probes was installed 27 in. above the tunnel floor (Fig. 11) for a 0.2-scale/full-scale probe calibration.

Additional test article details may be found in Refs. 3 and 4.

2.3 INSTRUMENTATION

Up to 379 steady-state pressure measurements were made on wing surfaces, internal and external cowl surfaces, internal and external bypass door surfaces and ramp surfaces, in boundary-layer bleed compartment plenums and metering sections, on upper and lower sideplate surfaces and flow-diverter surfaces, at the engine-face station, in the primary flow-metering ducts, and on the local Mach number calibration probes and plate. Unsteady-state pressure measurements were made on the wing, ramps, upper and lower side plates and cowl surfaces, in the boundary-layer bleed plenums, and at the engine-face station. (See Figs. 12a-d for pressure orifice locations.)

Engine-face steady- and unsteady-state pressures were measured with dual purpose probes. Each engine-face array consisted of 40 probes in eight 5-probe rakes, as may be seen in Fig. 12d.

Complete model instrumentation details may be found in Refs. 3 and 4.

All steady-state transducer outputs were sequentially input to an on-line computer system in which the data were reduced to engineering units. From the engineering unit data all desired weight flows, Mach numbers, engine-face total-pressure recovery and distortion parameters, and other requested parameters were computed and tabulated in the control room. Selected parameters were also plotted and displayed on a cathode-ray tube in the control room. The immediate availability of the tabulated and plotted data permitted continual on-line monitoring of the test results, which aided in the test direction, particularly in the early configuration development phase of the test. Facility instrumentation and data reduction capabilities are given in Ref. 2.

Outputs of the 65 unsteady-state pressure transducers per inlet were recorded by constant bandwidth, multiplexed FM recording systems on magnetic tapes. The signals from the 40 engine-face probes on each inlet were paralleled to rms-to-dc converters to obtain the rms magnitude of engine-face turbulence; the signals were also paralled to the RI-furnished Analog Distortion Analyzer (ADA). The ADA calculated the various distortion parameters for both inlets in real time, digitally sampled the 40 engine-face pressures at each instant of successively higher peak distortion (engine fan stall margin ratio allowable for engine-face distortions, IDL—see Appendix A), and transferred the end results to the facility data acquisition system.

Model angle of attack was determined by means of a strain-gaged pendulum-type angle sensor. Model yaw angle and the positions of all remotely operable model component positions were sensed by potentiometers.

For the inlet drag portion of the testing in Tunnel 16T, 140 additional pressure orifices were installed on the inlet cowl external surfaces, outboard inlet ramp surfaces, and wing surfaces, at the outboard inlet cowl lip station (inlet total-pressure rakes), and at the outboard bypass door exit station (bypass discharge total-pressure rakes). A complete description of these additional instrumentation locations may be found in Ref. 4, Appendix A.

3.0 PROCEDURES

3.1 TEST OPERATING PROCEDURE

After the desired tunnel free-stream conditions had been established, the model was positioned to the desired pitch and yaw attitude. Model variables such as second ramp angle, inlet lip height, bypass door angle, BLCII door angle, mass flow control vane angle, etc., were systematically varied to study the desired effect. At most test conditions, steady-state data and 30 sec of unsteady-state data were obtained over a range of simulated engine airflow rates. Airflow variations were obtained by positioning the flow control vanes from values causing supercritical inlet operation to those causing subcritical or inlet instability. Onset of inlet instability and/or inlet buzz was determined by observation of inlet duct and engine-face unsteady-state pressure transducer signals on oscilloscopes.

The flow-control vanes were normally operated under AEDC-designed automatic computer control, whereby the vanes were moved to set a specific requested engine-face corrected airflow rate. Real-time sampling of the flowmeter pressure transducer outputs and engine-face total-pressure recovery from the ADA permitted this mode of operation, which resulted in desired engine-face airflows being set more accurately and faster than could be accomplished by manual operation. The exception to this mode of operation was in definition of inlet instability, where manual vane control operation was employed.

During portions of the latter Tunnel 16S test program, simulated inlet/engine airflow matching was achieved by controlling the bypass door positions with an AEDC-developed analog system to maintain a specific duct control pressure ratio, the normal shock parameter (NSP). NSP is the ratio of a static pressure (orifice No. X703 located in each inlet throat on the upper sideplate at NS 16.98, NWL 5.2, Fig. 12b) to a total pressure (orifice No. X702 located in each inlet throat on the cowl surface at NS 19.00, NWL 1.28, Fig. 12a). Using NSP and a schedule of NSP versus MA or ML (see Section 4.2), the A/V Air Inlet Control System (AICS) causes the bypass door to open if a value of NSP is sensed that is greater than scheduled, and to close if NSP is less than scheduled. In addition, at some

supersonic A/V maneuvering attitudes or on cold-day operation where engine airflow demand would tend to cause supercritical inlet operation (low NSP value) even with the bypass door closed, the AICS sends a signal to the engine control causing a fan speed rollback (and reduction in airflow) to maintain inlet operation on the NSP schedule. The AEDC controller simulated the action of the AICS in controlling the bypass door position as a function of NSP. However, the fan speed rollback (airflow reduction) feature of the AICS was simulated by the operational procedures; as a condition was approached where the bypass door was closed and NSP was less than scheduled for a given airflow, the airflow was reduced until NSP was again on schedule.

3.2 PRECISION OF MEASUREMENT

Listed in Table 1 are estimates of the precisions of measurement for selected parameters. The uncertainties in these parameters include the inaccuracies in the tunnel reference systems, the recording systems, and the measuring devices themselves. The errors presented are combined errors (the square root of the sum of the squares of the individual errors) and were derived for a 95-percent confidence level using the Taylor series expansion method. Any errors contributed by the user-provided ADA are not included in these calculations.

4.0 RESULTS AND DISCUSSION

4.1 PRODUCTION CONFIGURATION DEVELOPMENT

The first test period was primarily devoted to developing a production A/V inlet configuration that would have lower weight and drag penalties while maintaining the performance characteristics of the prototype inlet reported in Ref. 1. The major investigation to effect a weight savings involved reducing the length of the fourth (diffuser) inlet ramp up to 32 in. (full-scale dimension), thus reducing the structural requirements for the ramps and actuators. Also, the length of the bypass door was reduced and the height increased, thereby reducing the moment arm of the aerodynamic loads on the door and hence allowing a lighter weight actuator. However, the bypass door changes were not critical to the inlet performance characteristics with the bypass doors sealed closed, and the revised bypass door effectiveness will be shown in Section 4.3. Drag reduction investigations involved reducing the boundary-layer bleed discharge areas and changing to a sharper cowl lip contour. Also investigated were the effects of eliminating the inlet side plates bleed and the possible inlet stability improvements that might be achieved by increasing the ramp bleed porosities or using a blunter cowl lip contour.

Data were obtained only at M0 = 2.2 and at selected combinations of angles of attack and yaw where suspected effects would be most significant. All data presented

herein were obtained with the inlet ramps in the same MA/ML schedule positions as for the prototype testing (Ref. 1) and with the bypass door sealed so that effects are noted on a one-for-one basis. The performance data are presented in terms of engine-face total-pressure recovery (R2), steady-state maximum-minus-minimum-over-average total-pressure distortion (D2), the average engine-face root-mean-square value of total pressure fluctuations ratioed to engine-face total pressure (TI2), the peak values of the circumferential (IDC8) and radial (IDR8) distortion indices, and the peak values of stall-margin ratio (IDL8) as a function of engine-face mass-flow ratio (MFR2). The value of IDL8 is particularly critical to inlet/engine compatibility because it is the ratio of engine-face distortion-caused fan stall-margin deterioration to the maximum distortion-caused fan stall-margin deterioration allowable for stall-free engine operation. Thus, as IDL8 exceeds 1.0 the probability of a distortion-induced engine stall increases beyond a value presumed to be tolerable. The peak distortion indices are those values recorded from the Analog Distortion Analyzer (ADA) within a 30-sec period at each data point and have been corrected for the zero shift of each of the dynamic transducers that was measured during the data point. (It should be noted that the constants used in the computations for the stall margin parameter, IDL, for this test series are as in Ref. 5, and have been changed since the Ref. 1 test phase; see Appendix A. All Ref. 1 data presented herein have been appropriately modified.) Noted on the plots are the values of engine airflow; a plot of the engine intermediate and idle power corrected airflow as a function of free-stream Mach number is presented in Fig. 13.

4.1.1 Effect of Reduced Fourth Ramp Length

At supersonic Mach numbers, the prime concern in reducing the fourth ramp length lay in the possibility of having separated flow in the subsonic diffuser because of the changed flow area distribution as seen in Fig. 4. The increased diffusion angle becomes more significant at the higher free-stream Mach numbers and attitudes where the value of HL and throat area is reduced. Inlet performance characteristics are presented in Figs. 14a through c at M0 = 2.20 for configurations having fourth ramp lengths simulating the prototype A/V (data from Ref. 1) as well as two reduced length fourth ramps. At the worst cases of a = -2 deg, ψ = 0 (Fig. 14a) and a = 9 deg, ψ = -3.0 deg (Fig. 14c), where the respective inboard and outboard inlet HL values are reduced from the cruise attitude condition, there appears to be no significant difference in the inlet performance characteristics because of reduced diffuser ramp length. (The difference in supercritical mass-flow ratio noted in Fig. 14a for the inboard inlet is attributed to a difference in lip height, and therefore throat area, rather than to the diffuser ramp length.) Engine-face total-pressure contours obtained at the same conditions for the prototype and 32-in. shortened ramp and presented in Figs. 15a through c give no indications of separation. The slight difference in contours may be attributed as much to the differences in airflow as to the difference in configuration.

area to 60 percent of the simulated prototype A/V or because of reducing the bleed zone I discharge area to 40 percent of the prototype. Typical data, obtained at the cruise attitude, are shown in Fig. 18a for zone II area variations with zone I at the simulated prototype A/V exit area, and in Fig. 18b for zone I variations with zone II at 60 percent of the simulated prototype valve.

For all subcritical inlet mass flow ratios, and most supercritical ratios, the bleed flows were choked at the discharge doors, never at the ramp surfaces. However, bleed flow rates were not reduced proportionally to the exit area reduction because of the increase in bleed plenum pressure as the exit area was reduced (see Fig. 19). Therefore, a slight drag reduction was obtained in that the total bleed door area (including forward-facing areas) was reduced, and the unit energy of the bleed discharge air was increased. As a result, bleed exit areas equal to about 60 percent of the prototype A/V were selected for the production A/V inlet.

4.1.5   M0 = 0 Effects

During the development test period, the effects of the reduced length fourth ramps were determined also at M0 = 0. This investigation was conducted because of the high distortion levels associated with the M0 = 0 conditions as reported in Refs. 1 and 5; any increase in distortion at M0 = 0 associated with the reduced length ramps would eliminate them as candidates for use in the production A/V inlet. The basic inlet performance characteristics are presented for the two shortened ramp configurations in Fig. 20, and the outboard inlet prototype configuration data from Ref. 1 are also presented. All data were obtained with the cowl lip in the takeoff position.

As is seen in Fig. 20, the inboard and outboard performance characteristics are very similar at the M0 = 0 conditions, as would be expected. Also, there is no significant difference between the configurations. Considering the time-dependent nature and the inherent uncertainty associated with the peak distortion parameters, the variations between the IDL8 values for the different ramp configurations are not felt to be significant. This opinion is reinforced by consideration of the similarity of the steady-state distortion (D2) values and the average root-mean-square (TI2) values of pressure fluctuations at the engine face.

The effects of sealing the gap between the cowl lip and sideplates when the cowl is in the takeoff position and the effect of opening the bleed zone II discharge doors were also investigated in this test phase. Summarizing the results of these investigations, it was seen that installing the cowl lip seals produced about a 1-percent increase in total-pressure recovery at the design engine airflow rate but had virtually no effect on the steady-state or peak distortion parameters. Opening the BLCII discharge doors appeared

to effect a marginal improvement in the peak distortion parameters, but insufficient data were obtained to be conclusive.

Because of the high distortion values attendant with the MO = 0 condition and the question of whether or not a crosswind would cause a further deterioration in inlet performance characteristics, the sensitivity of the inlet to crosswinds was investigated. Crosswind velocities were simulated up to 40 knots at 90 deg to the nacelle axis with the crosswind coming from the outboard side. The lack of sensitivity of both the outboard and inboard inlets to the simulated crosswinds is shown in Fig. 21 for the 32-in. shortened ramp configuration. Similar results were obtained for the 16-in. shortened ramp configuration.

4.2 INLET CONTROL SCHEDULES

The later test periods in Tunnels 16S and 16T were devoted to defining the performance characteristics of the selected production inlet configuration, but before this could be accomplished it was first necessary to prepare the inlet control schedules.

The logic used in the selection of the ML sensor (located on the bottom of the engine nacelle) for control of the inboard inlet and the MA sensor (located on the outboard inlet first ramp) for control of the outboard inlet is given in Ref. 1. Briefly, these control sensors were selected for the respective inlets as the single indicators that would allow development of ramp position schedules in which an acceptable compromise could be achieved between engine airflow demand and inlet local-flow conditions that resulted in stable inlet operation and satisfactory inlet performance characteristics throughout the A/V flight and maneuvering envelope. Selection of other possible sensors (e.g., MO, MA for the inboard inlet, and ML for the outboard inlet) would have restricted the A/V maneuvering envelope because of inlet instability (buzz) or extremely supercritical inlet operation and attendant excessive engine-face distortion levels.

The ML/MA data matrix obtained for the proposed production configuration is presented in Figs. 22a through f. It is quite apparent that the outboard inlet sensor, MA, is sensitive to yaw angle, but relatively insensitive to pitch angle. Conversely, the ML sensor is quite sensitive to angle of attack and less sensitive to yaw angle (except at yaw angles greater than ±3 deg). This occurs because, at supersonic free-stream conditions, the Mach number over the lower fuselage decreases as angle of attack increases and the magnitude of the flow outwash angle increases with angle of attack. For a given angle of attack, the under-fuselage Mach number does not change greatly with yaw angle, but the flow outwash angle on the leeward side of the fuselage is proportional to the magnitude of the yaw angle. Thus, the measured ML value is fairly insensitive to yaw angle because

the probe is located in a position which makes it relatively insensitive to local flow angle. However, the measured MA value, being the outboard first ramp local Mach number, is quite sensitive to the local flow angle approaching the first ramp leading edge and the resultant expansion (or compression) around the leading edge. Consequently, the effect of reduced under-fuselage Mach number as a function of angle of attack is cancelled by the increased flow outwash and expansion around the first ramp leading edge. The consistency of these phenomena is not evident at the transonic free-stream conditions. As may be seen in Figs. 22e and f, ML and MA values near 1.0 are not stable and may present a problem which will be described below.

Presented in Figs. 23a to c are the 0.2-scale/full-scale local Mach sensor correlation data obtained during the parasite flat-plate test in Tunnel 16S. Presented are data for the ML and MA probes used in this test series (Figs. 23a and b) as well as the MA probe used for the test series reported in Ref. 1 (Fig. 23c). The data from that test were used to schedule the prototype A/V Air Inlet Control System (AICS). Using these correlation data and inlet ramp position schedules defined in Ref. 1 and previous tests, the schedules presented in Figs. 24a through c were constructed.

Concerning these schedules and the MA/ML data in Fig. 22, there are several points of special interest. As is seen in Fig. 24b, the AICS controls the lip height position for sensed local Mach numbers greater than approximately 0.85. As stated above, it is apparent that MA and ML are not stable near 1.0. Therefore, at the low supersonic free-stream Mach numbers, A/V pitch or yaw oscillations, or transients, could lead to abrupt movements or a slight instability in the positioning of the aft inlet ramp. As this discontinuity, or instability, may result only in an A/V HL movement up to $\pm 1/2$ in., it is not felt that this would significantly affect inlet performance (see Section 4.3.1).

Another peculiarity may be observed in Fig. 25 where the effect of engine, and therefore inlet, airflow on the measured local Mach numbers is shown. Data presented in Fig. 25 were obtained at M0 = 1.4, but the effect of inlet airflow on the inlet static pressure field, and consequently on MA and ML, occurs at all lower free-stream Mach numbers. Because of these phenomena, it may be inferred that MA, and probably ML, are also functions of RB and HL, which affect the static pressure field. But once again, the instabilities that might be created by engine transients or ramp position changes would be small and not deleterious to the propulsion system performance. It also should be noted that any instability would to a large extent be dependent upon the gains and threshold error signals programmed into the AICS and are thus beyond the scope of this report.

In Fig. 24c, the decrease in the inboard inlet NSP schedule above ML = 1.8 should be noted. For a given flight condition, NSP is very sensitive to inlet flow and therefore

is an ideal parameter to use for inlet/engine airflow matching. Using this characteristic, the AICS controls the bypass doors in a closed-loop system as a function of NSP, as described in Section 3.1. For most conditions, an NSP value of about 0.68 to 0.72 yields high recovery, low distortion inlet characteristics. However, at some conditions (e.g., MO = 2.2, a = 0, ψ = 3 deg), flow conditions and the scheduled inboard ramp positions are such that inlet instability occurs at values as low as 0.61. Therefore, the schedule must be reduced below that value to ensure stable operation for these conditions at some sacrifice in total-pressure recovery while maintaining inlet distortions less than the prescribed maximum allowable value of IDL8 = 1.0.

4.3 PROPOSED PRODUCTION INLET PERFORMANCE

After the inlet control schedules had been constructed, the inlet performance characteristics of the proposed production inlet configuration were verified and documented. Mach numbers of 2.2, 1.8, 1.4, 0.85, and the takeoff condition were of primary interest. Representative data and comments defining the effects of ramp positioning, bypass door effectiveness, scheduled inlet performance characteristics, interference effects of the weapons bay doors and EVS pods, and takeoff performance are given below.

4.3.1 Ramp Positioning Effects

At the nominal cruise attitude the effects of ramp positions are presented in Figs. 26a through c for MO = 2.2, 1.8, and 1.4, respectively. These data were obtained with the bypass doors sealed. At MO = 2.2 and 1.80 the desirability of the scheduled ramp position at the matched engine airflow is seen as the inlet is operating at about 95 percent of the supercritical mass-flow ratio with adequate inlet stability margin. In these cases, the matched airflow IDL8 value is below 1.0. At MO = 1.40 (Fig. 26c) it is seen that the effects of HL for values above 4.9 in. are negligible; however, at the lower HL values, the inlet becomes choked at the matched engine airflow point, and performance deteriorates.

In a failed geometry situation as is represented by the cases of HL = 5.45 in. or 2.95 in., engine operation and inlet stability become questionable at MO = 2.20 and 1.80. For the HL = 5.45-in. case, at MO = 2.20, excessive distortion would preclude stall-free engine operation even if the bypass doors could pass enough airflow to maintain stable inlet operation. At MO = 1.80, stable inlet operation would be possible, but engine operation would be marginal as the IDL8 values at matched engine airflows are about 20 percent greater than allowable (1.0). At MO = 1.40 and below, the failed-open inlet presents no operational problems. As would be expected, an inlet failed at the minimum HL position presents the opposite problem; in this case MO = 2.20 would be

possible, but deceleration to lower Mach numbers would cause supercritical inlet operation until an engine stall occurred because of excessive distortion.

4.3.2 Bypass Door Effectiveness

The effect of the bypass doors on the control parameter, NSP, is seen in Figs. 27a and b for Mach numbers 2.20 and 1.80, respectively. These data were obtained at the scheduled ramp position and cruise attitude. Noted on the figures are the inlet stability limits, the excessive supercritical (IDL8 $>$ 1.0) limits, and the engine intermediate and idle power airflow rates. The doors are capable of handling the equivalent of about 100 to 125 lb/sec of engine airflow at these supersonic speeds.

As the bypass doors are opened at a constant engine airflow, or as engine airflow is increased at a constant door angle, NSP decreases and the inlet tends to operate more supercritically. This process increases until IDL8 exceeds 1.0, at which point engine operation becomes marginal.

Of particular note in these figures is the uniformity of the inlet stability limit with NSP for all cases except the outboard inlet at M0 = 2.20. The apparent inconsistency in defining the M0 = 2.20 outboard inlet stability limit was also observed during the cold-pipe testing of the full-scale inlet/engine test reported in Ref. 5. In that test, and the test reported herein, there appeared to be some inlet/duct airflow resonance created at certain combinations of bypass door openings and simulated engine airflows. This is believed to be a function of the ramp oblique shock waves coalescing with the inlet normal shock inboard of the cowl lip buttock plane, the resultant shock strength (and consequently the NSP signal because of the location of the NSP total-pressure probe; see Section 3.1) thus being insensitive to small inlet airflow changes. The result of this phenomenon is a weak, localized instability.

4.3.3 MA/ML Scheduled Inlet Performance

The MA/ML scheduled inlet performance characteristics are presented for M0 = 2.20 and 1.80 as a function of corrected engine-face airflow rate in Fig. 28 for variations in angle of attack at ψ = 0 and in Fig. 29 for yaw variations at α = 2.5 deg. These data were acquired with the bypass doors operating under automatic NSP control as given in the Fig. 24c schedule. Airflows that would have required NSP values less than the scheduled value (and thereby caused the bypass doors to be closed) were not obtained; similarly, stability limits were not defined. This mode of operation was followed to simulate the AICS/engine operation of the A/V as explained in Section 3.1.

There is one condition at which IDL8 exceeds a value of 1.0: M0 = 1.80, ψ = -3.0 deg, and the minimum airflow tested (Fig. 29b). However, since this airflow is less than the engine idle airflow, the high distortion level is of no consequence.

19

Data are presented in Fig. 30 which completely map the inlet operating characteristics over the M0 = 2.20 and 1.80 maneuvering envelopes with simulated engine airflows representative of intermediate power settings having, if necessary, fan speeds rolled back as dictated by the AICS/NSP schedule. Satisfactory inlet performance characteristics are evident for both inlets at both Mach numbers for all attitudes presented. The only conditions where IDL8 is near 1.0 are at M0 = 2.20 for the inboard inlet (Fig. 30a), where the ML values are in excess of 1.85 (see Fig. 22a) and NSP is reduced (Fig. 24c), thus forcing the inlet towards more supercritical operation.

4.3.4 Effects of Mis-Scheduled Ramp Positions

The effect on the inlet performance characteristics that would occur if the A/V AICS mispositioned the ramps enough to cause a 1-in. full-scale error in the value of HL was determined at M0 = 2.20 for a few model attitudes. It is noteworthy that this much error can be caused by an MA or ML static-to-total pressure ratio error of only ±0.011 at these flight conditions. Data are presented in Figs. 31a and b for two cases showing the effect of HL being too large, and in Fig. 31c for a case of HL being too small. These data for the scheduled and off-scheduled ramp positions were obtained with the bypass door sealed.

As is seen, the outboard inlet stability and performance characteristics are not severely affected for any of the three cases. However, the situation is different for the inboard inlet; in both situations where HL is greater than that scheduled, instability occurs at values of airflow greater than the engine demand. Although the instability could be eliminated by increasing inlet airflow by opening the bypass door, such action would also increase the peak stall margin ratio to a value greater than 1.0. For the instance where the value of HL is less than scheduled, some gain in stability margin is achieved, but this is at the cost of a reduction in recovery and an increase in IDL8.

Thus, it is seen that errors in the positioning of the ramps by the AICS or any other cause could result in rather serious inlet stability and performance problems, particularly for the inboard inlet.

4.3.5 M0 Scheduled Inlet Performance

The data presented in Fig. 32 were obtained with the ramps positioned as a function of free-stream Mach number, i.e., the M0-scheduled positions. The values of RB and HL used for the M0 schedule are the same as for the MA/ML schedule at the cruise attitude (i.e., α = 2.5 deg. ψ = 0). They are not a function of the A/V attitude or inlet local Mach number; they are a function only of free-stream Mach number. All these data were obtained with the bypass sealed. The ψ = 0 data presented in Fig. 32a indicate that

satisfactory inlet performance and stability characteristics are obtainable for the outboard inlet; however, the inboard inlet is unstable at a = -2.0 deg for the design engine airflow. Increasing the inboard inlet stability by opening the bypass doors would cause an increase in IDL8, which is already above the limit of 1.0. Hence, the minimum angle of attack at M0 = 2.2 with this M0 ramp schedule would be about zero. In the yaw data in Fig. 32b, a similar situation occurs for the outboard inlet at ψ = -5.8 deg and for the inboard inlet at ψ = 3.2 and 5.8 deg. Thus, it is readily seen that the A/V maneuvering envelope would be severely limited if M0 inlet ramp scheduling was used.

4.3.6 Transonic Inlet Performance Characteristics

The inlet performance characteristics are presented as a function of mass-flow ratio for M0 = 1.4 and 0.85 in Fig. 33 at ψ = 0 and various angles of attack, and in Fig. 34 for various yaw angles at a = 3.0 deg. All these data were obtained with the ramps positioned as in the MA/ML schedule and with the bypass doors sealed. At and below the intermediate engine airflow operating points, the distortion values are well within the acceptable limits. Inlet stability is marginal at some of the near-idle airflow points for both Mach numbers. However, these instability points are only at maneuvering attitudes, and these maneuvering attitudes would not normally be attempted with an engine at reduced power or sub-idle. In addition, the bypass doors are presently scheduled to be active at the sensed local Mach numbers typical of the M0 = 1.4 cruise conditions. This would eliminate any of the stability problems predicted by these data for the inboard inlet at $a \leqslant 3.0$ deg and for the outboard inlet at $\psi \leqslant 0$ and $a > 3$ deg.

Only minimal amounts of data were obtained on the M0 ramp schedule in the Tunnel 16T tests. These data are not presented herein, but the inlet was shown to be insensitive to slight HL variations from the optimum which would result from an M0 schedule at these Mach numbers in Section 4.3.1.

4.3.7 Interference Effects of the Weapons Bay Doors and EVS Pods

The inlet performance effects of opened mid and forward weapons bay doors and of the EVS pods were determined at M0 = 0.85, a = 3 deg, ψ = -5 to 5 deg. Data presented in Fig. 35 show that opened doors and installed EVS pods have no deleterious effect on the inlet performance characteristics. In fact, the inboard inlet peak stall margin ratio, IDL8, is improved with the opening of the doors or installation of the pods because of the reduction in the peak circumferential distortion parameter. This effect tends to be most significant at the negative yaw angles (nacelle leeward of the doors and pods) and is lessened at the positive yaw angles.

4.3.8 Subsonic and Takeoff Performance

The inlet performance characteristics for Mach numbers from 0 to 0.85 are presented as a function of engine-face airflow in Fig. 36a with the cowl lip in the cruise position and in Fig. 36b for the T/O cowl lip position. (The T/O cowl position is not realistic for M0 > 0.4, as stated below, but the cowl could fail open, and therefore the data are presented herein.) These data have been crossplotted at the sea-level intermediate power airflow and are presented in Fig. 37 as a function of Mach number. It is evident that satisfactory inlet performance characteristics are obtainable at least up to M0 = 0.85 with the cowl lip in the T/O position. Even though the T/O cowl lip position demonstrates superior engine-face total-pressure recovery and reduced distortion characteristics up to M0 = 0.8, it also has higher drag penalties associated with it. Hence, determining the optimum Mach number at which to transition from the T/O to cruise cowl lip position is beyond the scope of this report. At present, however, the cowl lip positioning mechanism is linked to the A/V landing gear; i.e., if the landing gear is down, the cowl lip is in the T/O position, and if the gear is retracted, the cowl lip is in the cruise position. According to the peak fan stall margin ratio (IDL8) in Fig. 37, it appears landing gear retraction should be delayed until at least M0 = 0.30 (approximately 200 knots on a standard day), presuming takeoff engine power setting will be intermediate or above. On landing approach, gear extension could take place at a lower Mach number if engine power and airflow are reduced.

During this test, as in the full-scale test (Ref. 5), data were obtained during a tunnel Mach number transient from M0 = 0 to 0.20 with simulated engine airflow equivalent to the engine intermediate power setting. The instantaneous total-pressure recovery and distortion parameters as sensed and computed by the ADA are presented in Fig. 38 as a function of Mach number. Also shown in Fig. 38 are the loci of estimated peak fan stall margin ratio values based on the peak values obtained at M0 = 0 and 0.20 steady-state conditions. (IDL8 values were not available from the ADA during these transients.)

As may be seen for both inlets, there is a decline in IDL which starts at about M0 = 0.04 or 0.05 and is essentially complete by M0 = 0.10 to 0.13. This is caused by a reduction of the radial distortion component, IDR; the change in the circumferential component, IDC, is not so definite. These data validate the questionable data obtained during the Mach number transients reported in Ref. 5. Therefore, it is evident that as the A/V approaches 80 knots (less than rotation velocity), inlet-created engine-face distortion will be reduced to the point where the probability of an engine stall because of distortion is minimal.

4.4 TRANSONIC INLET DRAG CHARACTERISTICS

The outboard inlet drag characteristics were determined over a small angle-of-attack range about the nominal cruise attitude. Typical data are presented in the form of spillage drag as a function of mass-flow ratio in Figs. 39a to c for M0 = 0.85, 1.20, and 1.40, respectively. These data were obtained with the ECS closed, the bypass doors sealed, and the zone II BLC doors closed. The method of calculations for the inlet spillage drag term is given in Appendix B.

During the course of the test it became apparent that determination of inlet momentum by use of inlet total-pressure rakes and average static pressure would not yield valid answers, so the method of calculation was altered and the inlet momentum was determined by using the inlet airflows and the average inlet static pressure at the cowl lip plane.

The effects of opening the zone II BLC doors were determined at M0 = 1.40, where the doors are nominally scheduled to be opened on the A/V. The bleed drag term is also defined in Appendix B and is the loss in momentum of the bleed airflow for both bleed zones from free-stream conditions to door exit stations, plus the pressure-drag term of the opened BLCII doors. Data are presented in Fig. 40 for the zone II doors opened and closed. With the BLCII doors closed, CDBLC is the bleed zone I drag, and with the doors open it is the BLCI plus BLCII drag. Observing the spillage drag term in Fig. 40, one notes that the increase in BLC drag with the BLCII doors open is offset by a decrease in spillage drag. At the highest mass-flow ratios the decrease in spillage drag is greater than the increase in BLC drag, but at the lower mass-flow ratios the reverse is true. At the matched airflow point, the increase in BLC drag appears to be slightly greater than the decrease in spillage drag, but not significantly so.

5.0 CONCLUSIONS

An investigation was conducted in tunnels 16T and 16S of the Propulsion Wind Tunnel Facility on the 0.2-scale B-1 forebody/inlet model to develop an inlet configuration for the production B-1 A/V and to verify and document the performance characteristics of that configuration.

From the results of the developmental phase of the test series, the following conclusions were reached:

1. Shortening the inlet fourth ramp by up to 32 in. full scale from the prototype configuration did not significantly affect the inlet performance or stability characteristics.

2. Eliminating the inlet sideplate boundary-layer bleed porous areas did not reduce the inlet stability margin nor affect the inlet performance characteristics.

3. Increasing the porosity of the third and fourth ramp boundary-layer bleed porous areas did not improve inlet stability nor affect the inlet performance characteristics.

4. Replacing the prototype cowl lip with one having more blunt contours did not improve the inlet stability or performance characteristics but could be expected to increase inlet drag.

5. Replacing the prototype cowl lip with a more sharp-lipped cowl caused a reduction in stability margin at model attitudes where stability was already marginal.

6. Reducing the boundary-layer bleed discharge areas to approximately 60 percent of the prototype configuration was accomplished at no loss to inlet stability or performance while effecting an inlet drag reduction.

7. At takeoff (M0 = 0) conditions, the inlet performance characteristics were insensitive to crosswinds up to 40 knots velocity at 90 deg to the inlet.

8. At takeoff conditions, the use of seals to fill the gaps between the cowl lip in the takeoff position and the sideplates increased inlet total-pressure recovery by about 1 percent but did not affect the distortion parameters.

9. At takeoff conditions, opening the throat bleed discharge doors may effect a slight improvement in the inlet peak distortion parameters.

From the results obtained during the production inlet verification test phase, the following conclusions have been reached:

1. The outboard inlet control sensor is sensitive to yaw angles but relatively insensitive to angles of attack, while the reverse is true for the inboard inlet control sensor. ML.

2. Using the outboard and inboard inlet control sensor schedules presented herein, stable inlet operation with distortion parameters below the fan stall margin distortion limit were demonstrated for all conditions tested at representative engine airflows.

3. Above Mach number 1.8, with the inlet failed at maximum lip height position, inlet instability or excessive distortion will prevent stall-free engine operation. Conversely, with the inlet failed at minimum lip height, low supersonic and subsonic engine operation will be prevented by excessive engine-face distortion except at very low engine airflow rates.

4. Mis-positioning of the fourth ramp (i.e.. lip height) up to 1 in. full scale will result in inboard inlet instability and/or excessive distortions at matched engine airflows for Mach number 2.20 maneuvering attitudes.

5. If free-stream Mach number rather than outboard and inboard inlet control sensors were used to control the inlet ramp positions, the air vehicle maneuvering envelope would be severely limited at the higher supersonic Mach numbers because of reduced inlet stability margin and/or excessive peak total-pressure distortion.

6. Neither the opened weapons bay doors nor the electro-optical visual system pods caused any significant effects on the inlet performance characteristics at the Mach number 0.85 condition tested.

7. Up to about Mach number 0.80. inlet total-pressure recovery is increased and distortion reduced with the cowl lip in the takeoff position. The cowl lip may be translated from the takeoff position to the cruise position and vice-versa at Mach numbers ≥ 0.3 with intermediate power engine airflow settings while maintaining the peak fan stall margin distortion parameter at less than 1.0.

8. During a Mach number transient simulating takeoff, the peak fan stall margin ratio decreases from about 1.0 at Mach number 0 to a value of about 0.70 at Mach number 0.12 with airflows representative of intermediate engine power setting.

REFERENCES

1. German, R. C. "0.2-Scale B-1 External-Compression Inlet Verification Model Test at Transonic and Supersonic Mach Numbers (Phase II)." AEDC-TR-74-52 (AD921416), August 1974.

2. Test Facilities Handbook (Tenth Edition). "Propulsion Wind Tunnel Facility, Vol. 4." Arnold Engineering Development Center, May 1974.

3. "B-1 Test Plan/Procedure, Inlet Verification Model PWT-16, Test 3." NA-70-550-2, Vol. VII, April 1974.

4. "Pretest Information for the 0.20-Scale B-1 Inlet Verification Model in the AEDC Propulsion Wind Tunnels - 16S, 16T (Test 4)." NA-70-550-2, October 1974.

5. McDill, H. E. "Results of a Full-Scale B-1 Inlet/Engine Compatibility Test at Subsonic and Supersonic Mach Numbers." AEDC-TR-75-3 (ADB001545L), January 1975.

SOLID AREA
PERFORATED WALLS
NOZZLE
TEST SECTION
DIFFUSER

FS 154.5

TUNNEL ℄

AUXILIARY
PITCH TABLE

PITCH TABLE PIVOT

YAW TABLE PIVOT

℄
PITCH
TABLE

SUCTION SYSTEM FOR
INLET AIRFLOW

TUNNEL FLOOR

-16
-4.2
0
FS 0.00
20
40
46.4

TUNNEL STATIONS IN FEET
FUSELAGE STATIONS IN INCHES
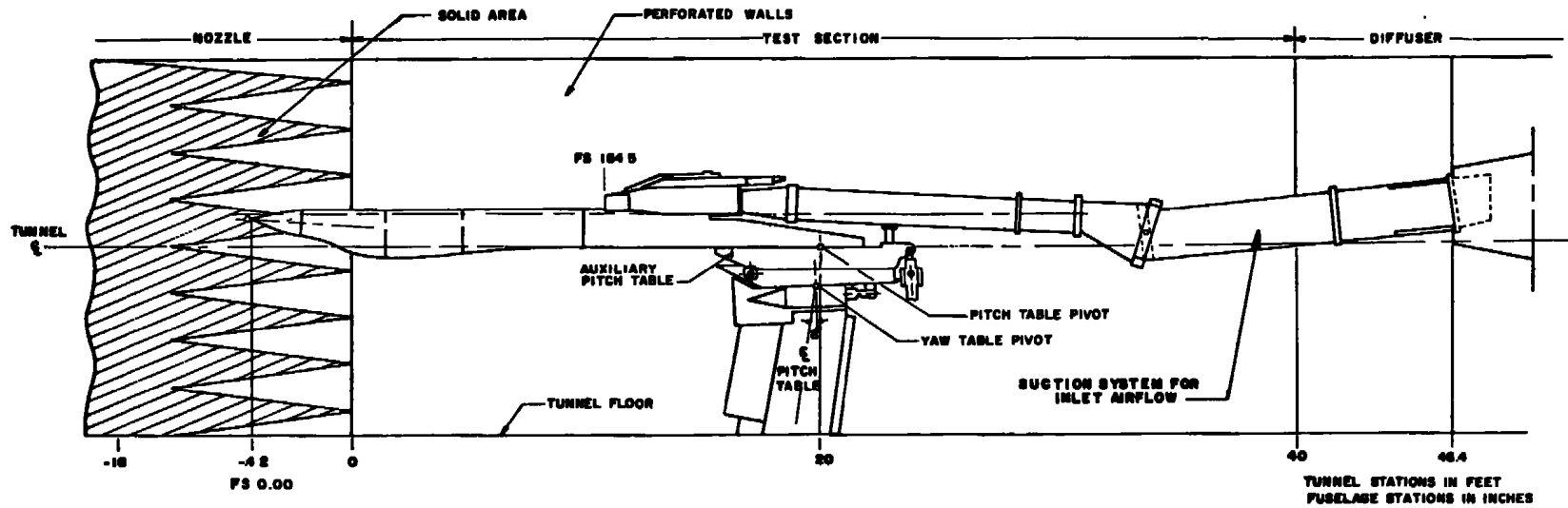
a. Tunnel 16T
Figure 1. Sketches of model installation.

NOZZLE — TEST SECTION — DIFFUSER

TUNNEL TOP WALL

FS 184.5'

PITCH TABLE PIVOT

FS 388.5

FS 0.0

TUNNEL ₵

TUNNEL ₵

AUXILIARY
PITCH TABLE

YAW TABLE
PIVOT

₵
PITCH
TABLE

TUNNEL FLOOR

-14.2   0   10   18.2 20.0   40.0

TUNNEL STATIONS IN FEET
FUSELAGE STATIONS IN INCHES
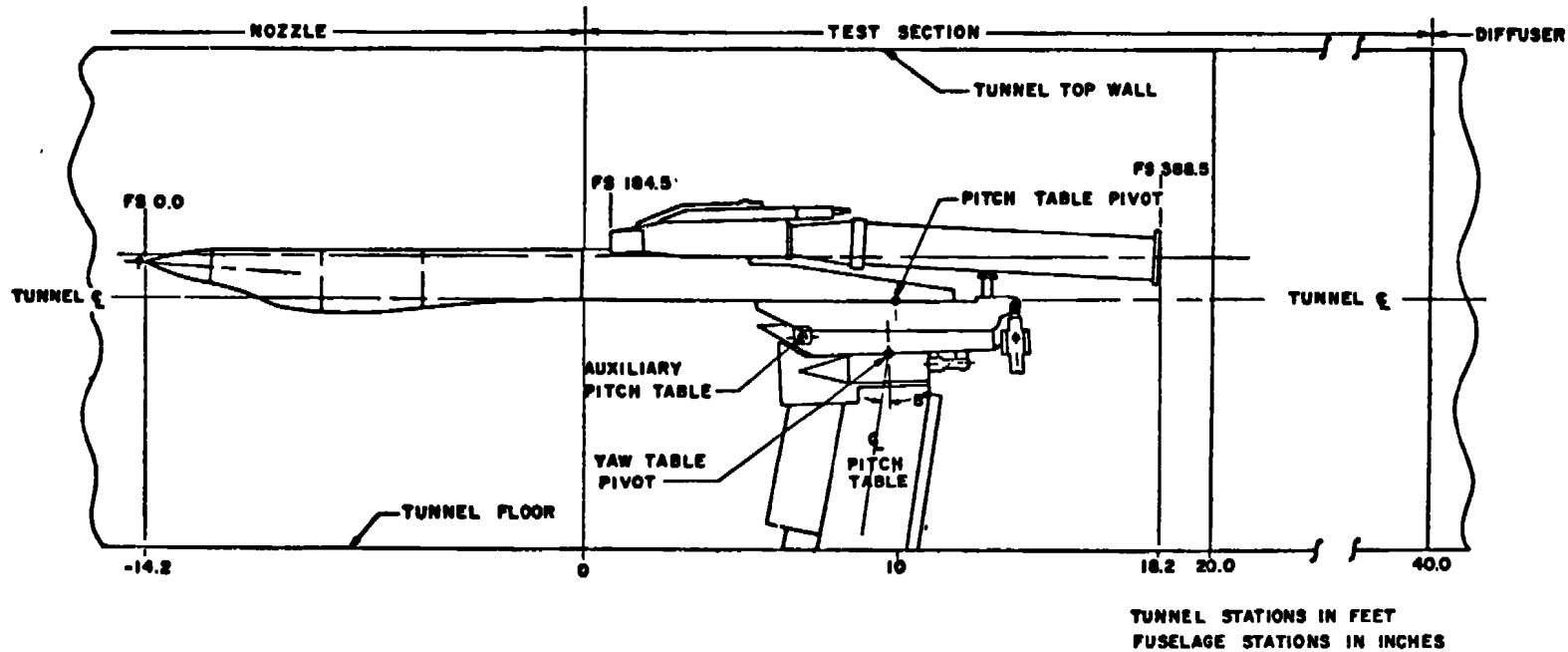
b. Tunnel 16S
Figure 1. Concluded.

a. Tunnel 16T
Figure 2. Installation photographs.

b. Tunnel 16S
Figure 2. Concluded.
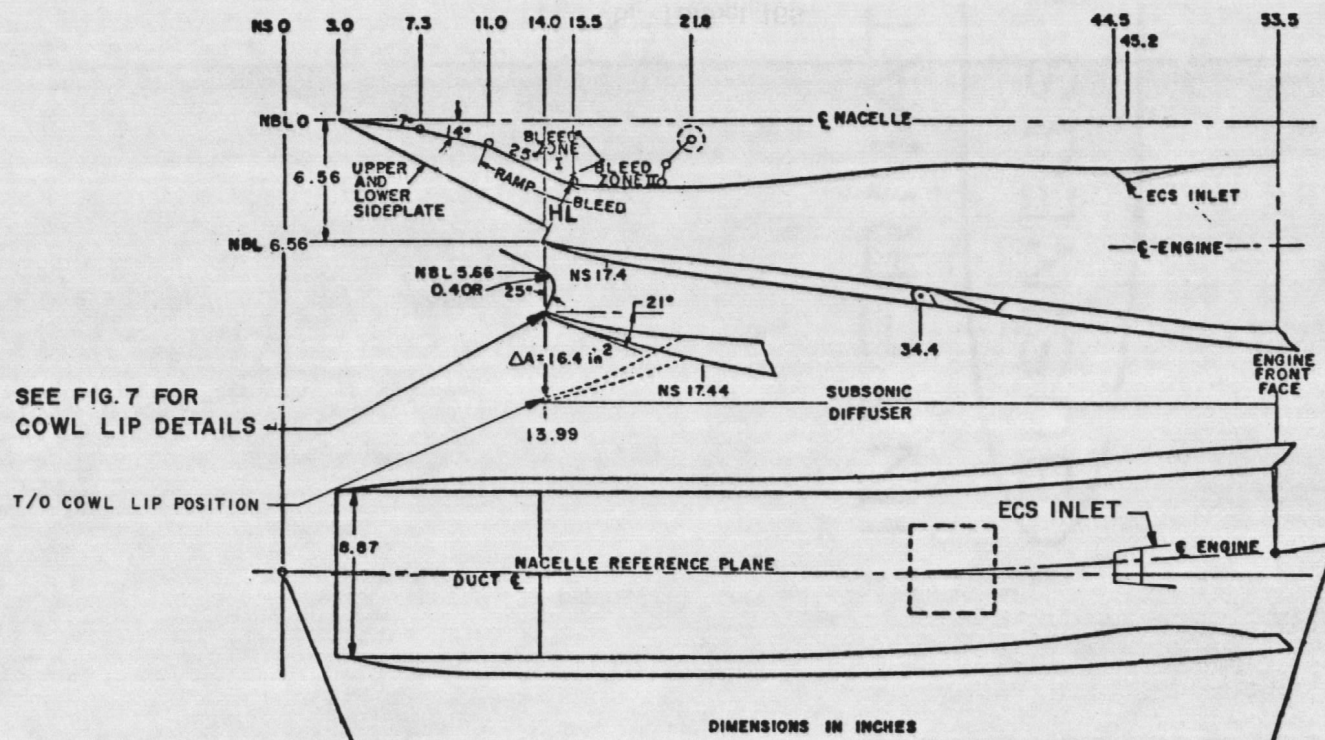
DIMENSIONS IN INCHES

REFERENCE SYSTEM		
NACELLE	FUSELAGE	ORIENTATION NACELLE
NBL = O	FBL = 28.53	ΔPITCH = 1°-10'-00" NOSE UP
NS = O	FS = 181.53	ΔYAW = 0°-33'-4.7" NOSE IN
NWL = O	FWL = - 6.38	Δ ROLL = 2°-30'-1.9" INBOARD DOWN

REFERENCE SYSTEM			
NACELLE	FUSELAGE	ENGINE	ENGINE ORIENTATION
NBL = 6.70	FBL = 35.69	O	ΔPITCH = 2°-00'-00" NOSE DOWN
NS = 53.50	FS = 234.99		ΔYAW = 0°-48'-34.8" NOSE OUT
NWL = 1.17	FWL = - 6.01	O	

a. Schematic
Figure 3. Inlet geometry.

31

AEDC-TR-75-57
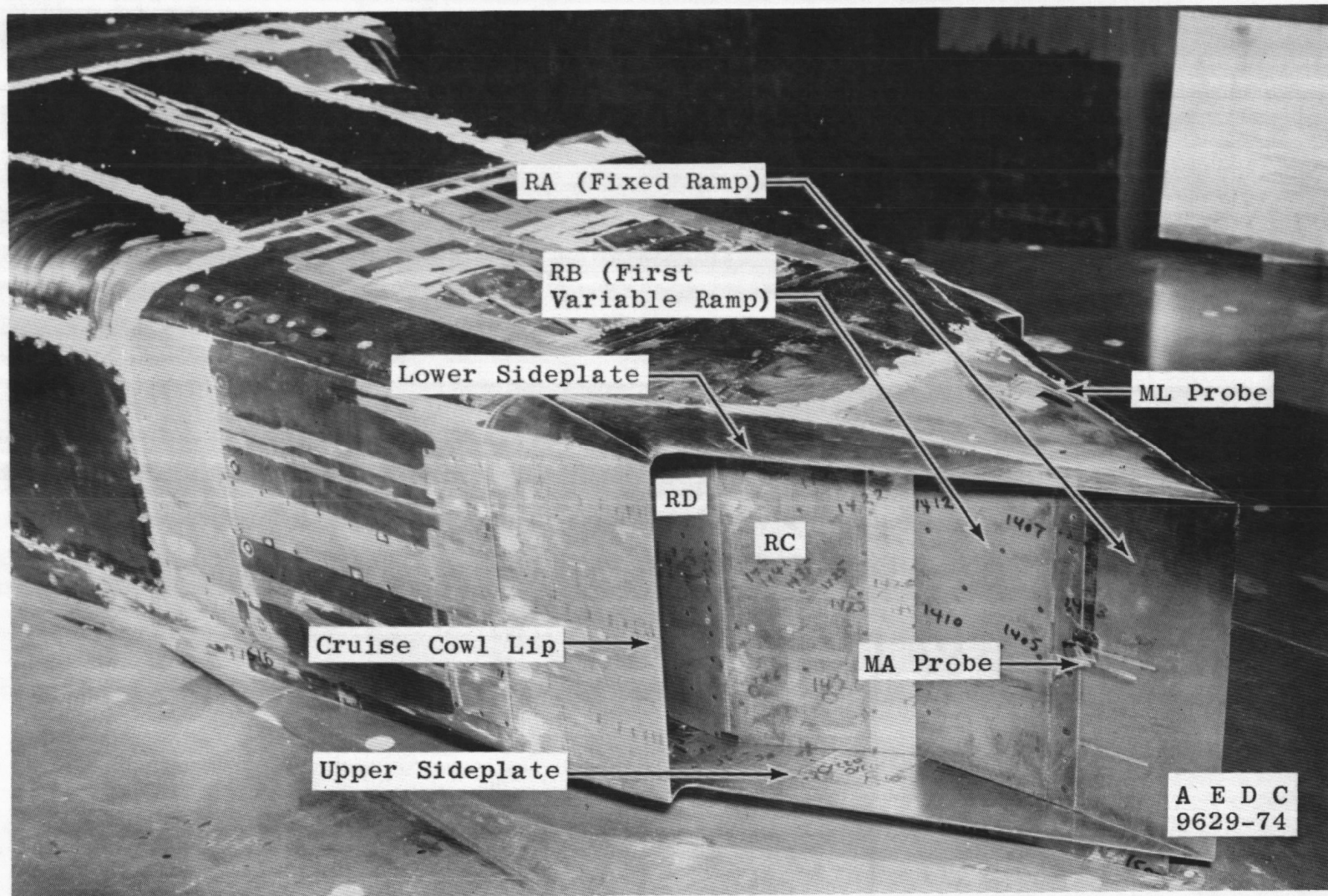
b. Photograph
Figure 3. Concluded.
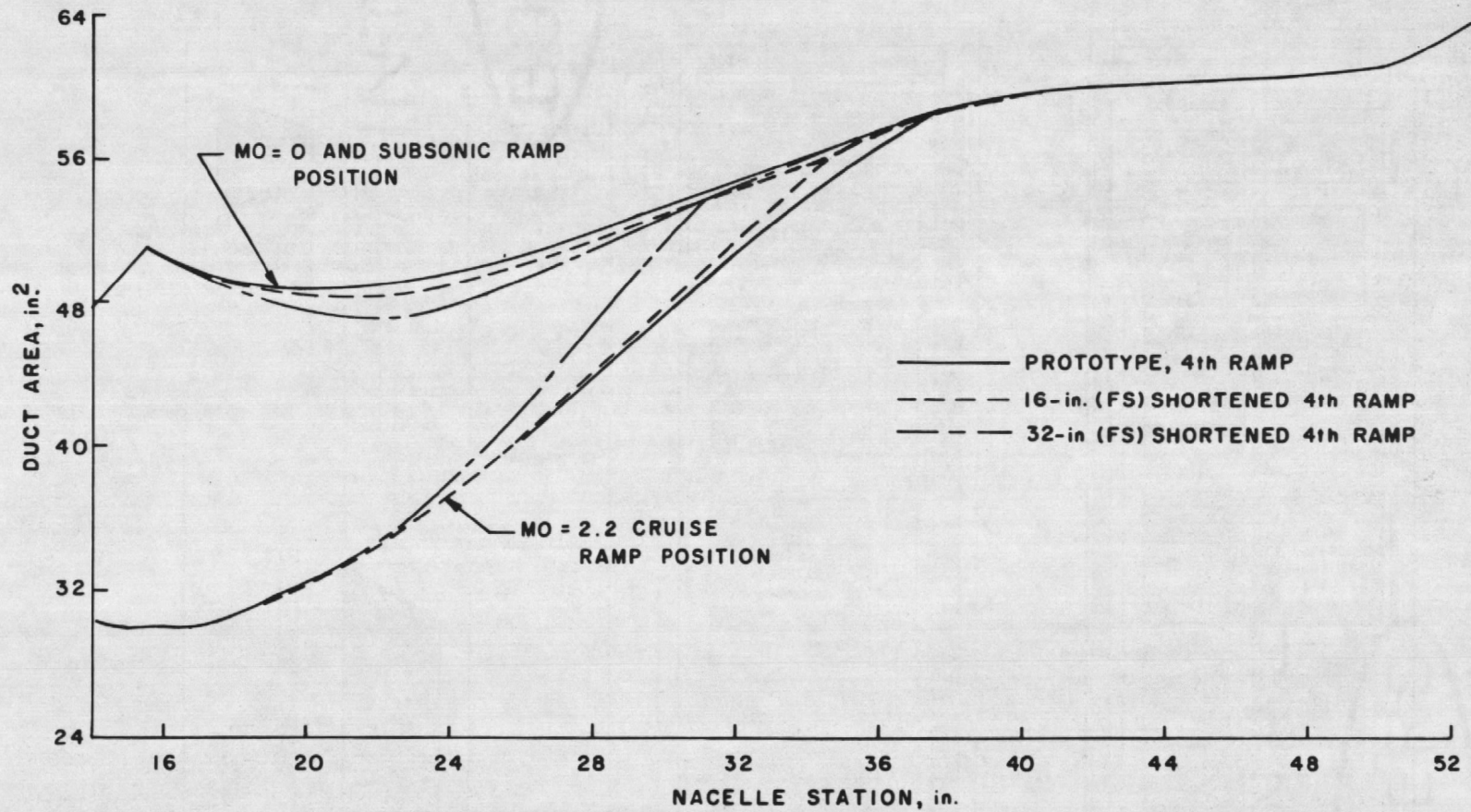
Figure 4. Duct area distribution.
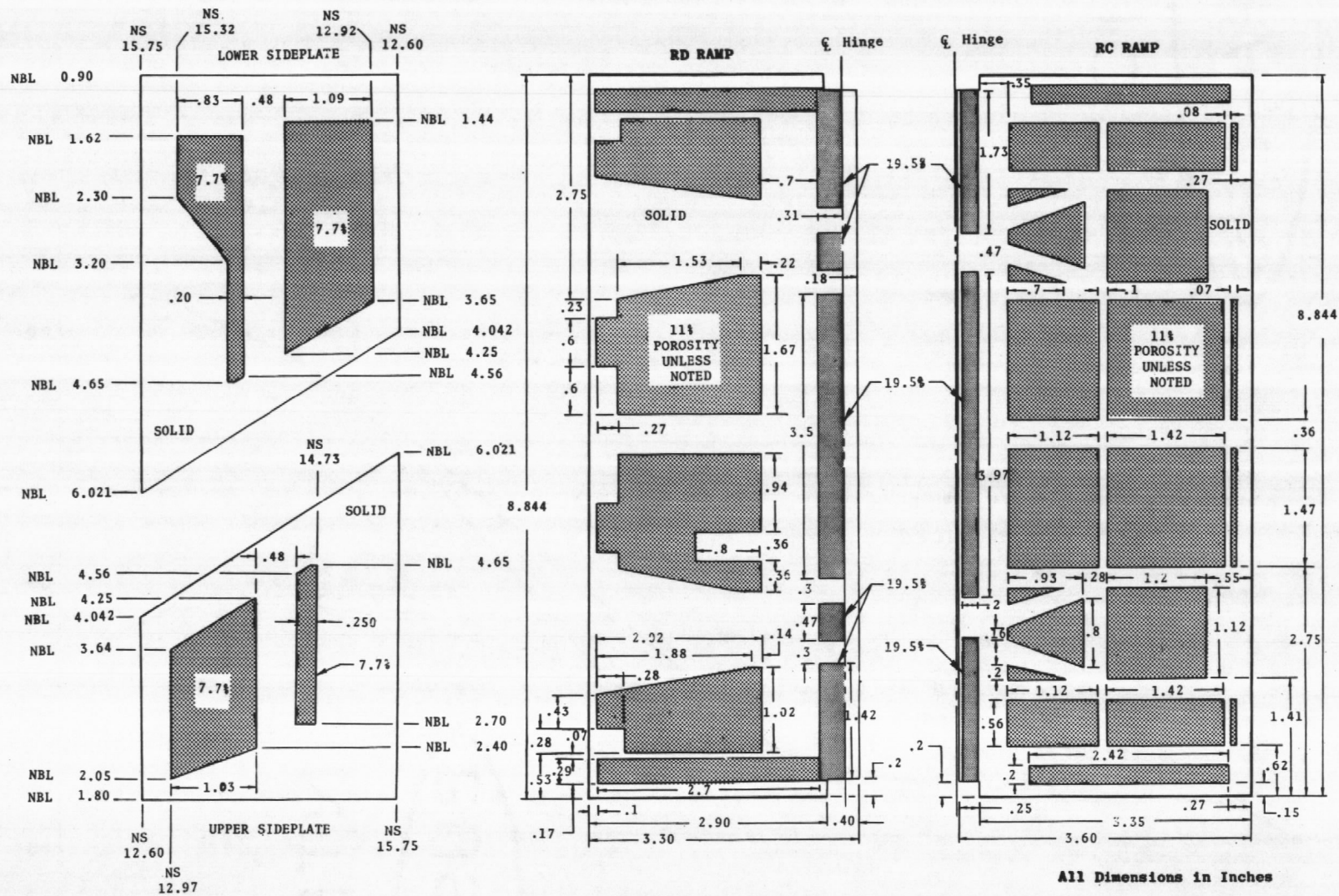
Figure 5. Inlet boundary-layer bleed porosity configuration.

BLCI Fixed Exit Doors:

Door 3

Door 4

Inboard Doors →

Outboard Doors →

Door 3   Door 2   Door 1

BLCII Variable
Exit Doors

A E D C
9630-74
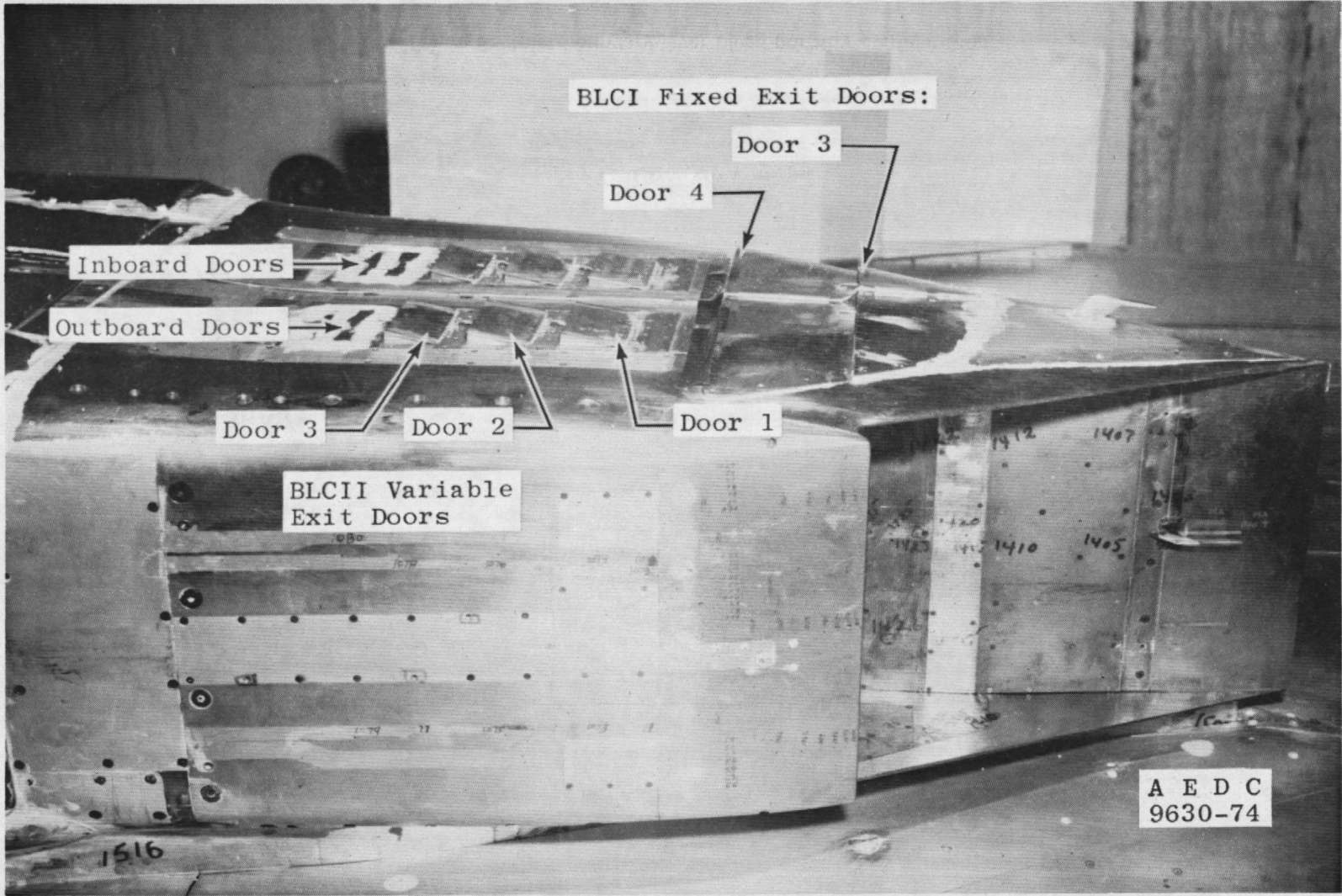
Figure 6. Production configuration bleed zone discharge doors.
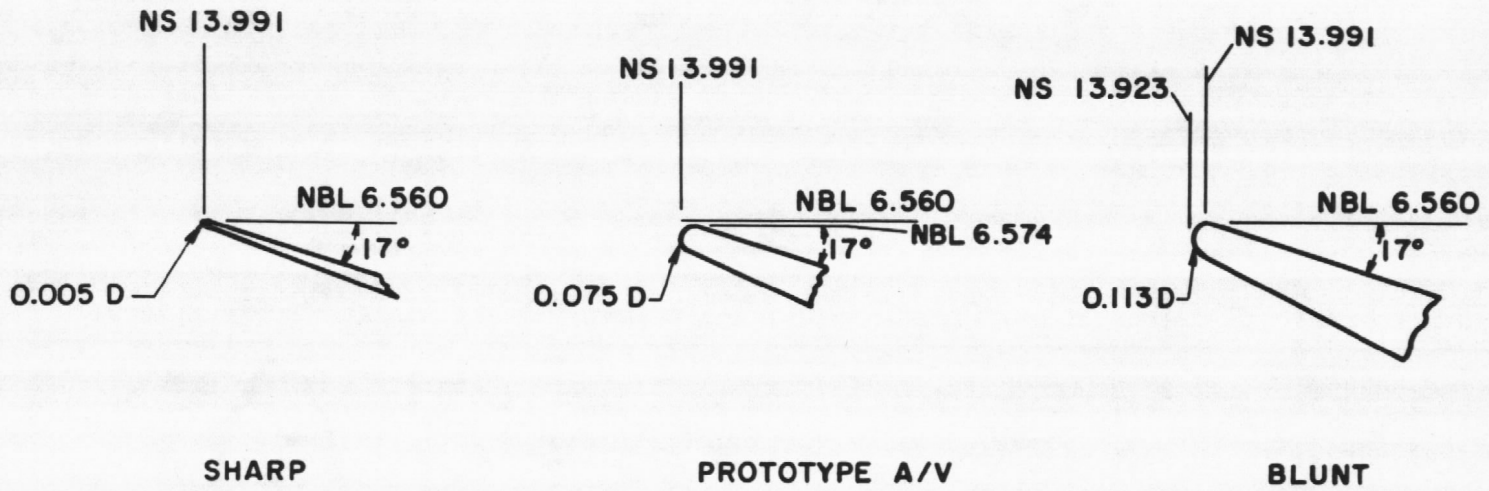
DIMENSIONS IN INCHES

Figure 7. Cowl lip contours.
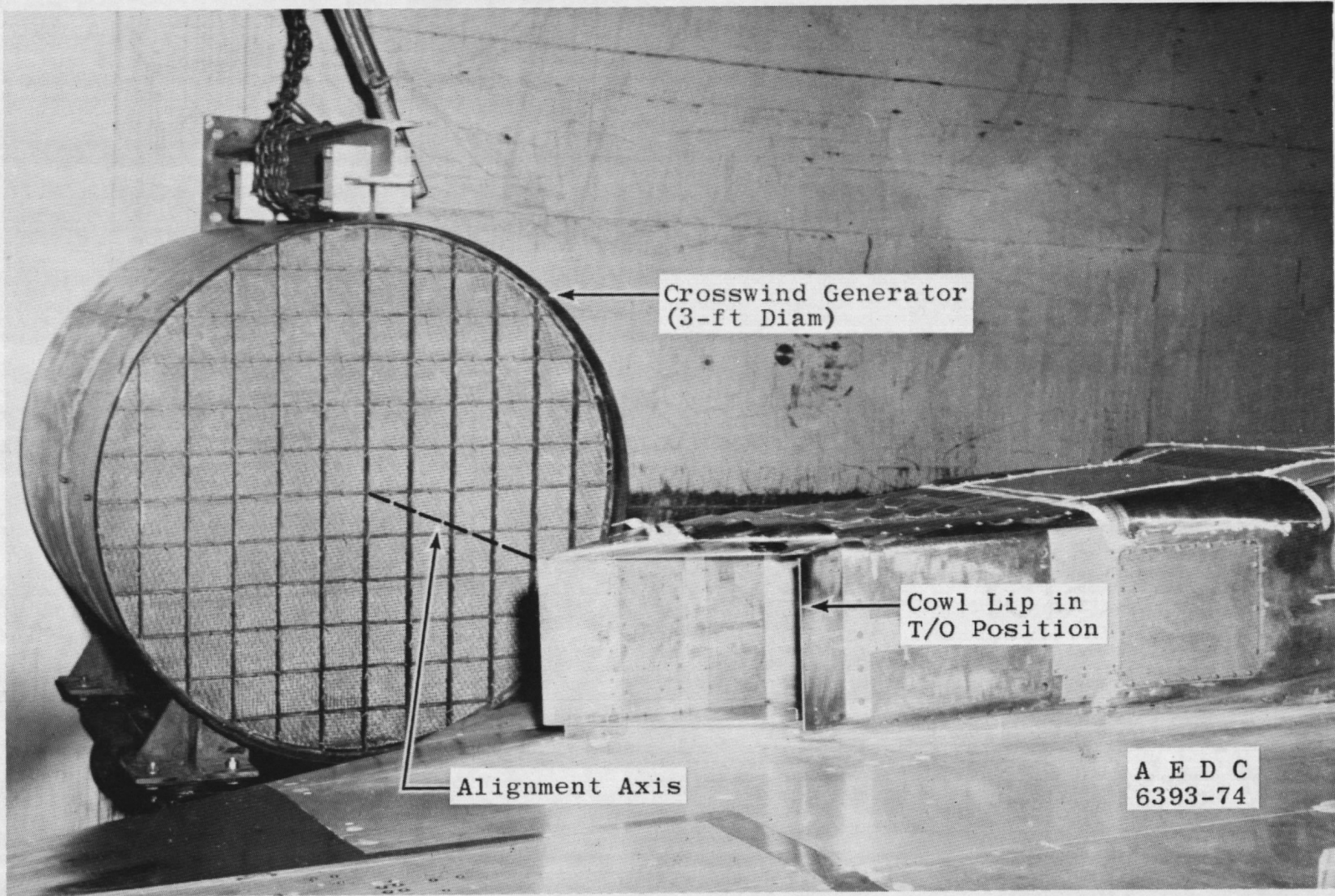
Figure 8. Crosswind generator installation.

Figure 9. Bypass door schematic.

FS 94.42

FS 94.58

Forward Weapons Bay Doors

A E D C
10725-74
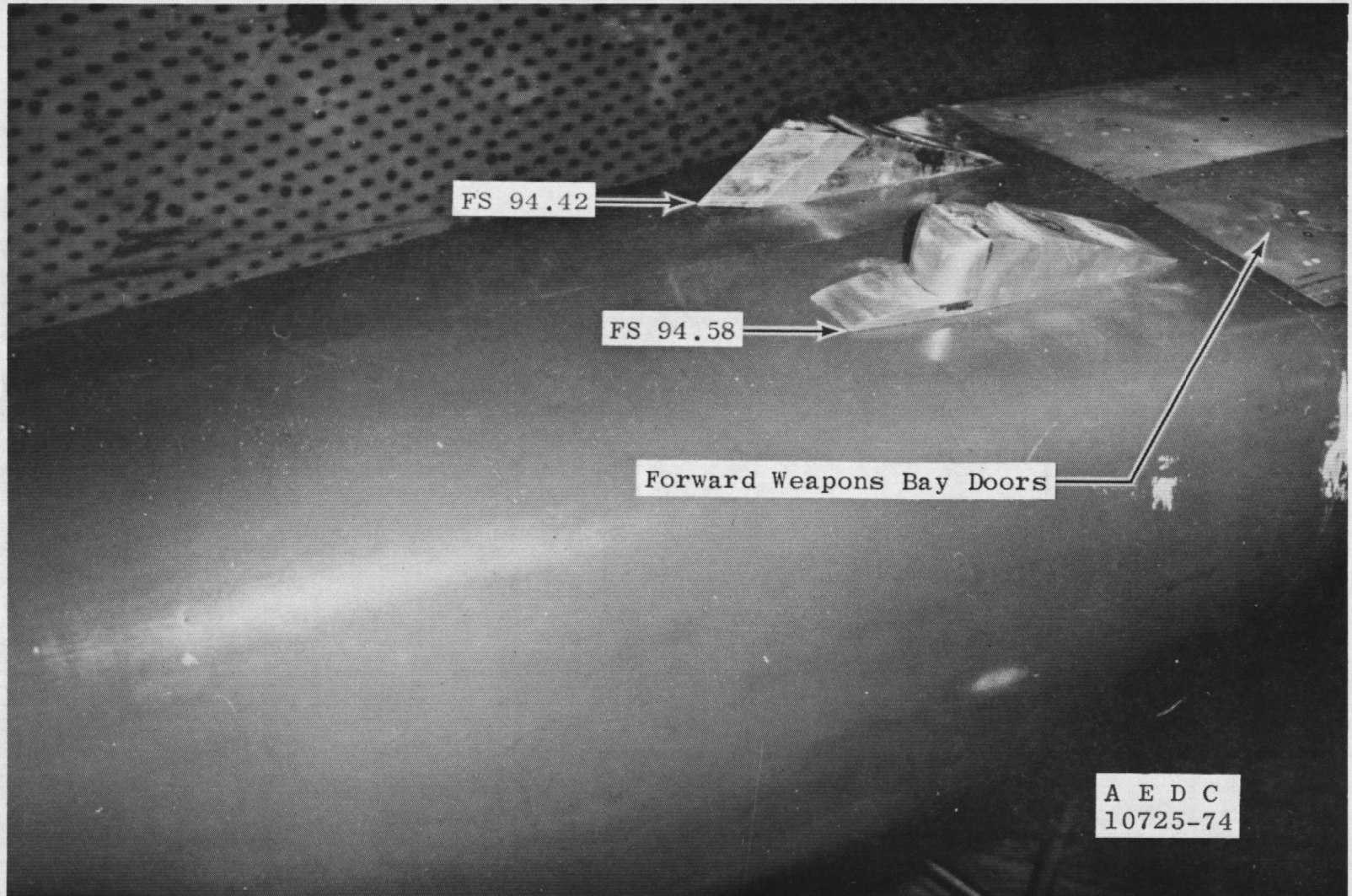
Figure 10. EVS pod installation.
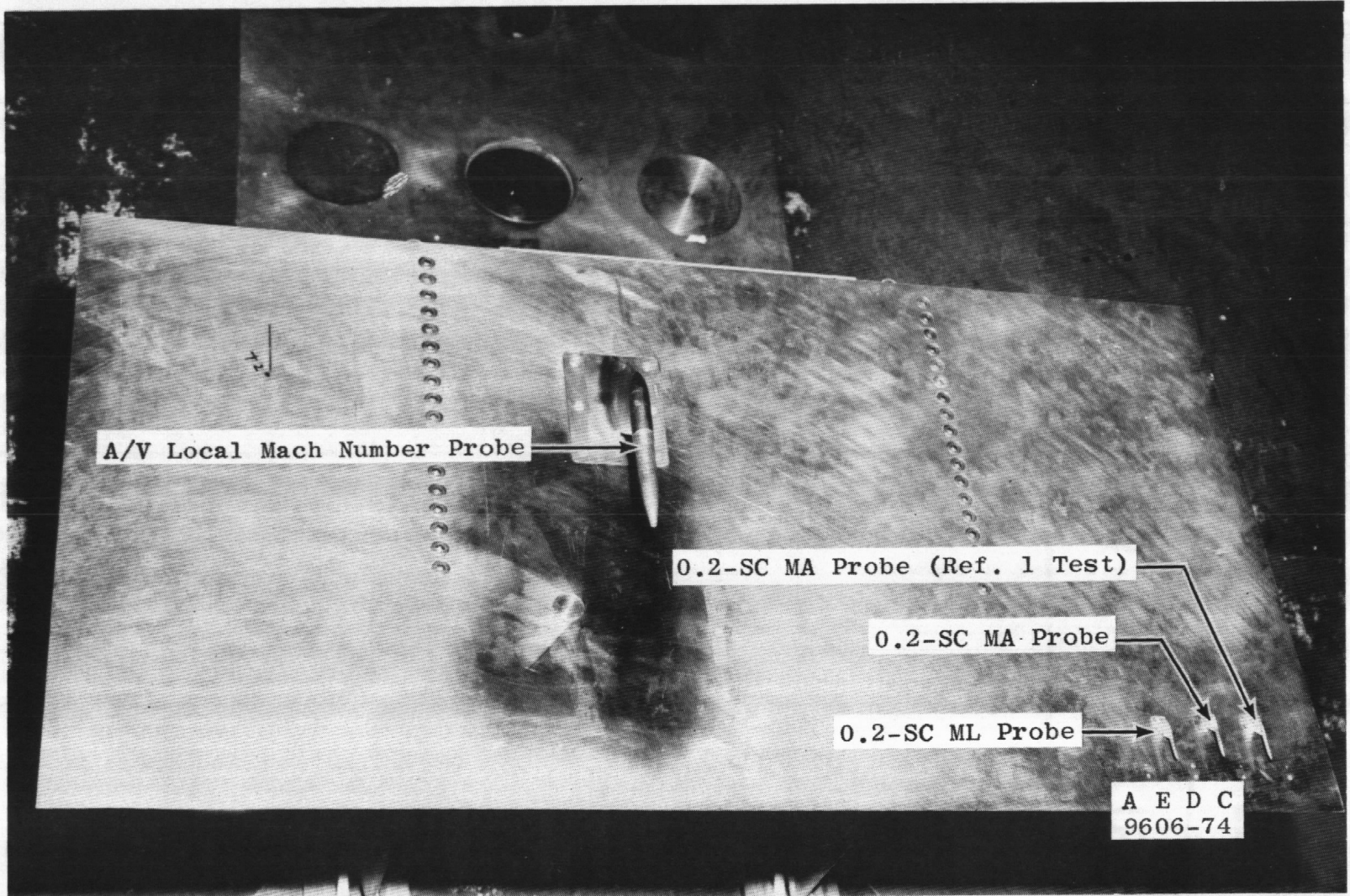
Figure 11. MA/ML probe calibration plate.
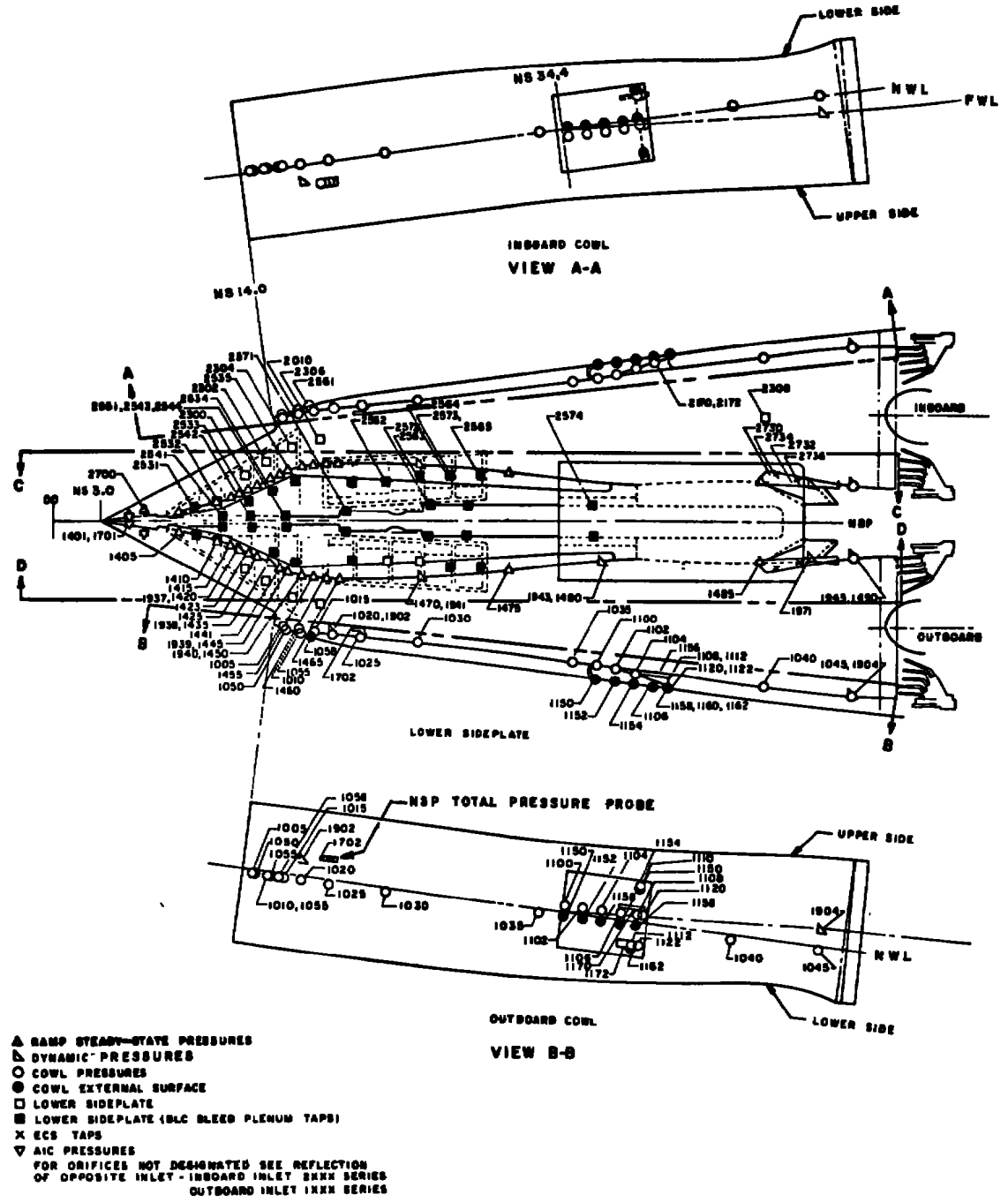
a. Inboard cowl, lower sideplate, outboard cowl
Figure 12.   Instrumentation locations.
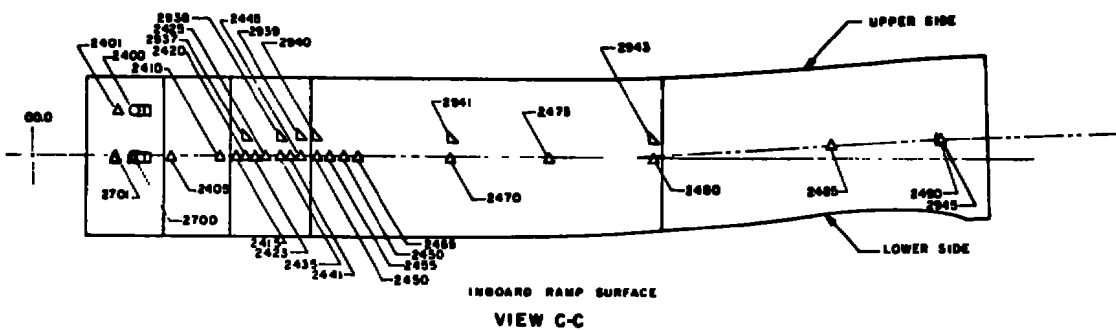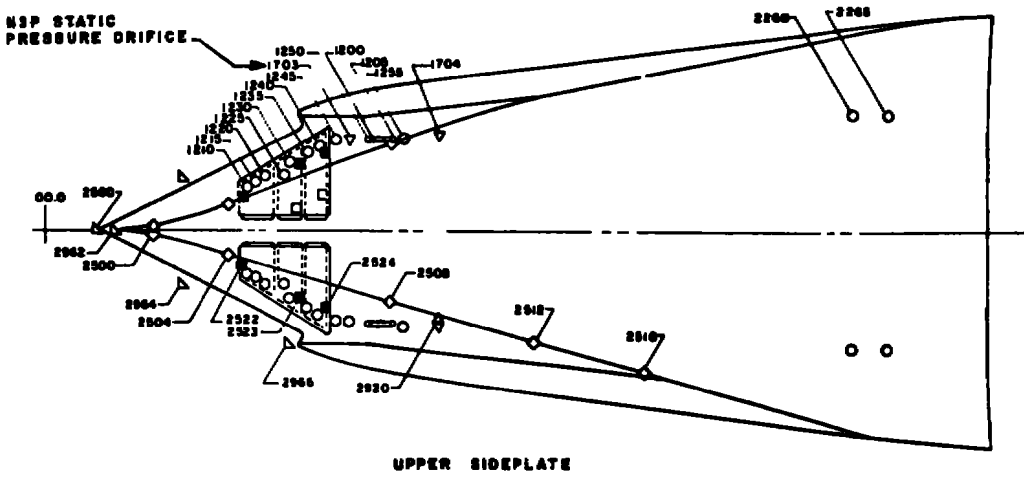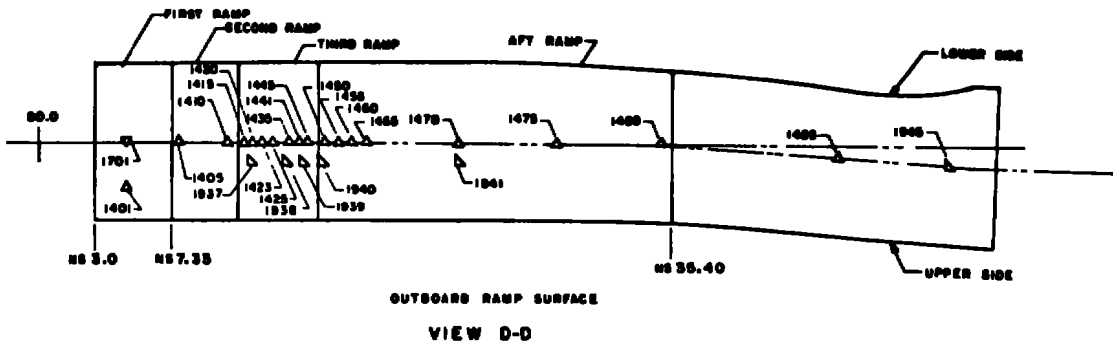
b. Outboard ramp, inboard ramp, upper sideplate
Figure 12. Continued.

c. Schematic of boundary-layer control system instrumentation
Figure 12. Continued.
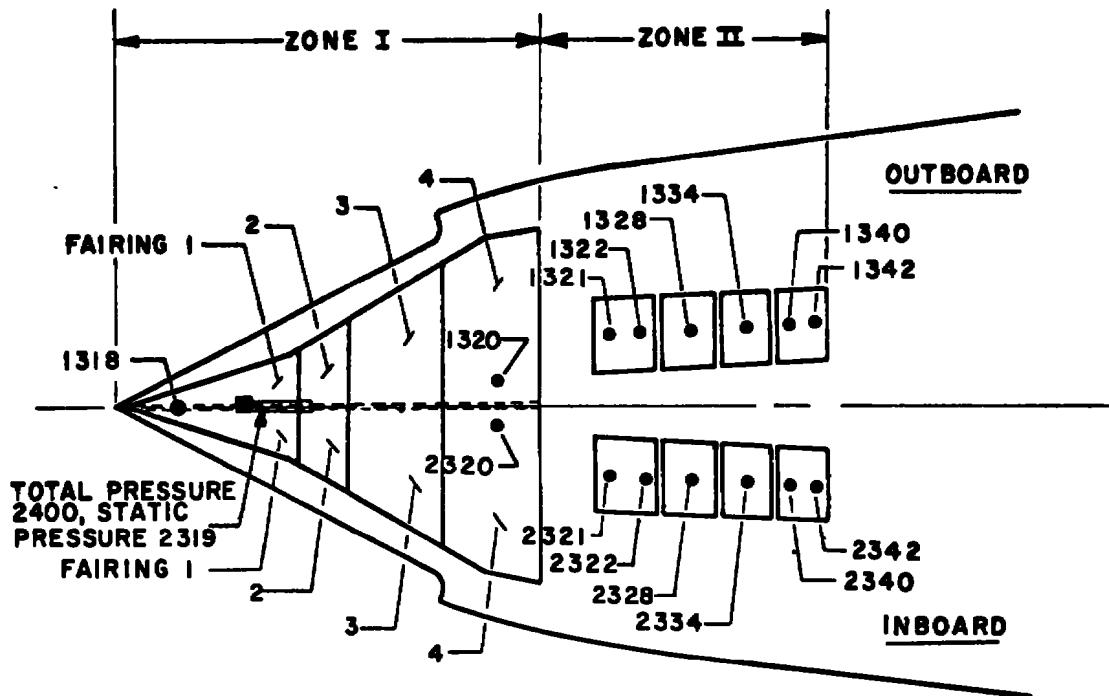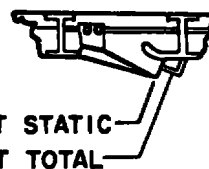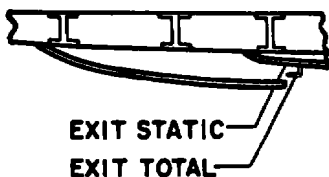
FAIRING	EXIT STATIC	EXIT TOTAL
1	X311	X310
2	X313	X312
3	X315	X314
4	X317	X316

X = 1, OUTBOARD
X = 2, INBOARD

DOOR	EXIT STATIC	EXIT TOTAL
1	X326	X324
2	X332	X330
3	X338	X336
4	X346	X344

43

r0 = 14490	
r1 = 19783	
r2 = 27486	
r3 = 33429	
r4 = 38477	
r5 = 42936	
r6 = 45000	
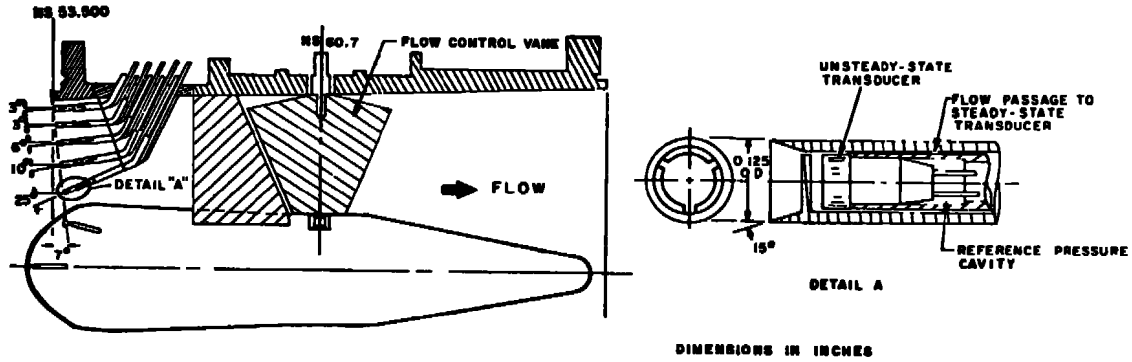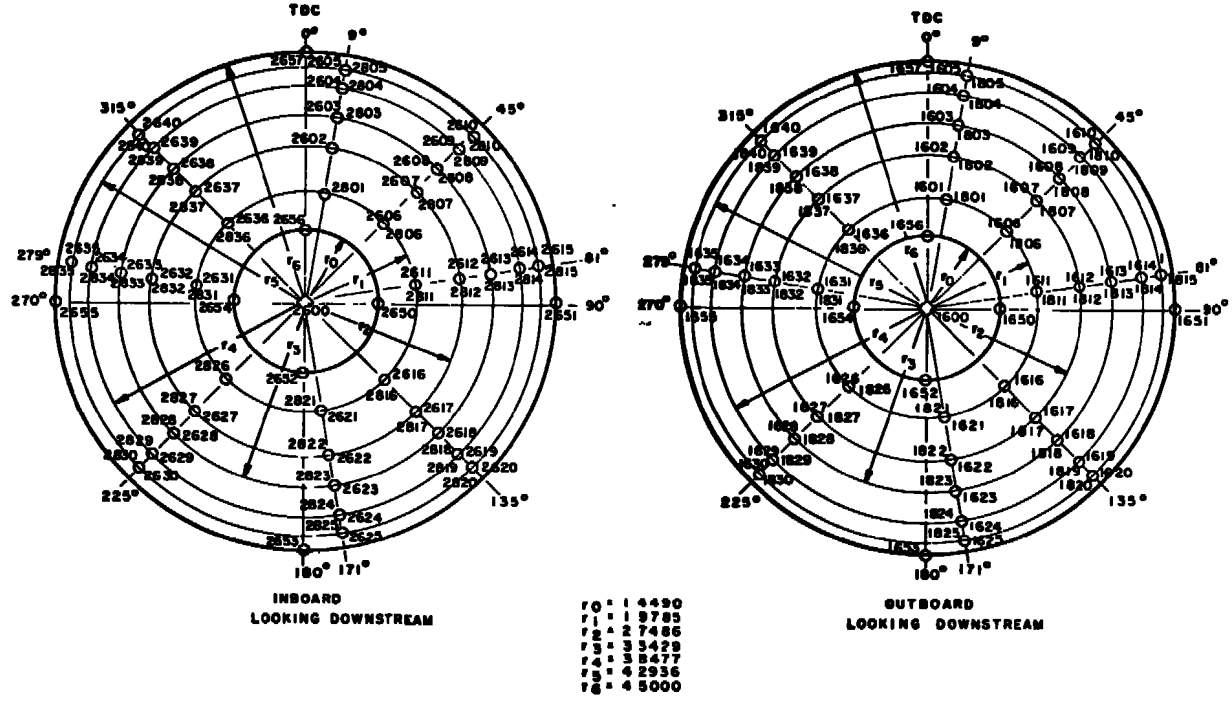
d. Pressure instrumentation at compressor face

Figure 12. Concluded.
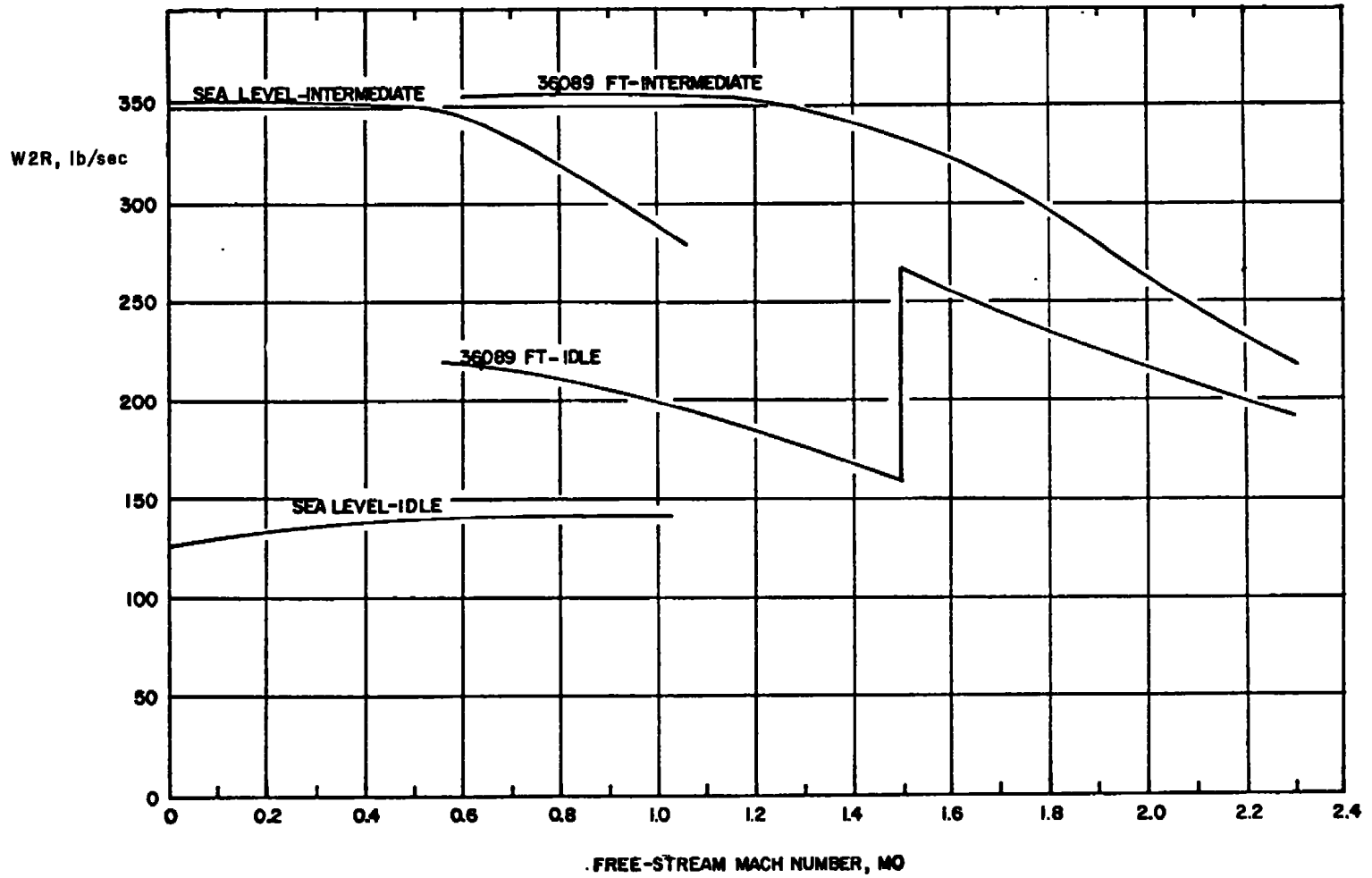
Figure 13. Variation of corrected engine airflow with free-stream Mach number.
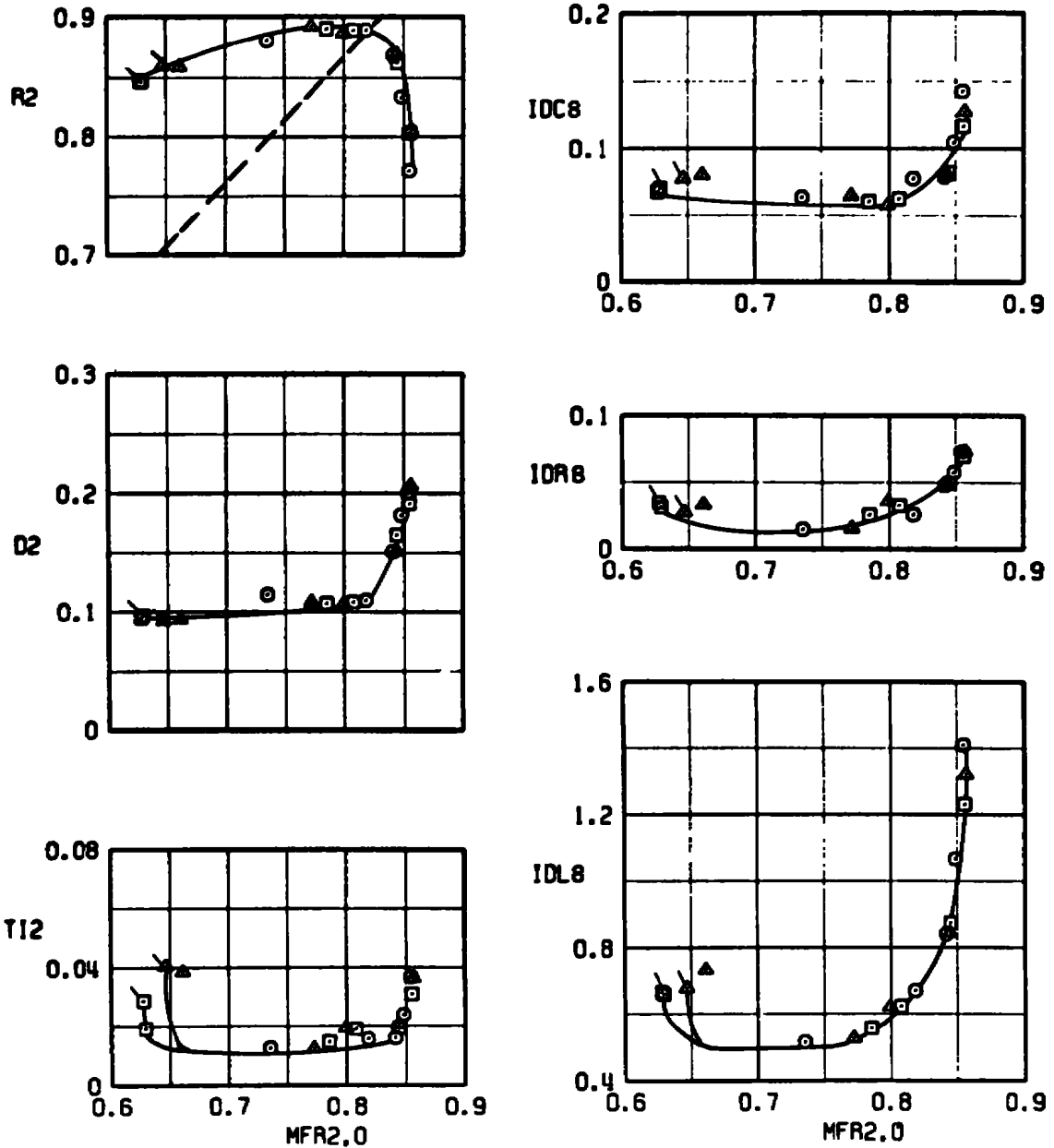
a. α = -2 deg, ψ = 0, outboard

Figure 14. Inlet performance effects of shortened inlet fourth ramp at M0 = 2.20.

a. Concluded, inboard
Figure 14. Continued.

AEDC-TR-75-57

SYMBOL	α	ψ	RB	ML	FOURTH RAMP	
⊙	2.5	0.0	14.0	3.36	PROTOTYPE	1021
▫	2.5	0.0	14.0	3.36	16-in. SHORTENED	1534
▲	2.5	0.0	14.0	3.36	32-in. SHORTENED	1583

FLAGGED SYM - STABILITY LIMIT
— — — INTERMEDIATE POWER AIRFLOW, 36K ft

b. a = 2.5 deg, ψ = 0, outboard
Figure 14. Continued.

SYMBOL	α	ψ	RB	HL	FOURTH RAMP	
⊙	2.5	0.0	14.0	3.36	PROTOTYPE	1021
⊡	2.5	0.0	14.0	3.36	16-in. SHORTENED	1534
△	2.5	0.0	14.0	3.36	32-in. SHORTENED	1583

FLAGGED SYM   STABILITY LIMIT
— — — INTERMEDIATE POWER AIRFLOW, 36K ft

b. Concluded, inboard
Figure 14. Continued.

SYMBOL	α	ψ	RB	ML	FOURTH RAMP	
⊙	9.0	-3.0	16.0	3.10	PROTOTYPE	1044
▢	9.0	-2.9	16.0	3.10	16-in. SHORTENED	1556
▲	9.0	-2.9	16.0	3.10	32-in. SHORTENED	1584

FLAGGED SYM - STABILITY LIMIT

— — —INTERMEDIATE POWER AIRFLOW, 36K ft

c. a = 9 deg, ψ = 5 deg, outboard

Figure 14. Continued.
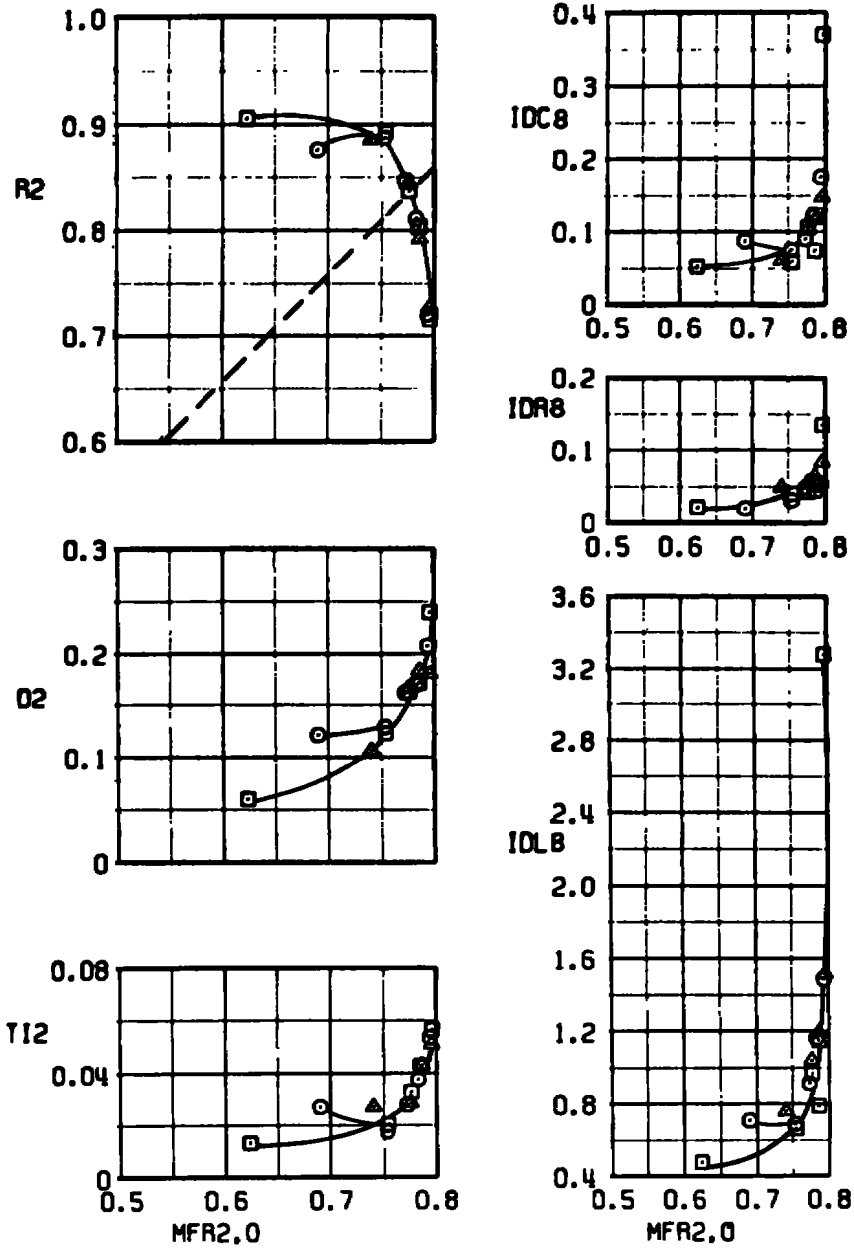
c. Continued, inboard
Figure 14. Continued.

SYMBOL	α	ψ	RB	HL	FOURTH RAMP	
⊙	9.0	-3.0	13.2	3.81	PROTOTYPE	1044
▣	9.0	-2.9	13.2	3.81	16-in. SHORTENED	1556
△	9.0	-2.9	13.2	3.81	32-in. SHORTENED	1584

FLAGGED SYM - STABILITY LIMIT

— — — INTERMEDIATE POWER AIRFLOW, 36K ft
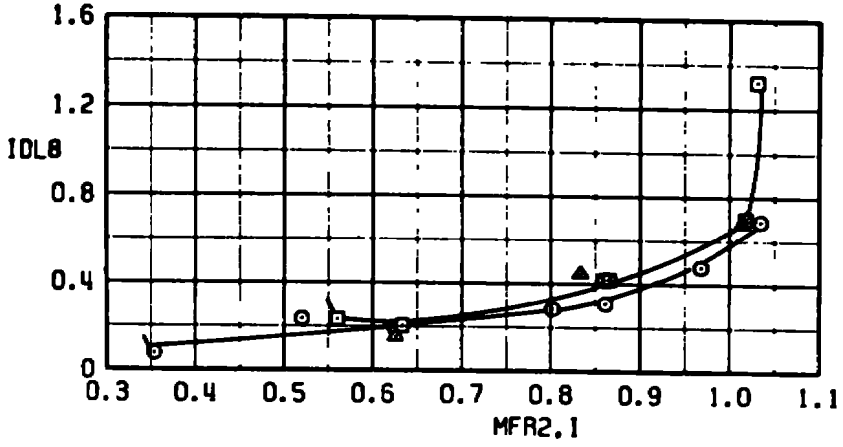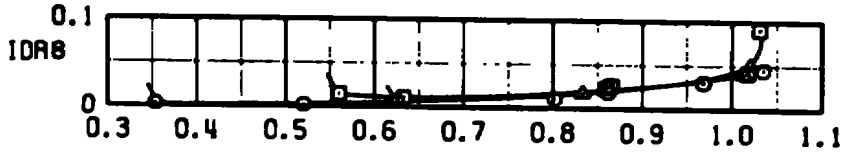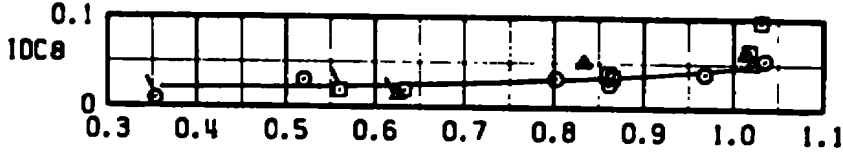
c. Concluded, inboard
Figure 14. Concluded.

52

PROTOTYPE FOURTH RAMP

WING

INBOARD
R2 = 0.833
D2 = 0.176
W2R = 226 lb/sec
RB = 16.7 deg
HL = 3.10 in.

OUTBOARD
R2 = 0.889
D2 = 0.110
W2R = 232 lb/sec
RB = 14.0 deg
HL = 3.37 in.

32-in. SHORTENED FOURTH RAMP

WING

P_{t2} / P_{t0}
DEVIATION FROM R2

INBOARD
R2 = 0.827
D2 = 0.189
W2R = 230 lb/sec
RB = 16.7 deg.
HL = 3.14 in.

OUTBOARD
R2 = 0.886
D2 = 0.106
W2R = 225 lb/sec
RB = 14.0 deg.
HL = 3 38 in.
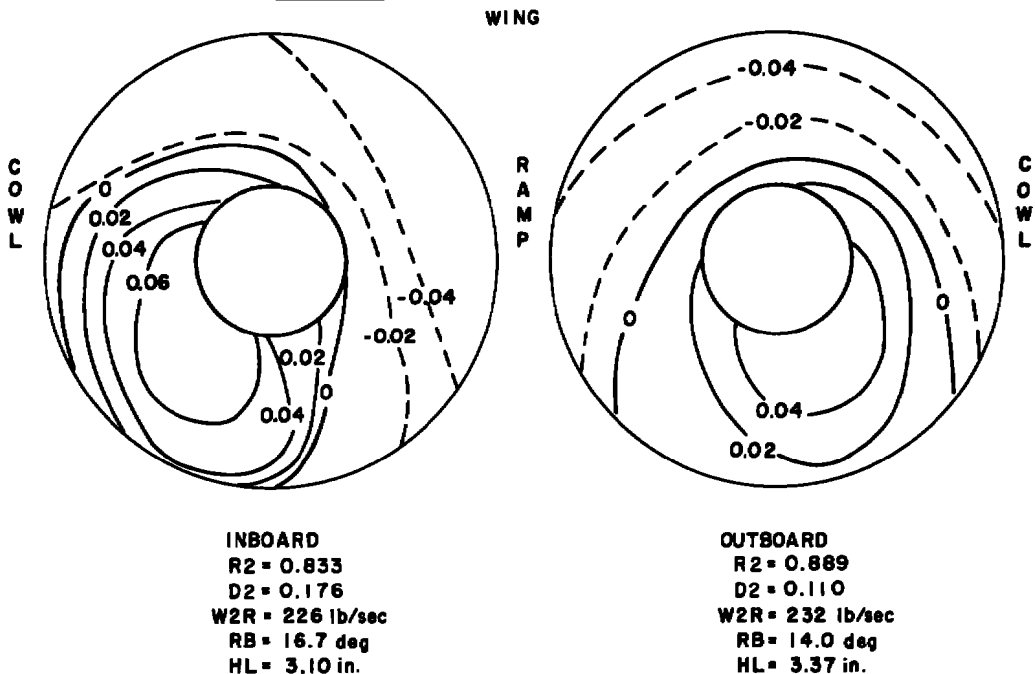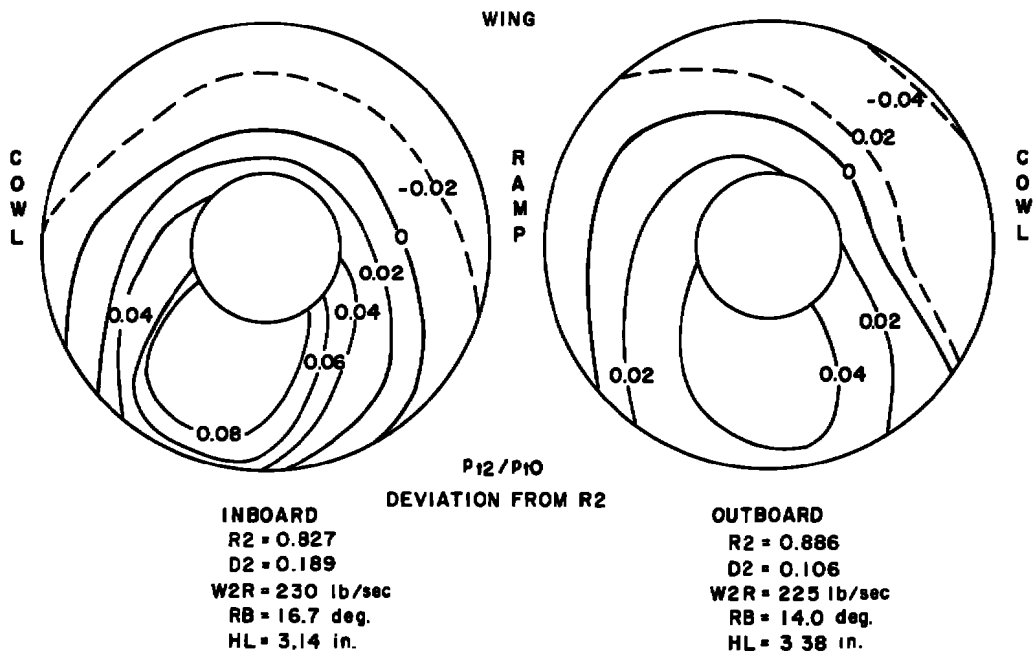
a. $a = 2$ deg, $\psi = 0$

Figure 15. Effects of shortened inlet fourth ramp on engine-face
total pressure contours.

53

PROTOTYPE FOURTH RAMP

WING

INBOARD
R2 = 0.925
D2 = 0.084
W2R = 226 lb/sec
RB = 14.0 deg.
HL = 3.36 in.

OUTBOARD
R2 = 0 920
D2 = 0.100
W2R = 226 lb/sec
RB = 14.0 deg
HL = 3 36 In.

32-in. SHORTENED FOURTH RAMP

WING

P_{t2}/P_{t0}
DEVIATION FROM R2

INBOARD
R2 = 0.909
D2 = 0.100
W2R = 231 lb/sec
RB = 14.0 deg.
HL = 3.36 in.

OUTBOARD
R2 = 0.906
D2 = 0.106
W2R = 230 lb/sec
RB = 14.0 deg.
HL = 3.36 In.
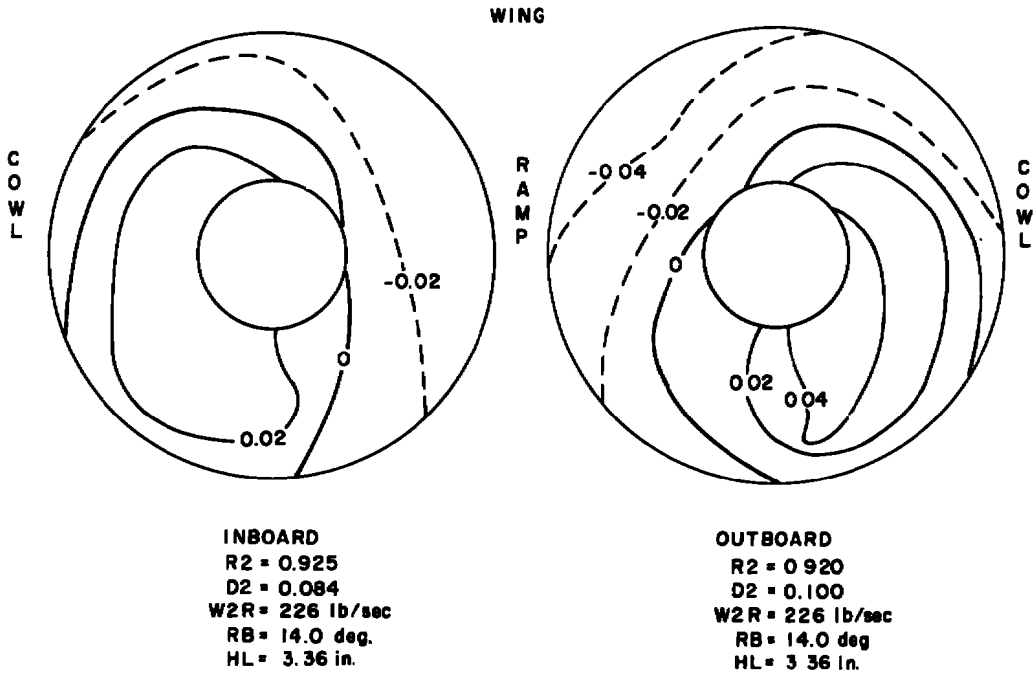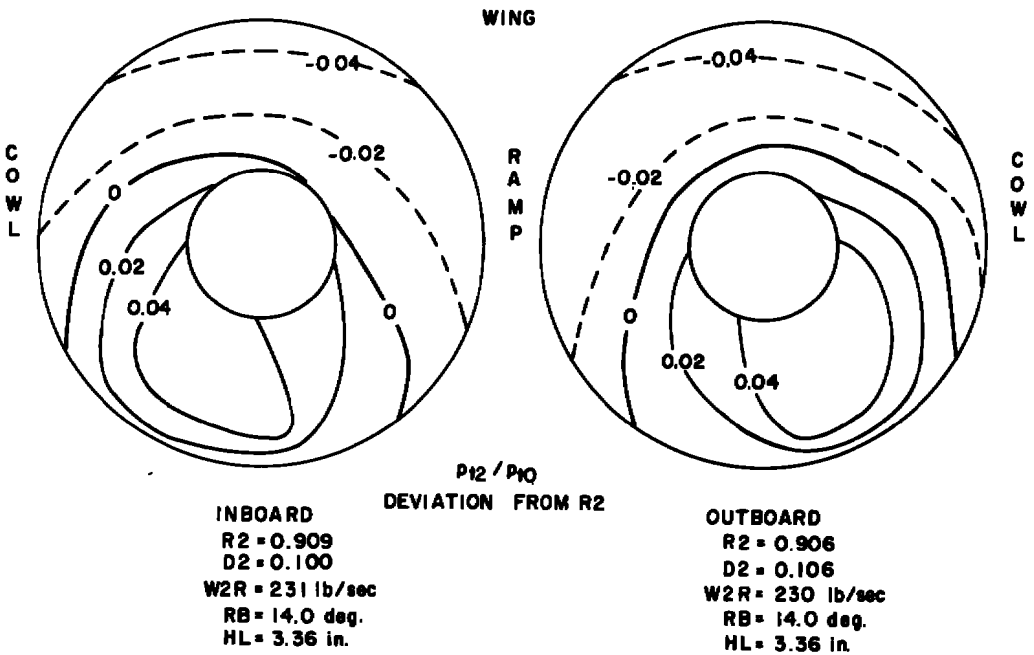
b. $a = 2.5$ deg, $\psi = 0$
Figure 15. Continued.

54

PROTOTYPE FOURTH RAMP

INBOARD
R2 = 0.930
D2 = 0.062
W2R = 233 lb/sec
RB = 13.2 deg.
HL = 3.81 in.

OUTBOARD
R2 = 0.847
D2 = 0.163
W2R = 230 lb/sec
RB = 16.0 deg.
HL = 3.10 in.

32-In. SHORTENED FOURTH RAMP

P_{t2} / P_{t0}
DEVIATION FROM R2

INBOARD
R2 = 0.924
D2 = 0.060
W2R = 225 lb/sec
RB = 13.2 deg
HL = 3.81 in.

OUTBOARD
R2 = 0.844
D2 = 0.167
W2R = 230 lb/sec
RB = 16.0 deg.
HL = 3.10 in.
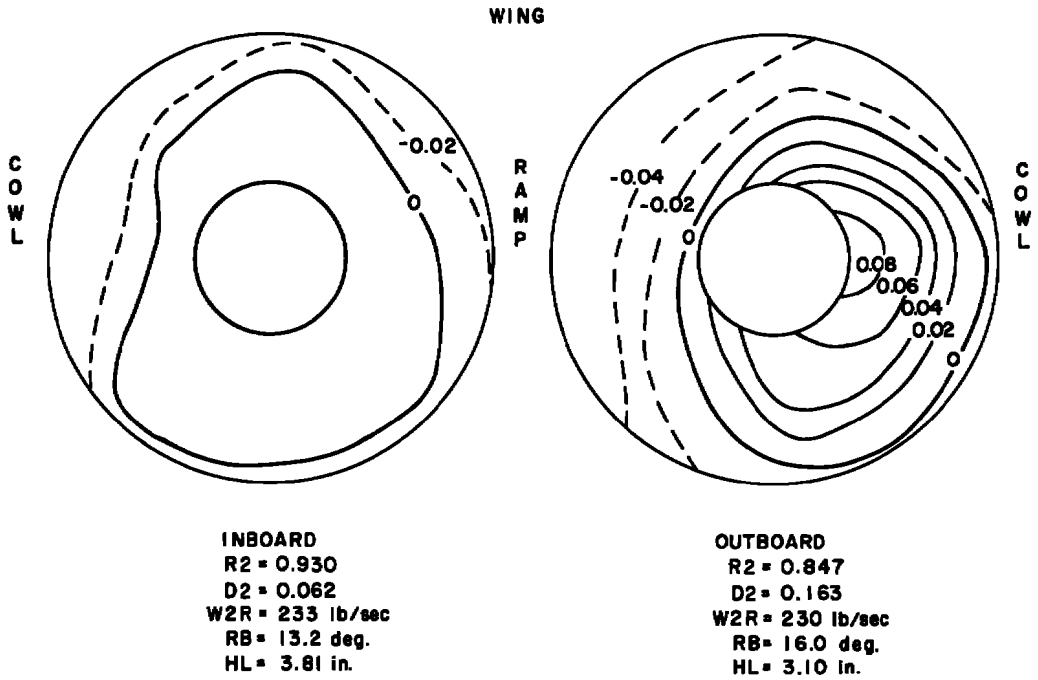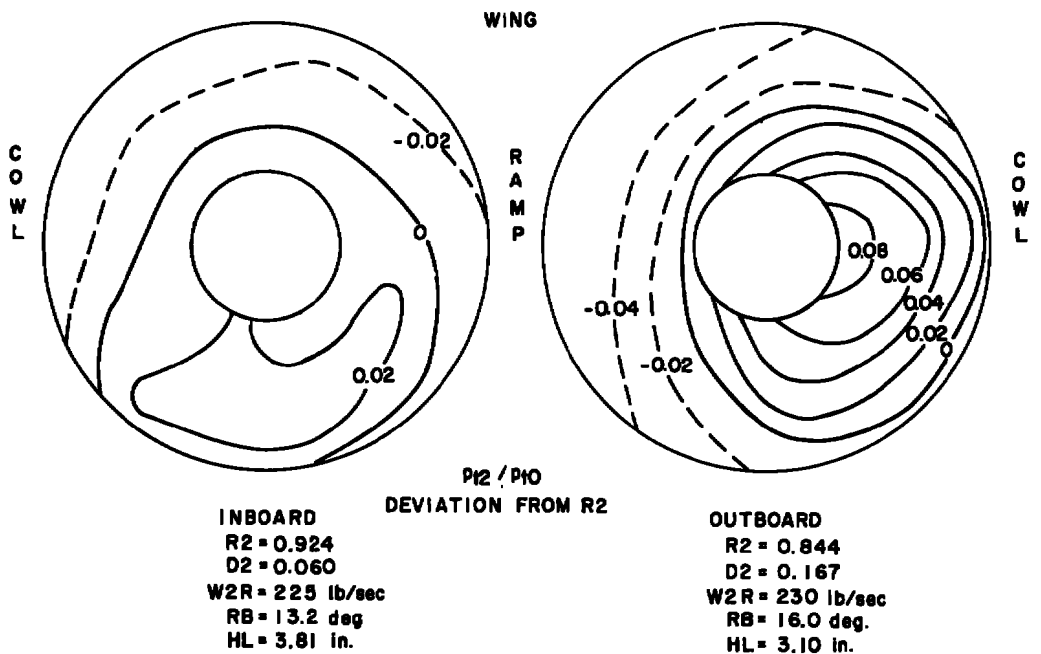
c. a = 9 deg, ψ = -3 deg
Figure 15. Concluded.

SYMBOL	α	ψ	RB	HL	BLEED	
⊙	2.5	0.1	14.0	3.36	PROTYPE	1583
⊡	2.5	0.0	14.0	3.36	NO SIDE PLATE	1672
▲	2.5	0.0	14.0	3.36	INCREASED RC	1712
◇	2.5	0.0	14.1	3.36	INCREASED RD	1693

FLAGGED SYM - STABILITY LIMIT

— — — INTERMEDIATE POWER AIRFLOW, 36K ft
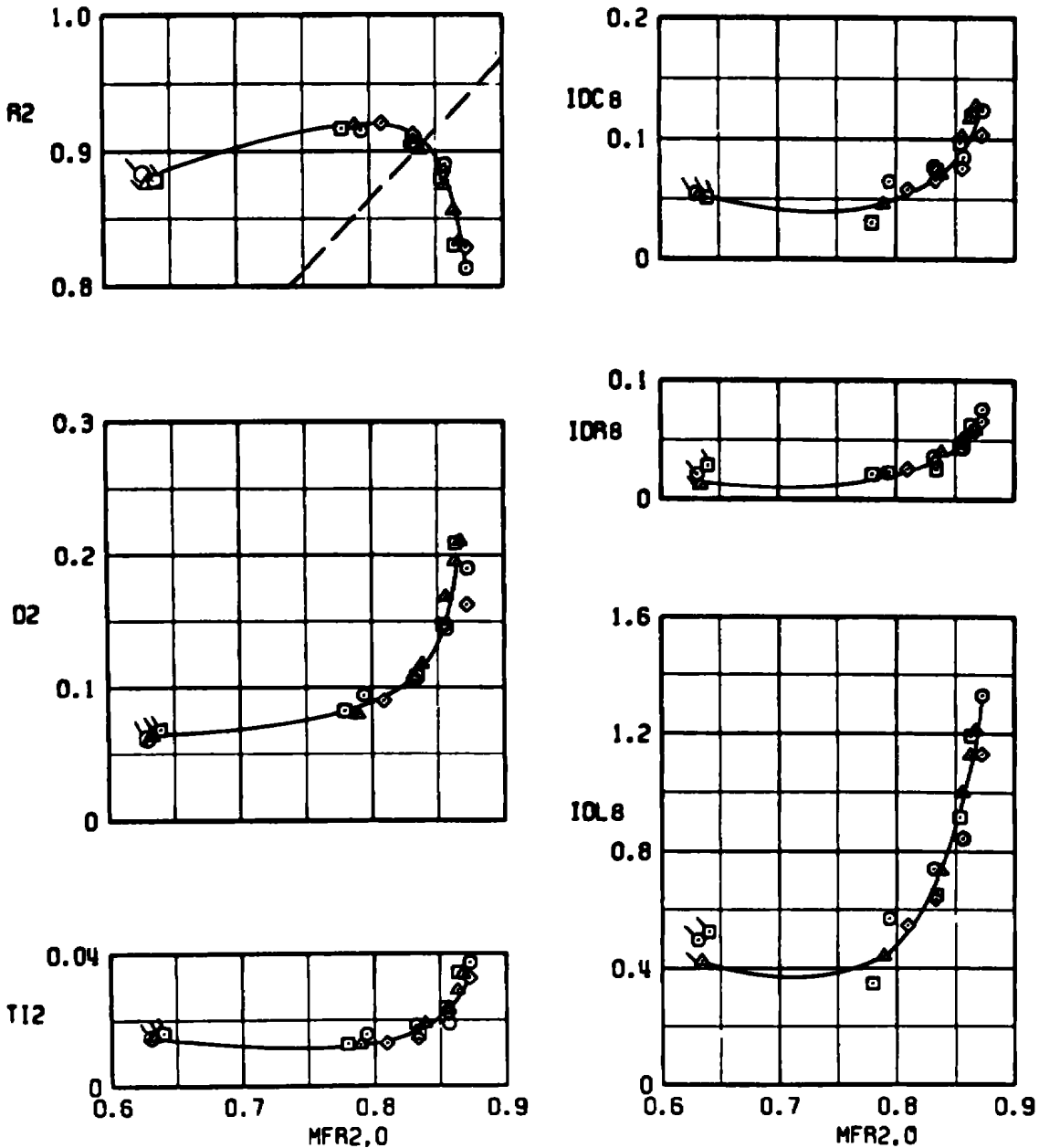
a. a = 2.5 deg, ψ = 0, outboard

Figure 16.   Effects of bleed porosity configurations on inlet at M0 = 2.20.
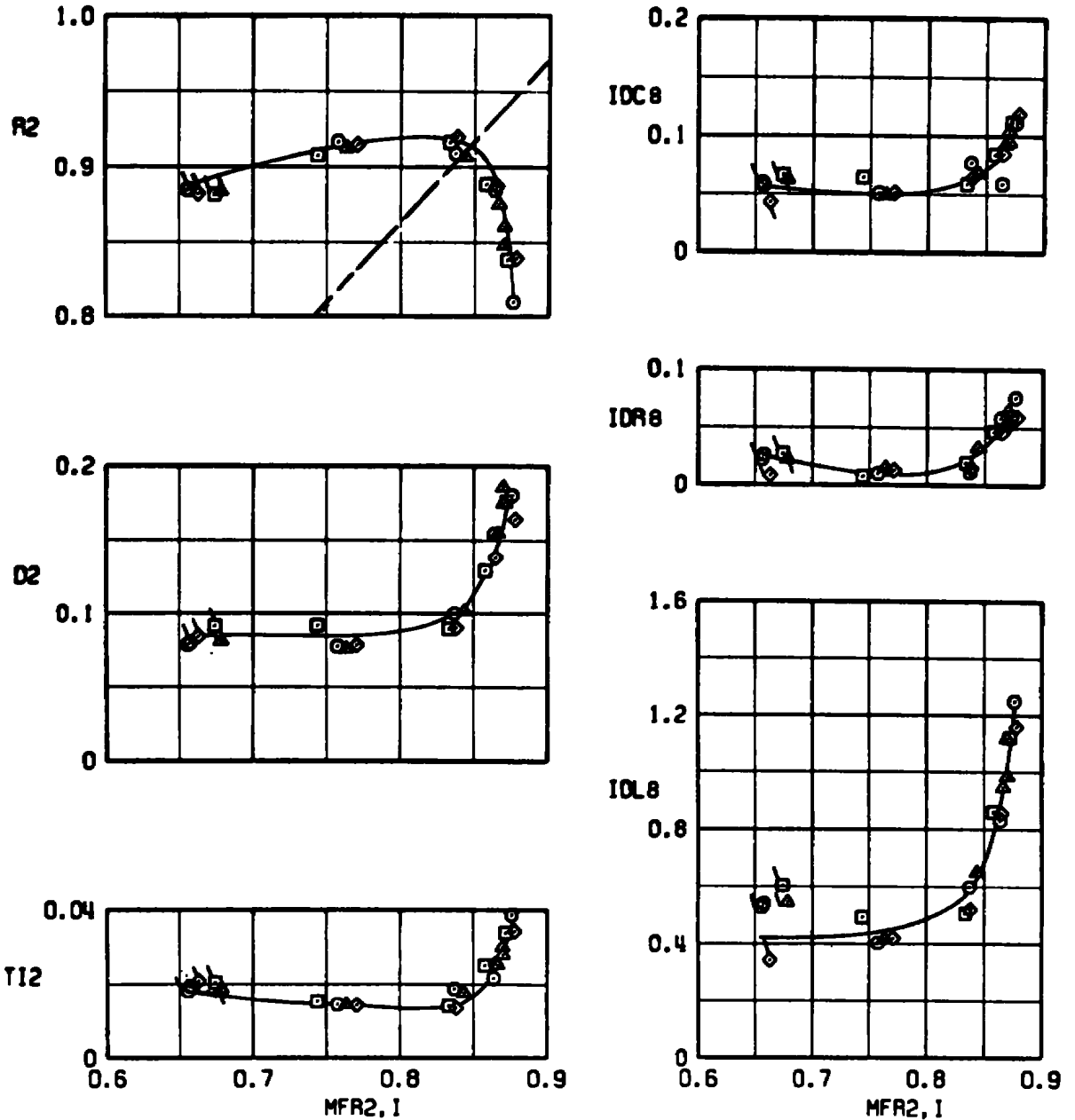
a. Concluded, inboard
Figure 16. Continued.

SYMBOL	α	ψ	RB	HL	BLEED	
⊙	0.0	3.0	15.2	3.13	PROTOTYPE	1585
▣	0.0	2.9	15.2	3.13	NO SIDE PLATE	1673
▲	0.0	2.9	15.2	3.13	INCREASED RC	1713
◈	0.0	2.9	15.2	3.13	INCREASED RD	1695

FLAGGED SYM - STABILITY LIMIT

— — — INTERMEDIATE POWER AIRFLOW, 36K ft
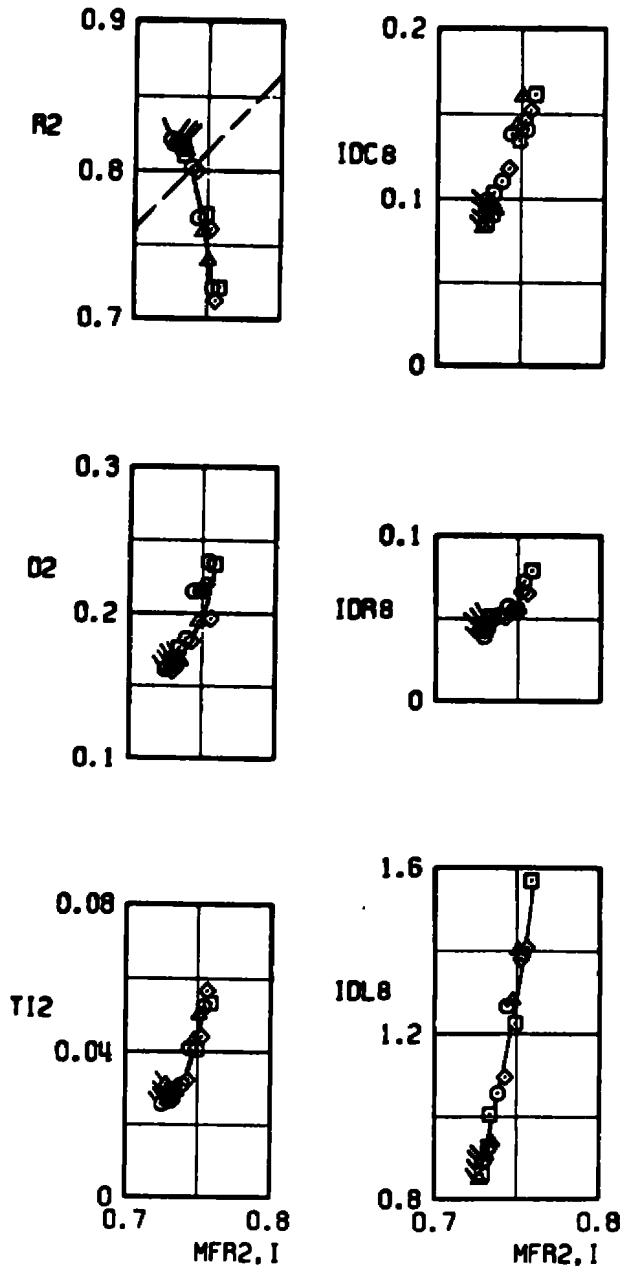
b. $a = 0$, $\psi = 3$ deg, inboard
Figure 16. Concluded.

SYMBOL	α	ψ	RB	HL	COWL	
⊙	2.5	0.0	14.0	3.36	PROTOTYPE	1751
▫	2.5	0.0	14.0	3.36	SHARP	1845
▲	2.5	0.0	14.0	3.36	BLUNT	1854

FLAGGED SYM-STABILITY LIMIT

— — —INTERMEDIATE POWER AIRFLOW,36K ft
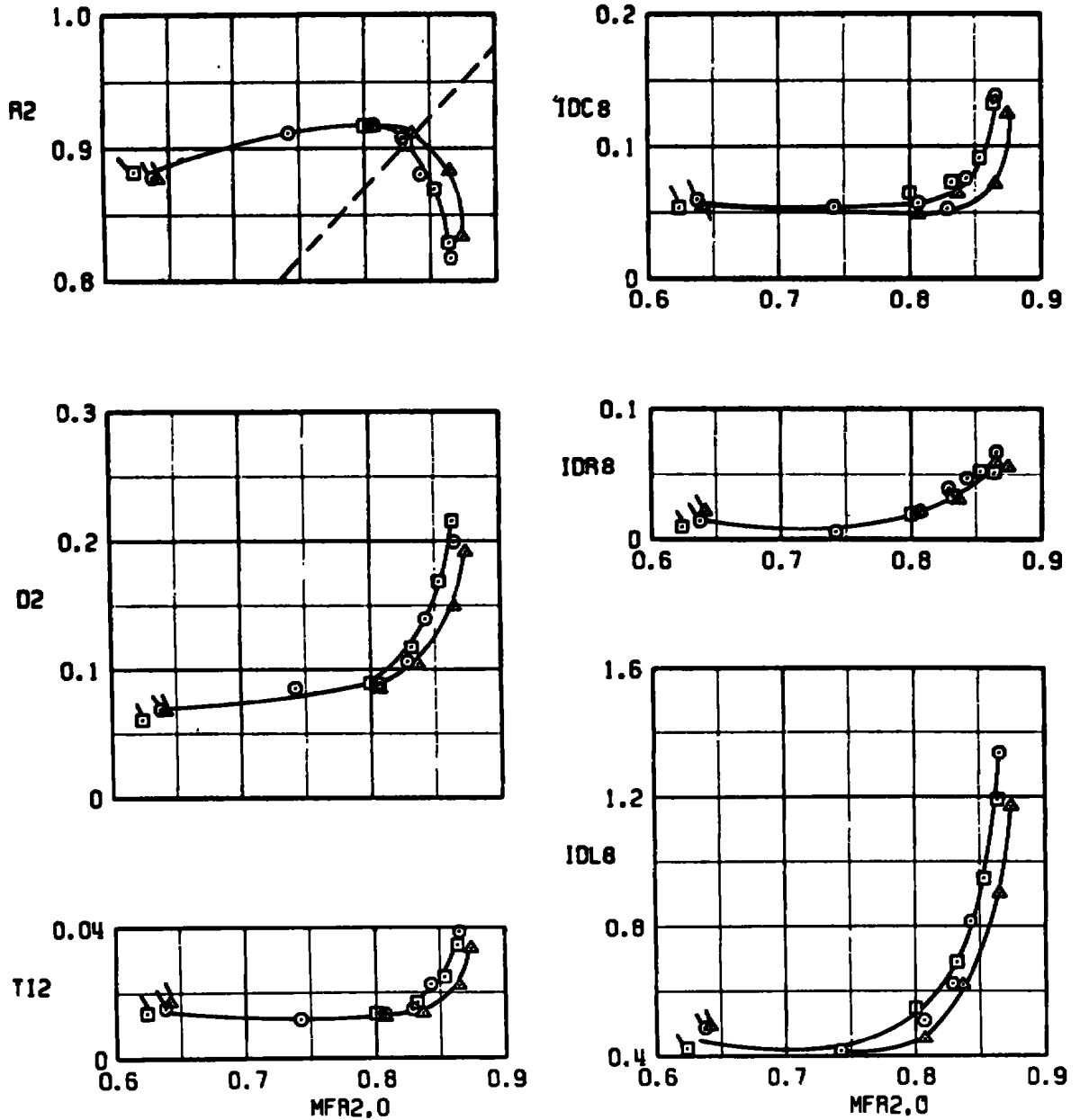
a. a = 2.5 deg, ψ = 0, outboard

Figure 17.   Effects of cowl lip contours on inlet performance at M0 = 2.20.
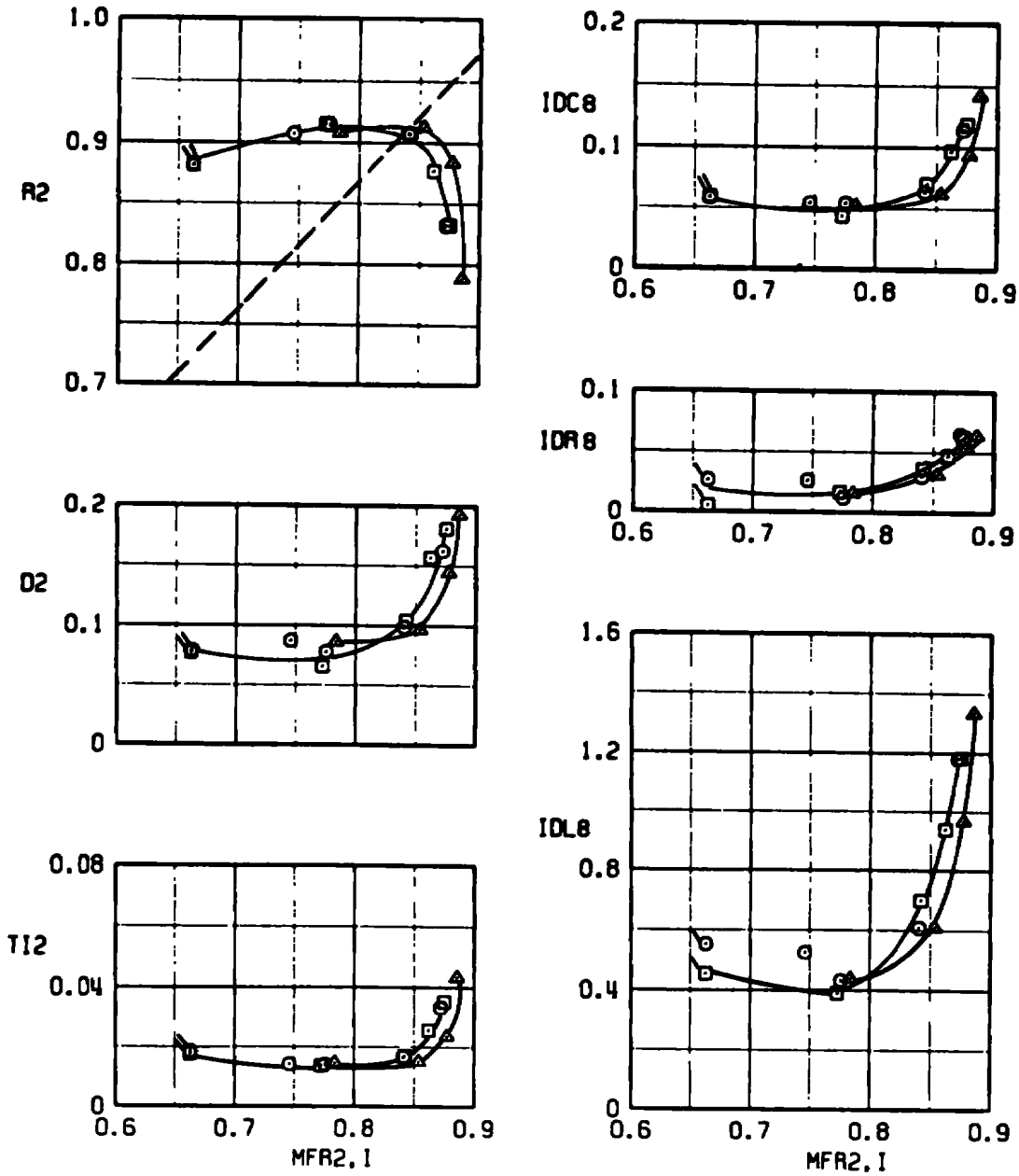
a. Concluded, inboard
Figure 17. Continued.
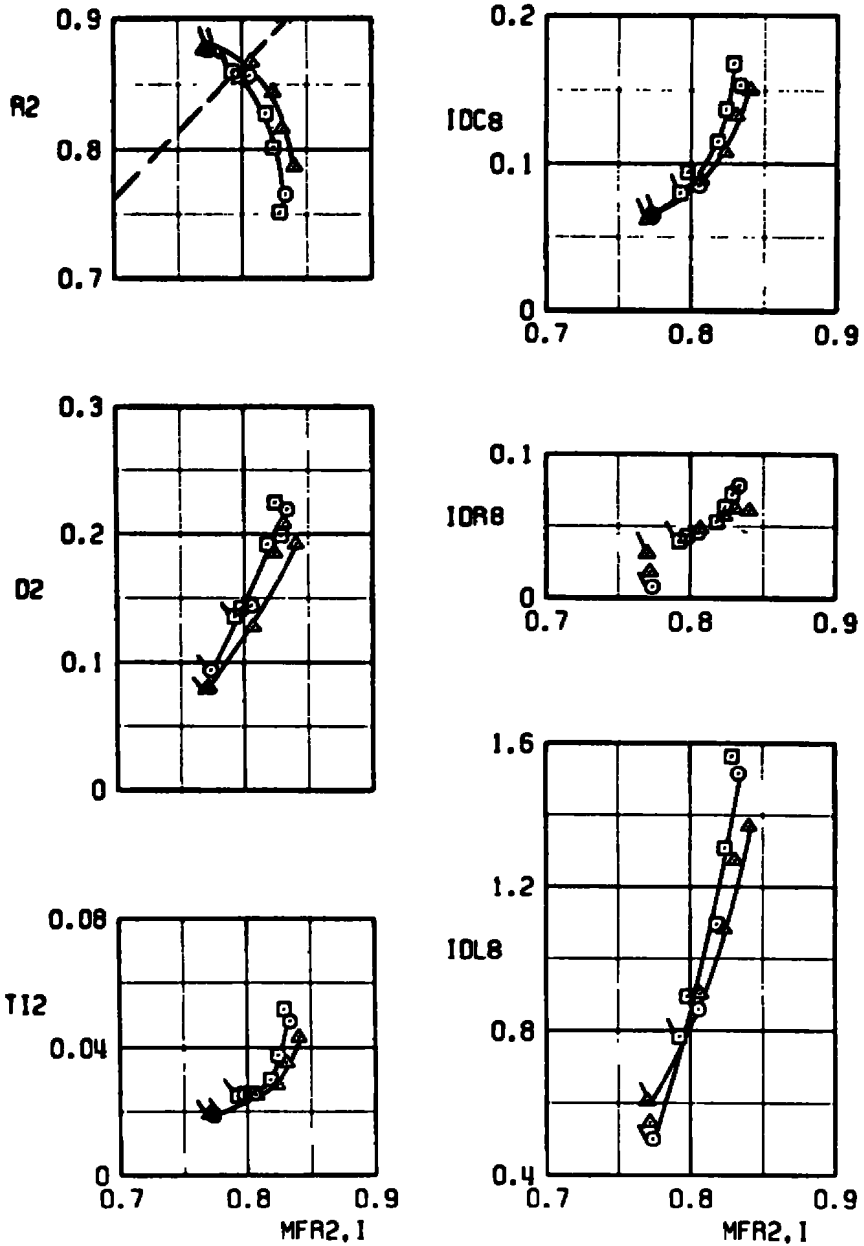
b. a = 2.5 deg, ψ = 3 deg, inboard
Figure 17. Concluded.

SYMBOL	α	ψ	RB	HL		ABLCII, in^2
⊙	2.5	0.0	14.0	3.36	3.34	1751
⊡	2.5	0.0	14.0	3.36	2.68	1757
▲	2.5	0.0	14.0	3.36	1.98	1765

FLAGGED SYM - STABILITY LIMIT

— — — INTERMEDIATE POWER AIRFLOW, 36K ft
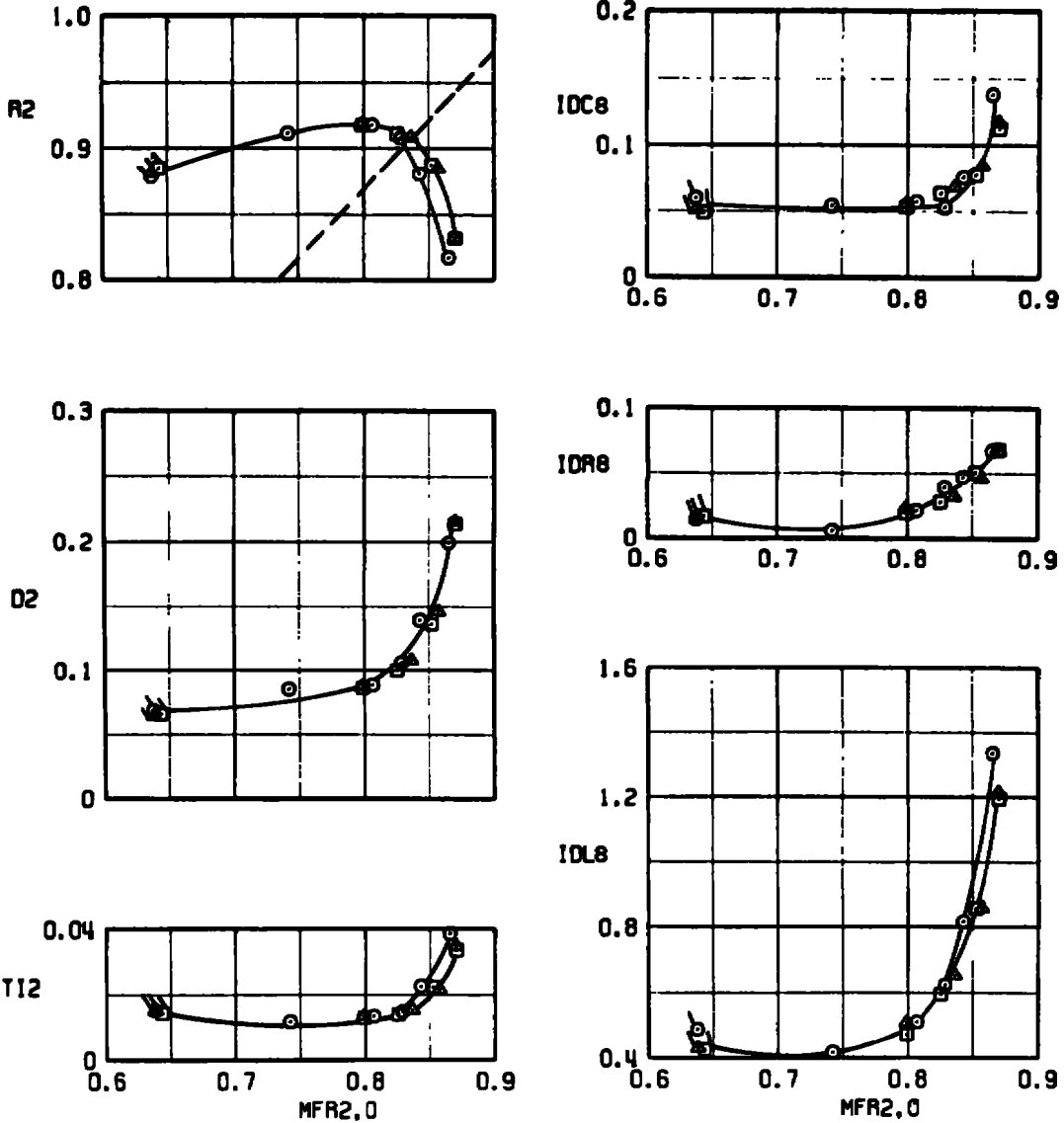
a. a = 2.5 deg, ψ = 0, outboard

Figure 18. Effects of reduced BLCI and II discharge areas on inlet performance at M0 = 2.20.
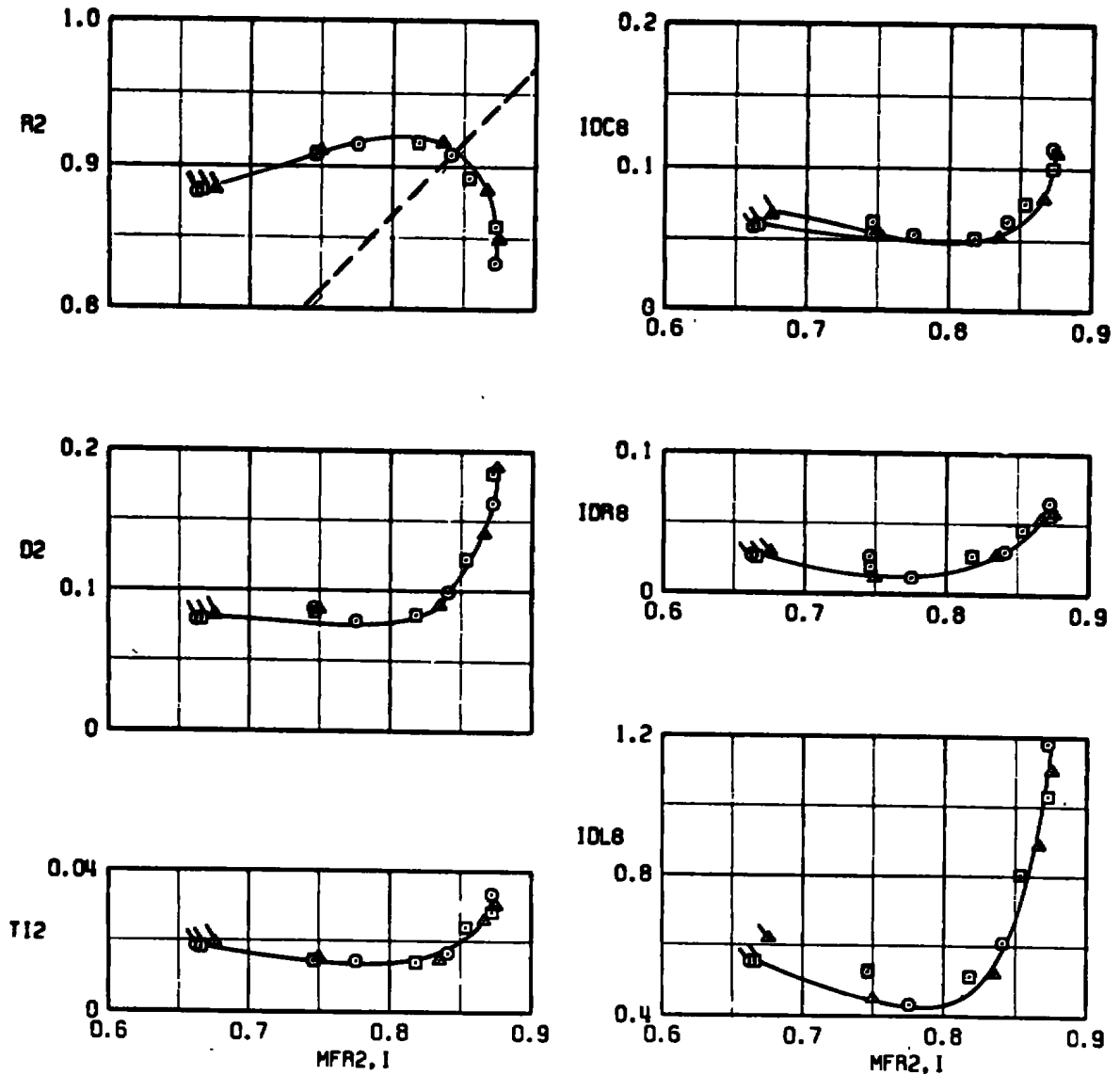
a. Concluded, inboard
Figure 18. Continued.

| SYMBOL	α	ψ	R8	HL	ABLCI, in^2	
⊙	2.5	0.0	14.0	3.36	1.82	1765
▣	2.5	0.0	14.0	3.36	1.11	1802
▲	2.5	0.0	14.0	3.36	0.79	1820

FLAGGED SYM - STABILITY LIMIT

— — — INTERMEDIATE POWER AIRFLOW, 36K ft
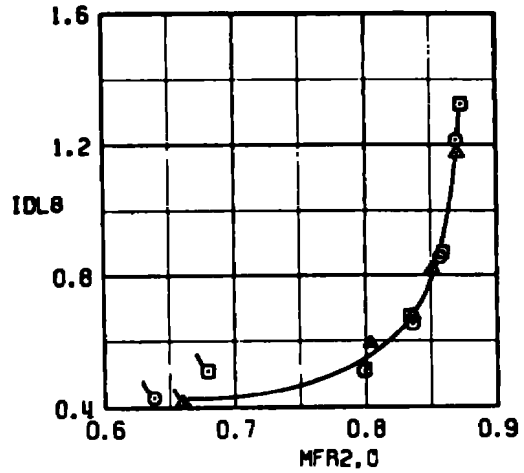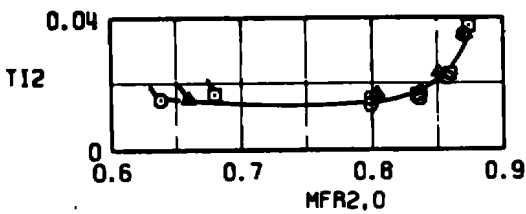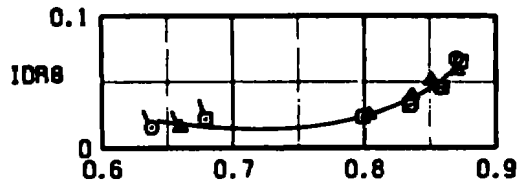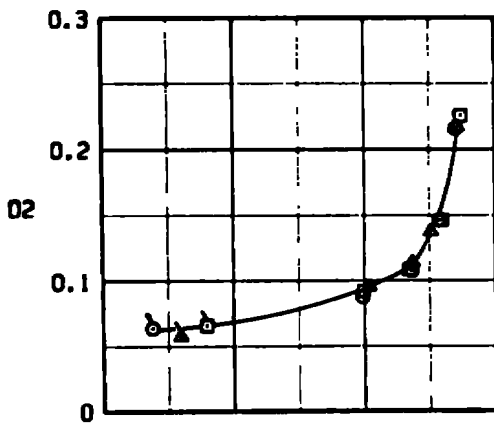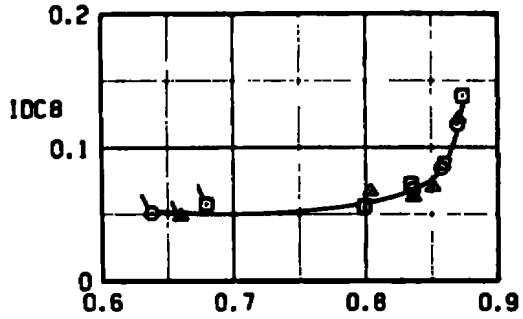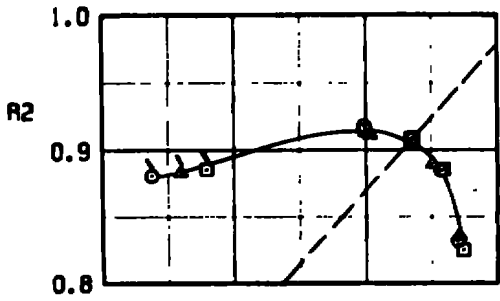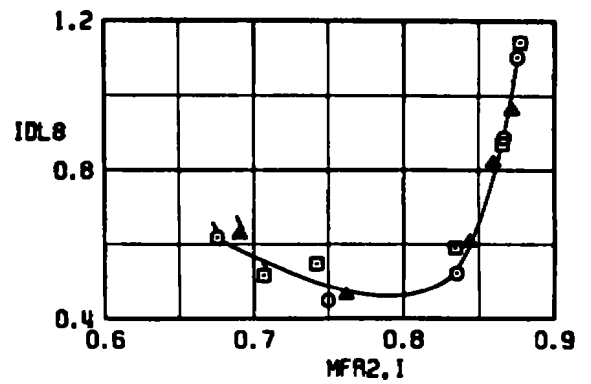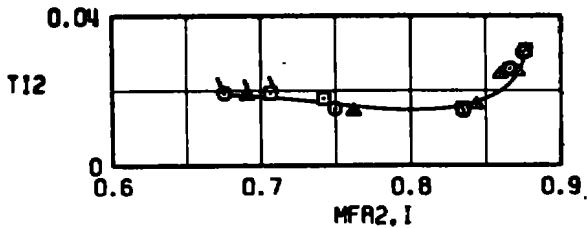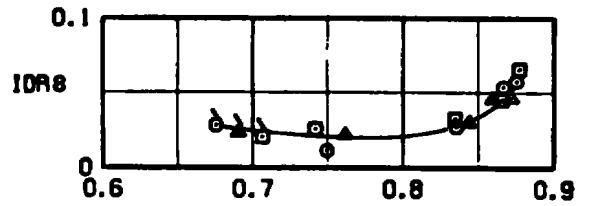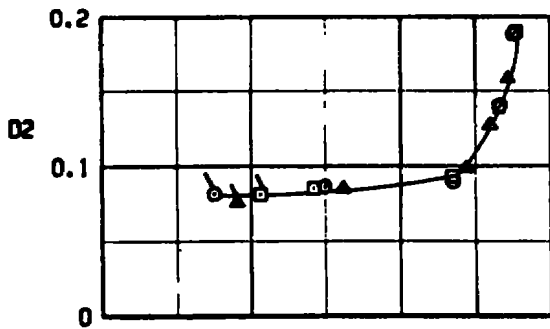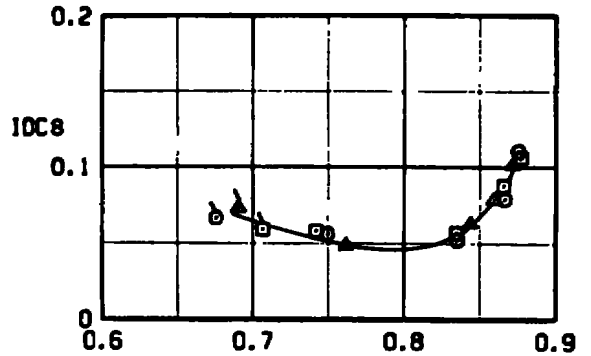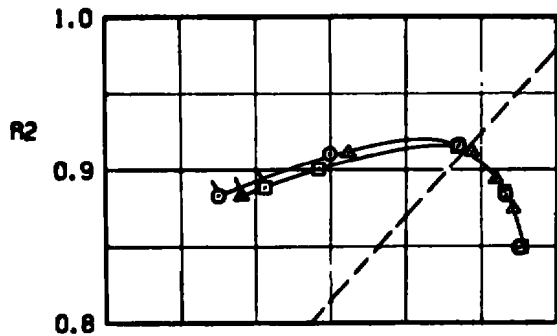
b. $\alpha = 2.5$ deg, $\psi = 0$, outboard
Figure 18. Continued.
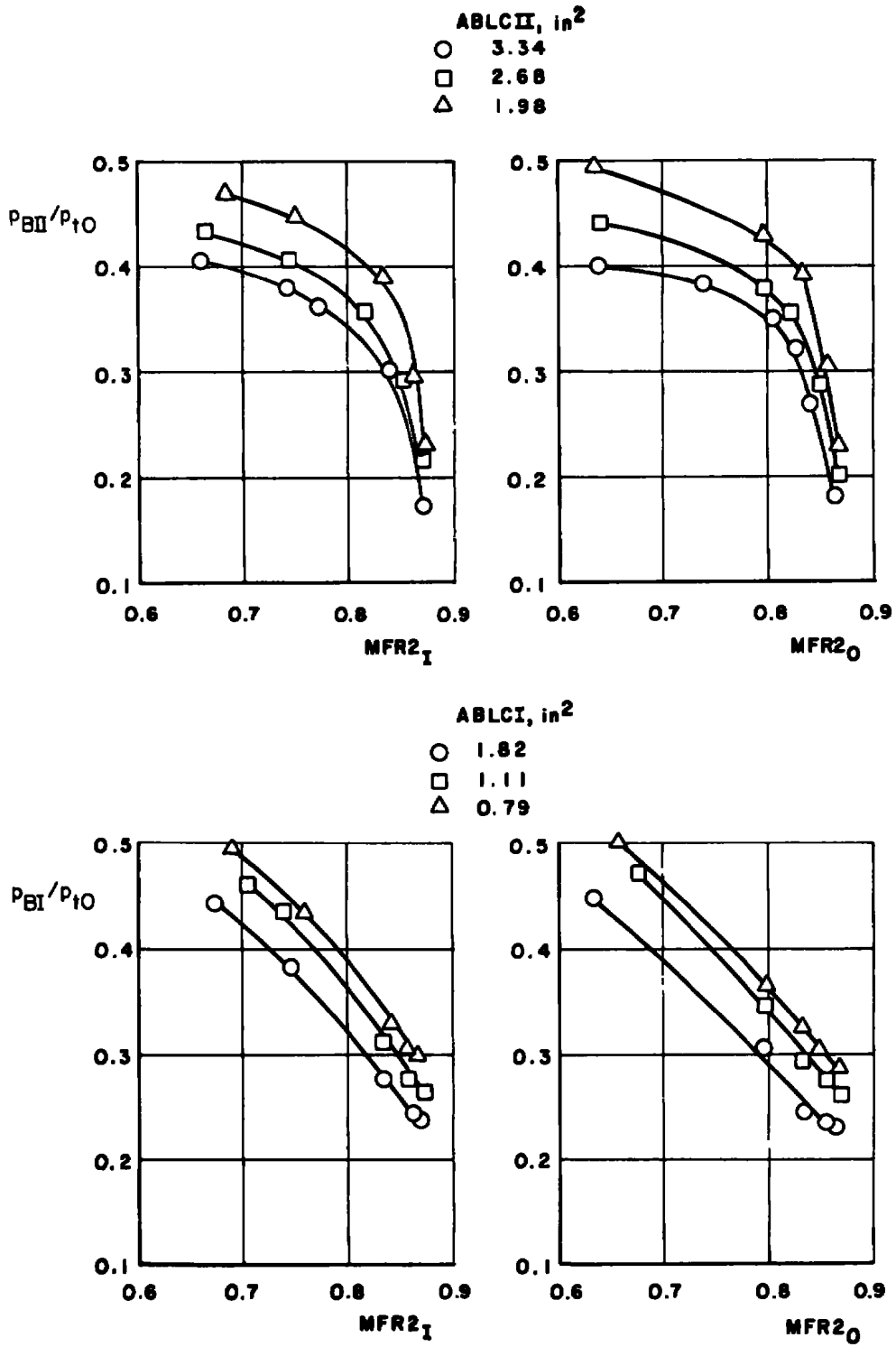
Figure 19. Effects of reduced BLCI and II discharge areas on the BLCI
and II plenum pressures.
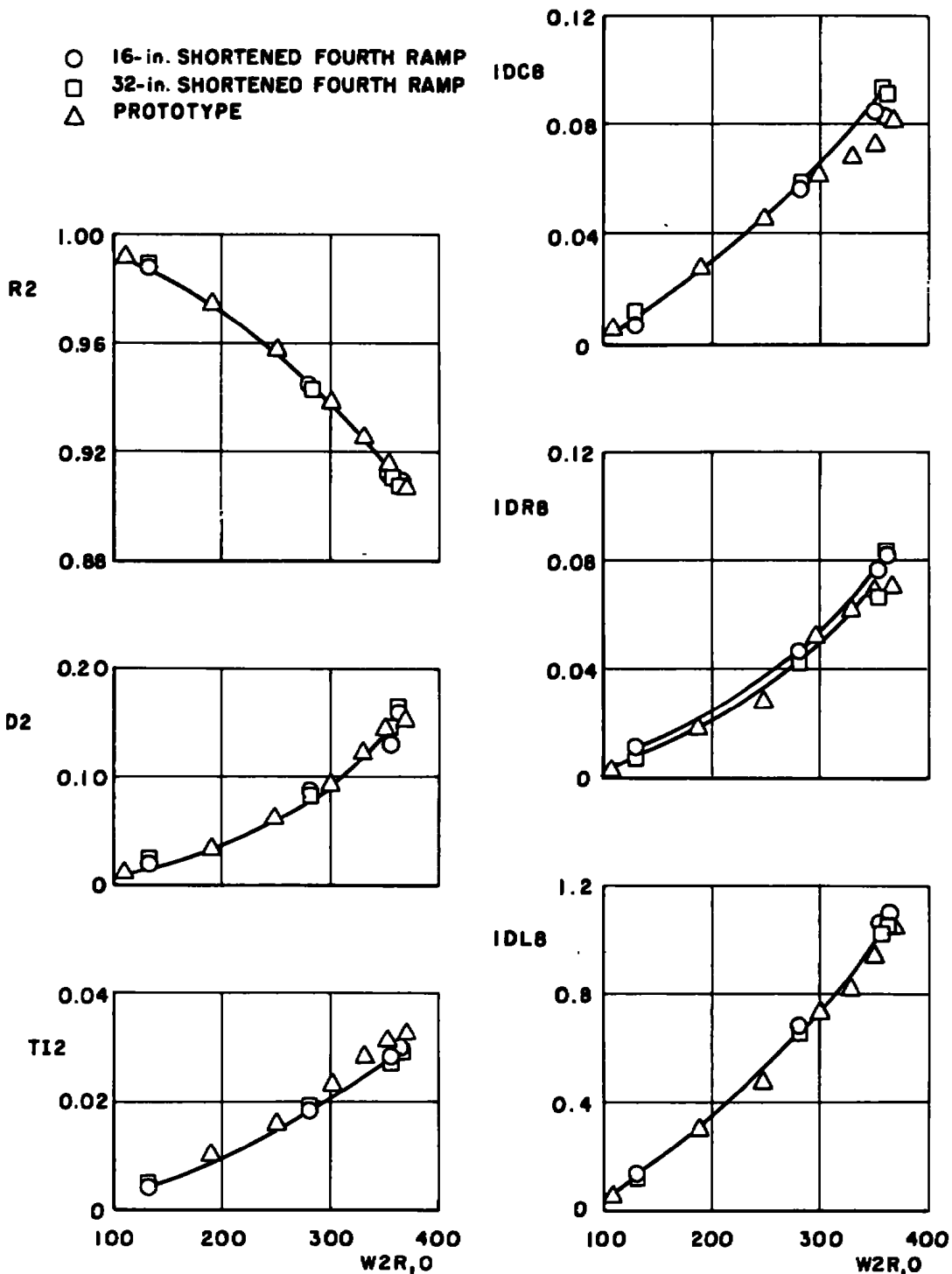
a. Outboard

Figure 20. Effects of reduced fourth ramp length on inlet performance at M0 = 0.
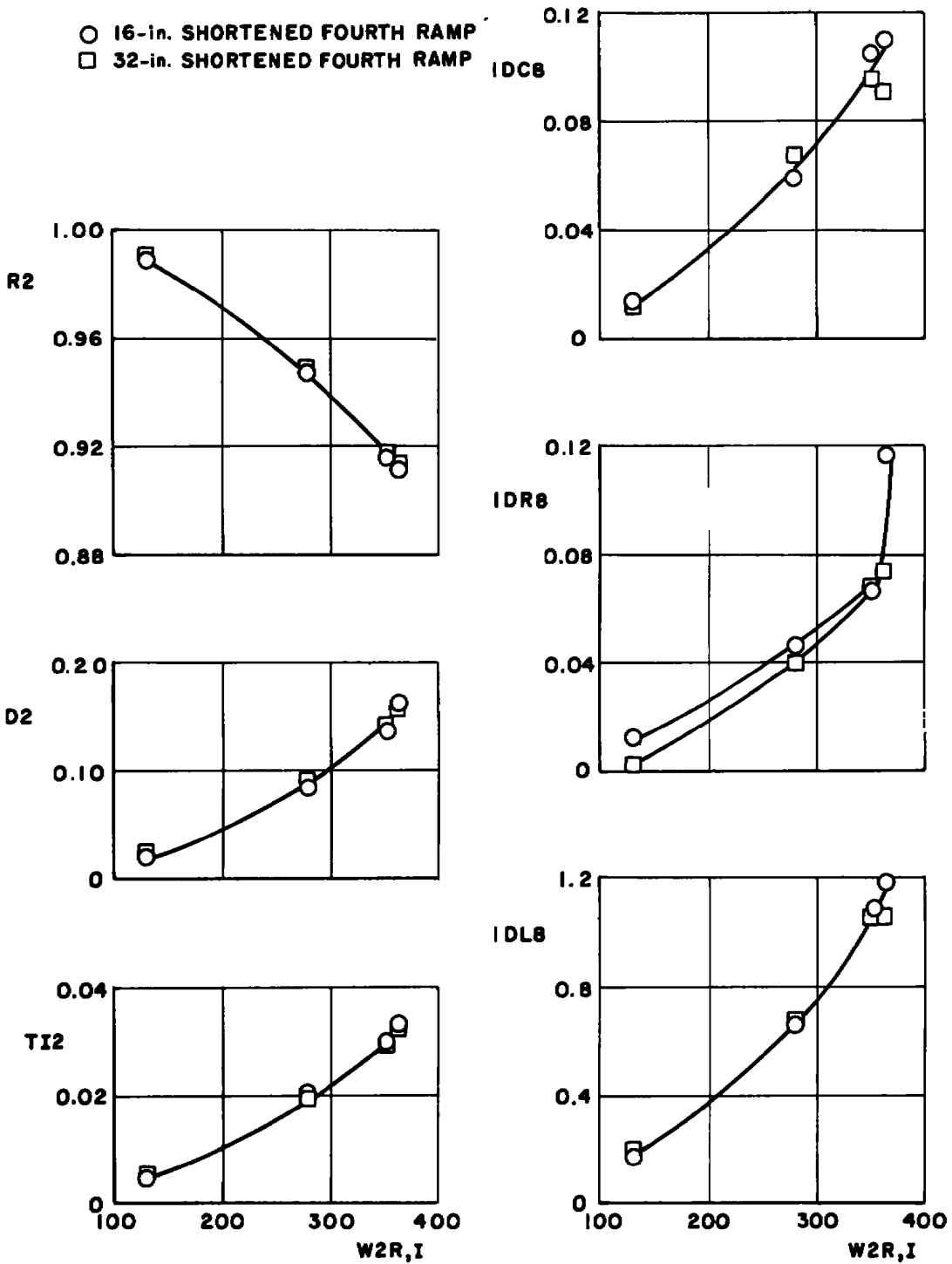
b. Inboard
Figure 20. Concluded.
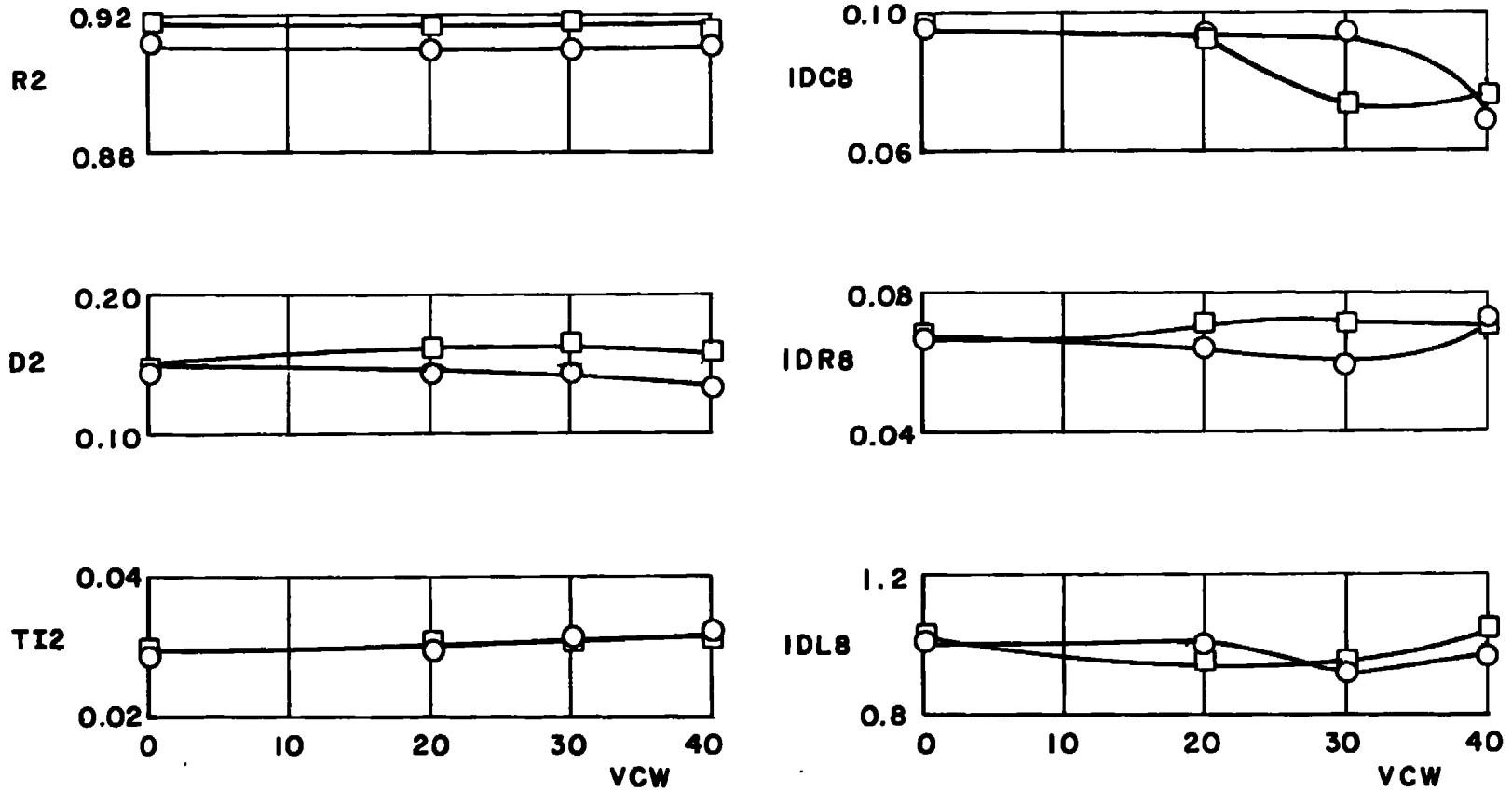
Figure 21. Effects of crosswind on inlet performance at takeoff conditions.
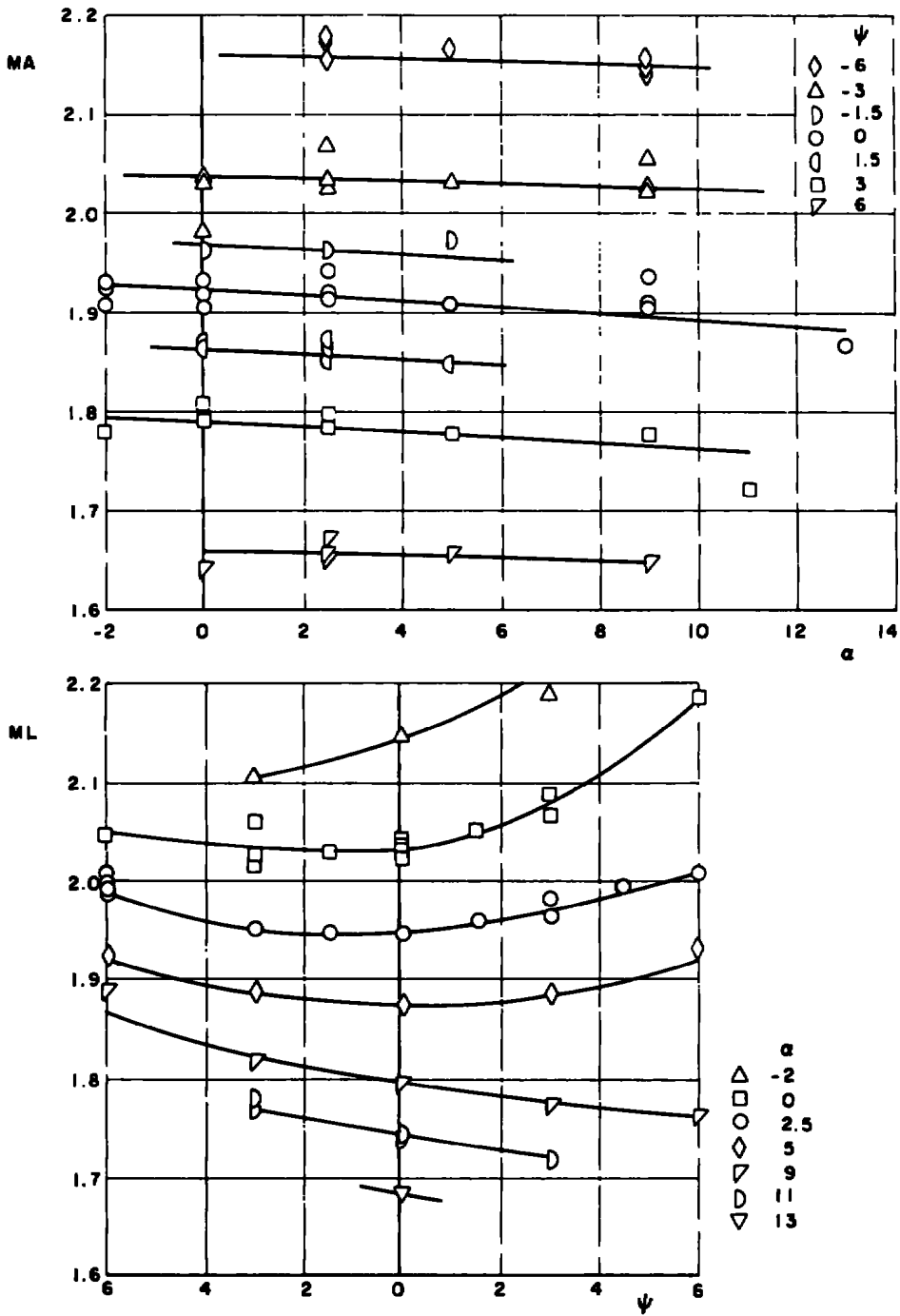
a. M0 = 2.2

Figure 22. MA/ML local Mach number data matrix.
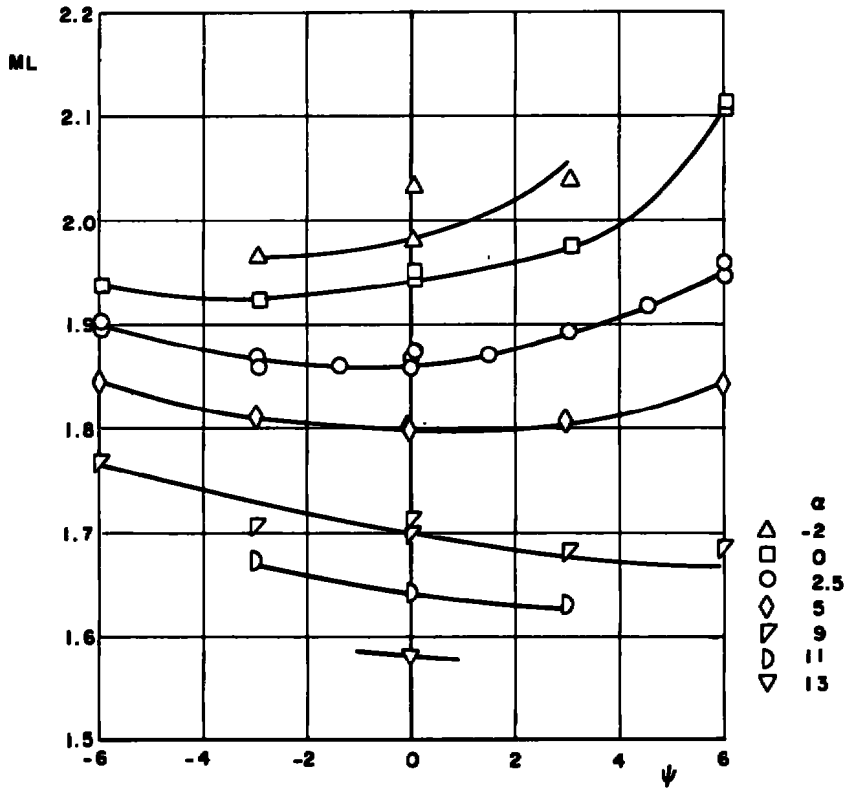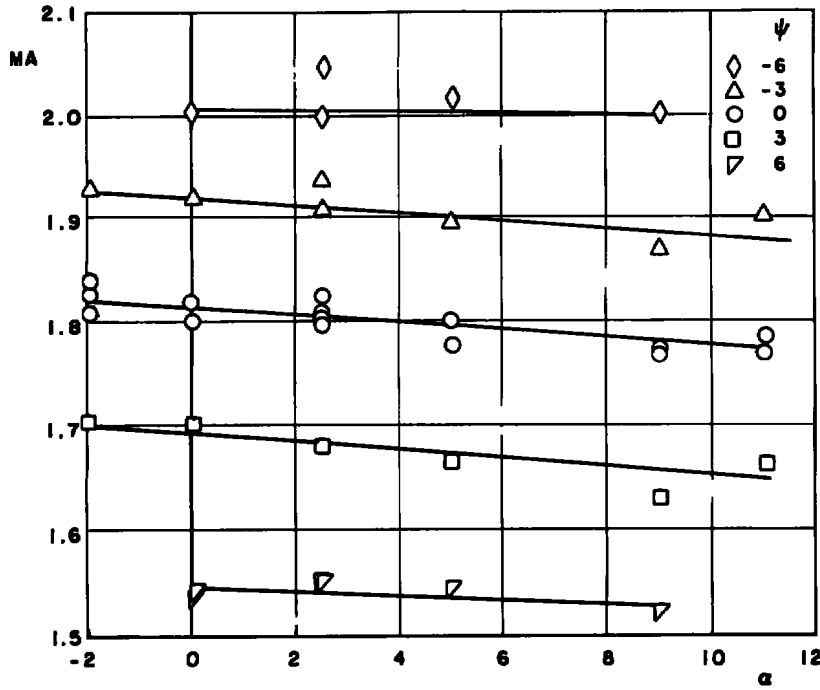
b. M0 = 2.1
Figure 22. Continued.
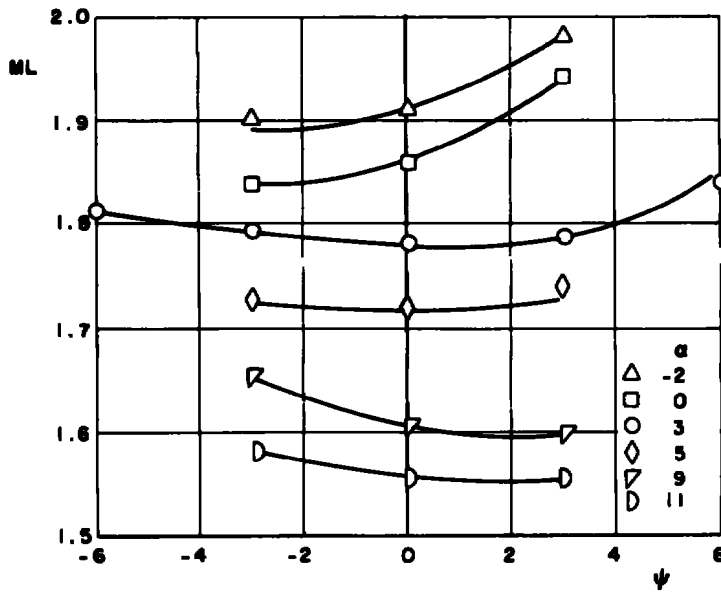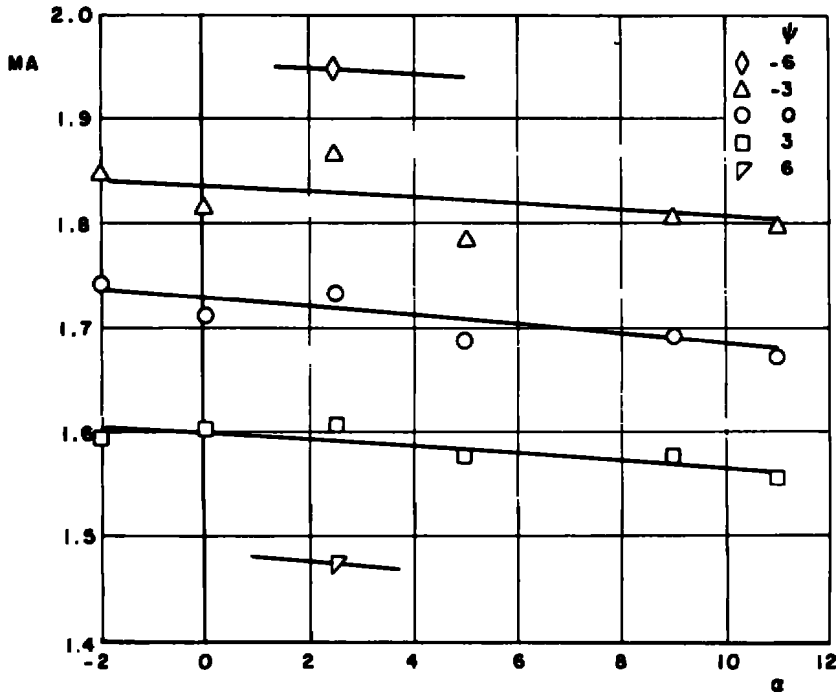
c. M0 = 2.0
Figure 22. Continued.
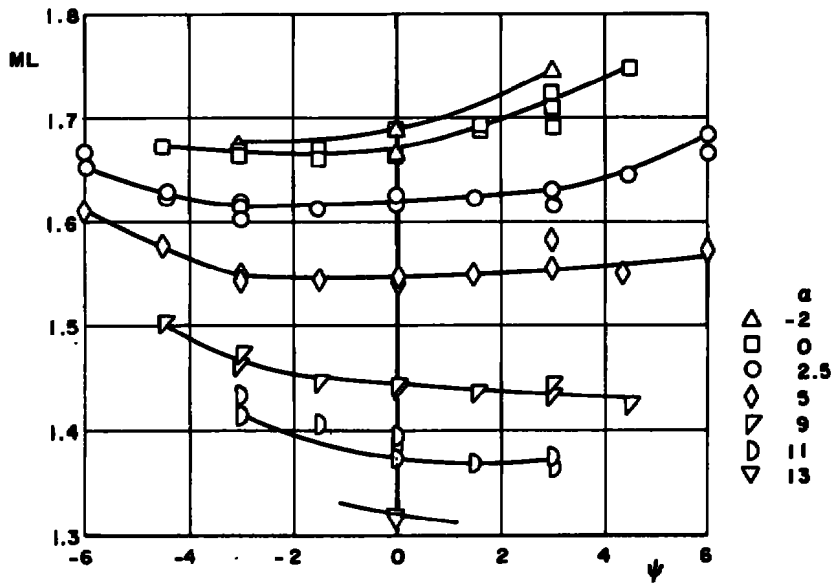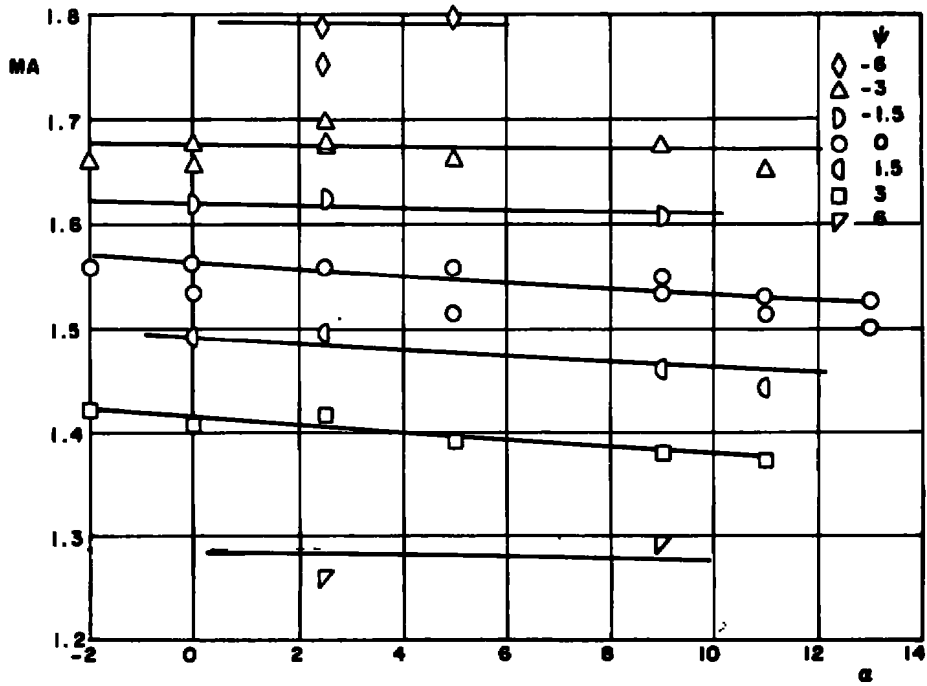
d. M0 = 1.8
Figure 22. Continued.

73
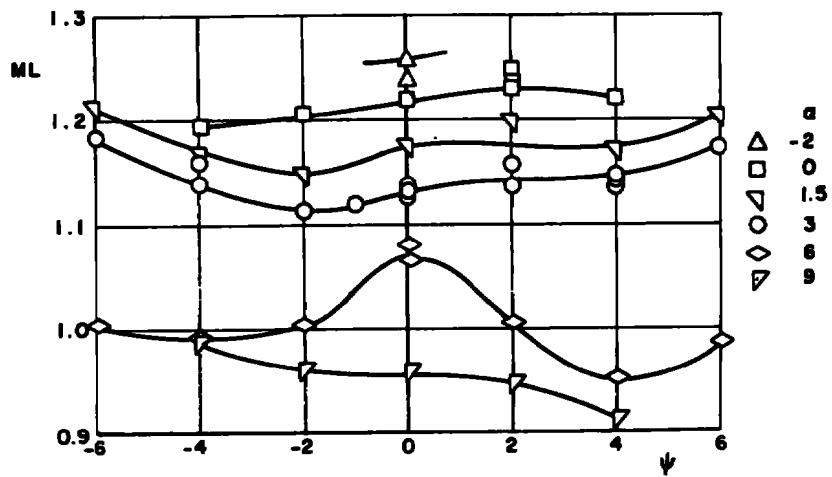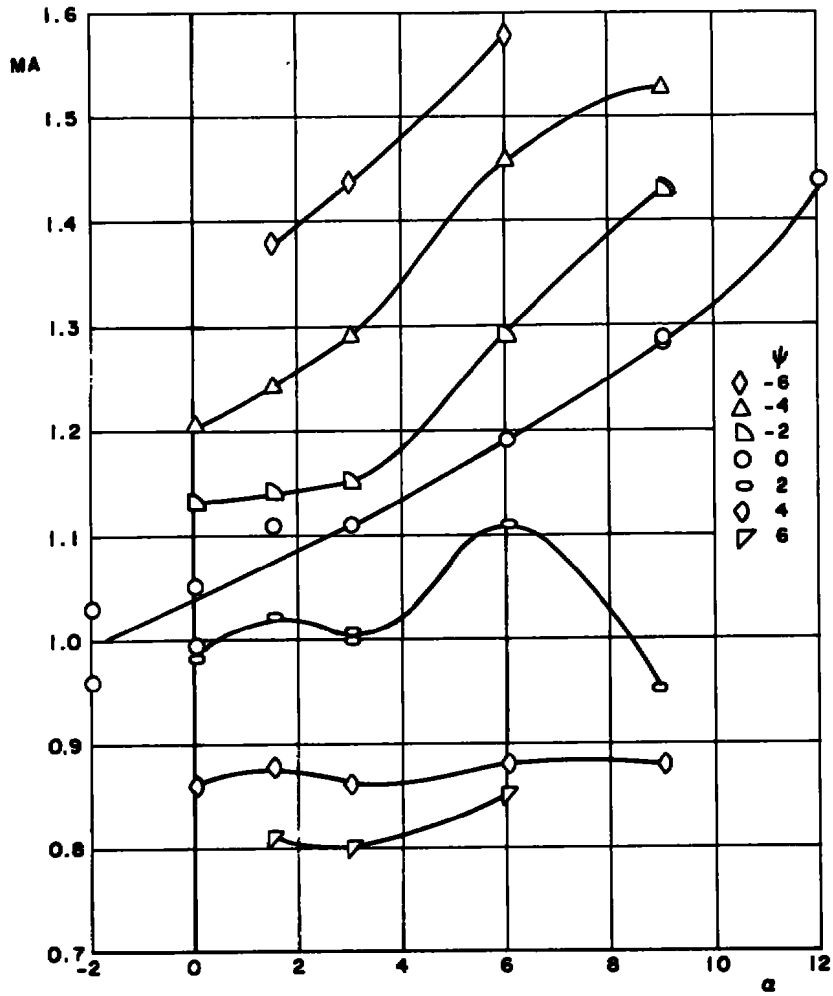
e. M0 = 1.4
Figure 22. Continued.
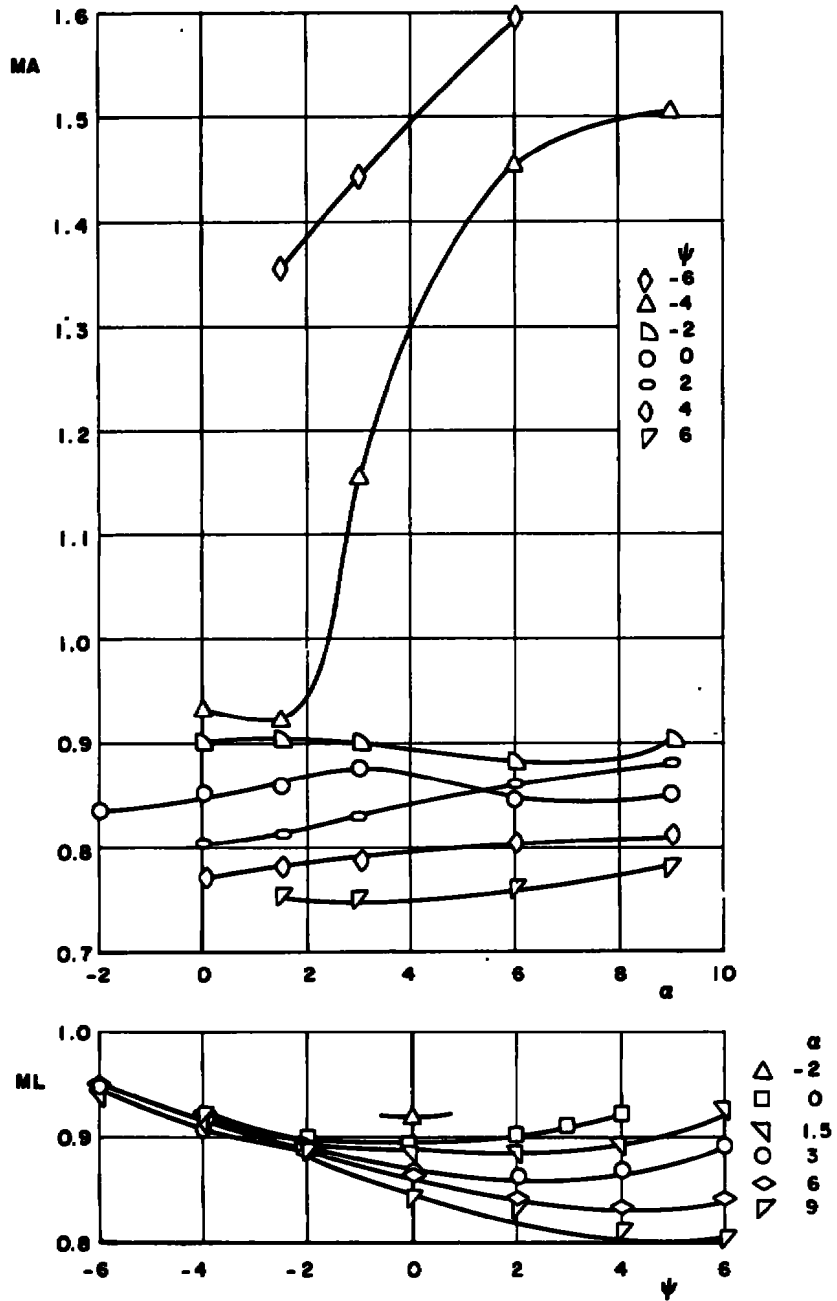
f. M0 = 1.2
Figure 22. Concluded.
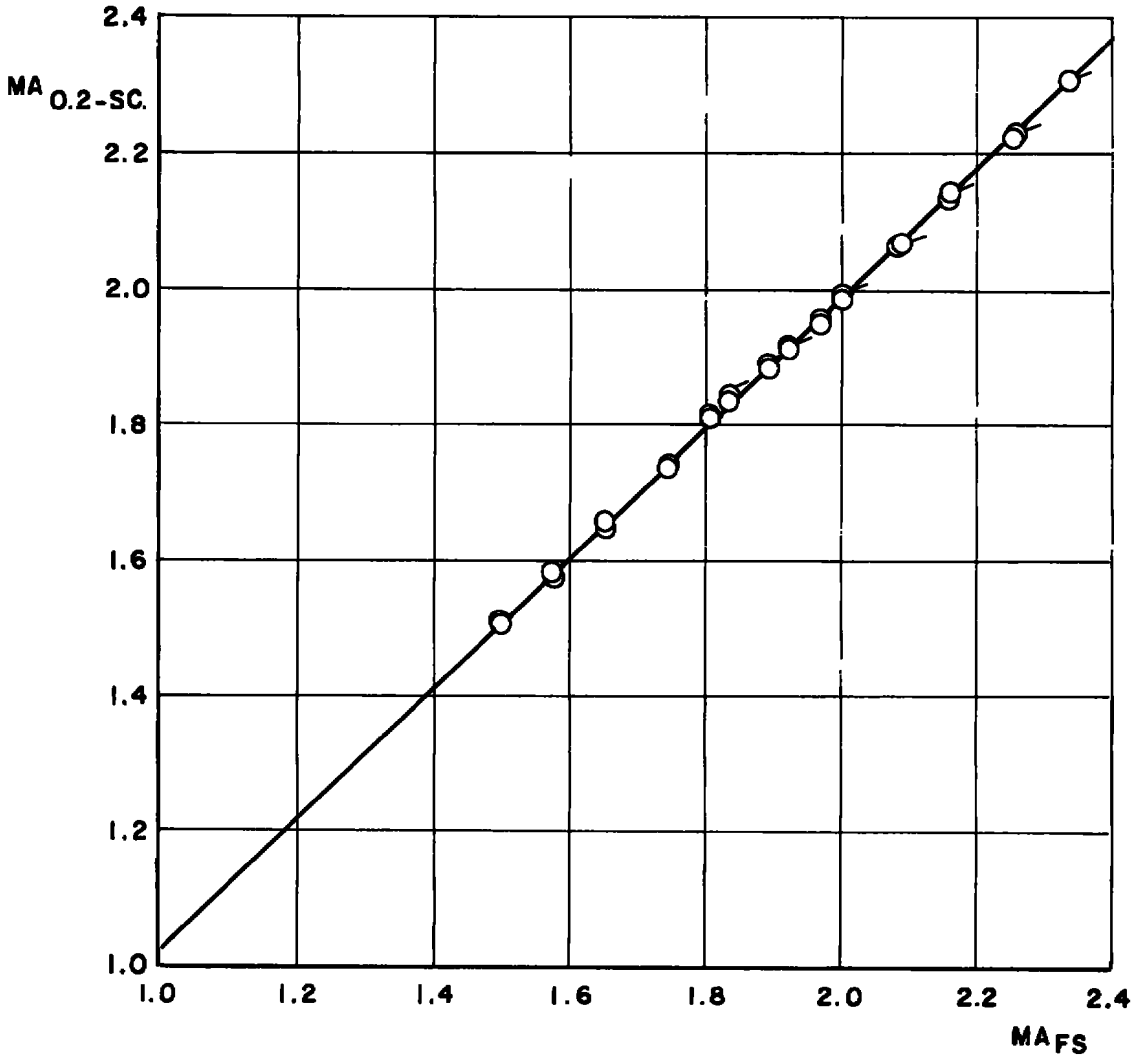
a. Inboard inlet, ML probe
Figure 23. 0.2-scale/full-scale local Mach sensor correlation.

PLAIN SYM - DATA OBTAINED AT MO = 1.8
FLAGGED SYM - DATA OBTAINED AT MO = 2.1
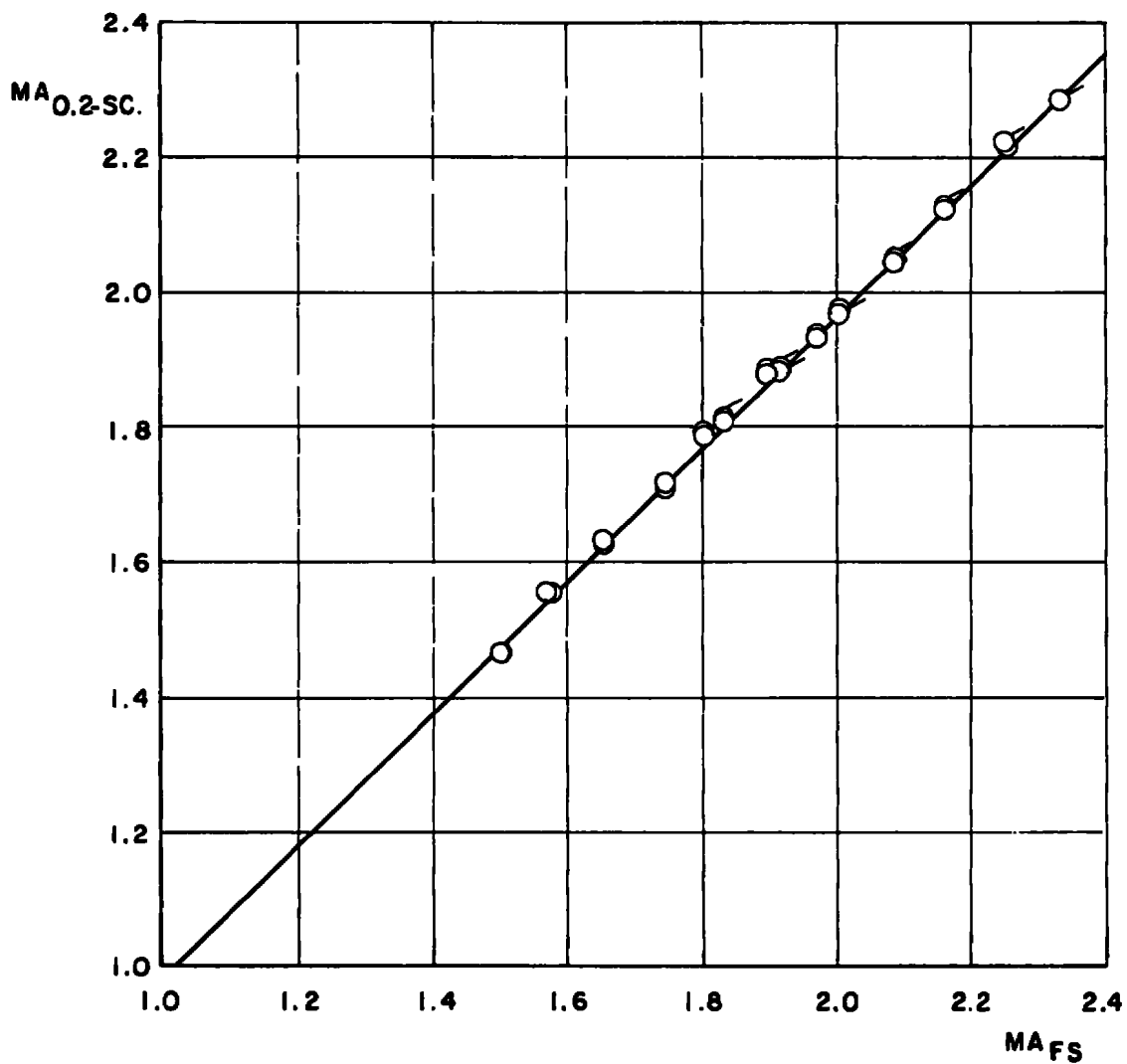
b. Outboard inlet, MA probe
Figure 23. Continued.

PLAIN SYM - DATA OBTAINED AT MO = 1.8

FLAGGED SYM - DATA OBTAINED AT MO = 2.1
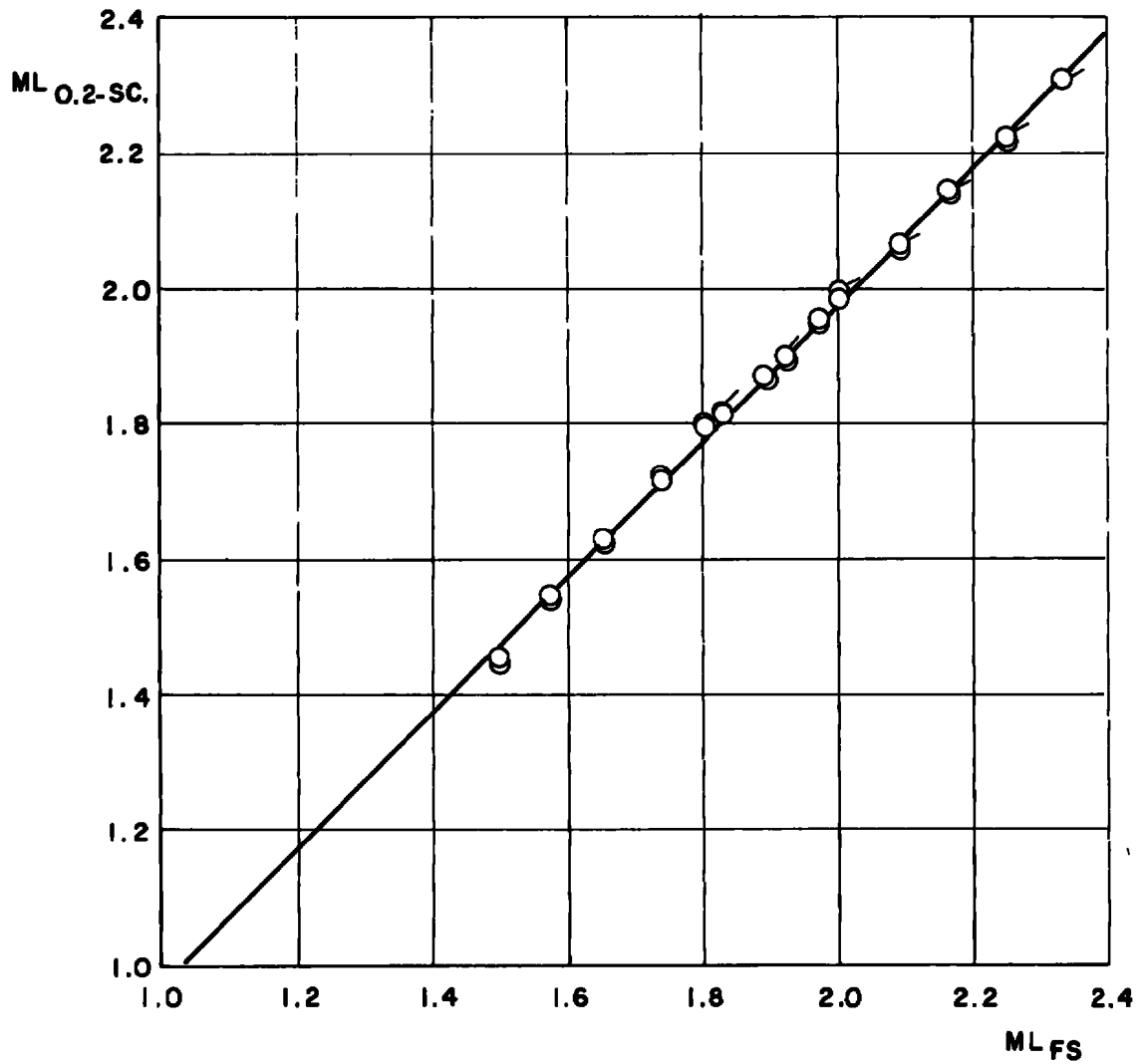
c. Outboard inlet, Ref. 1 MA probe
Figure 23. Concluded.
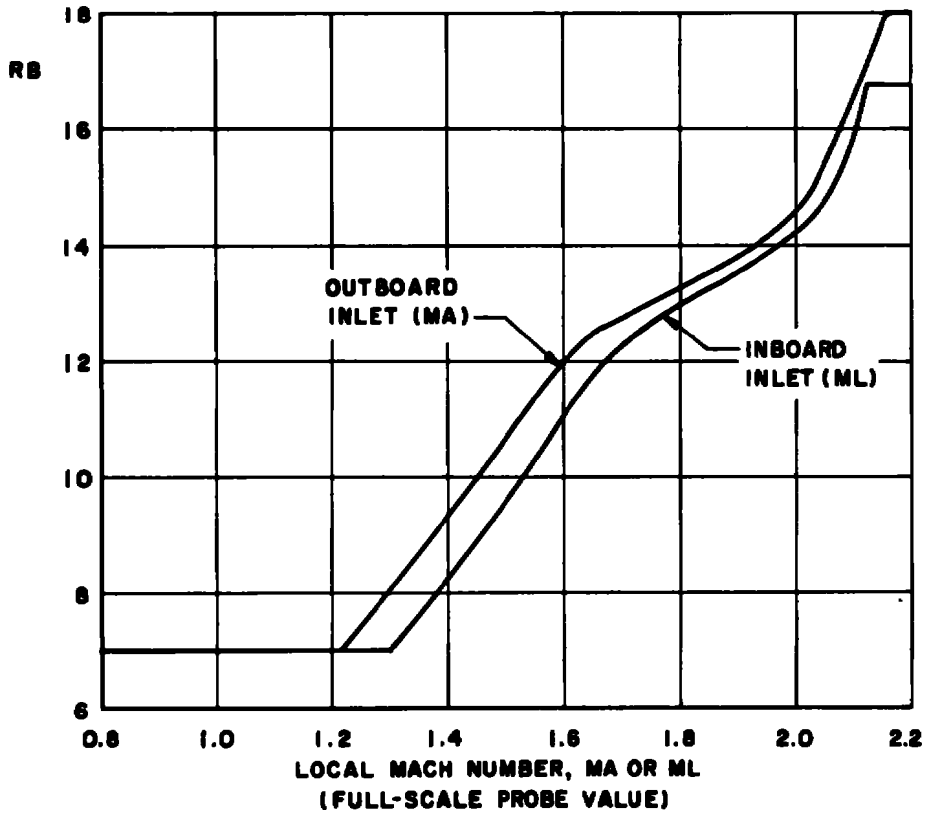
a. Second ramp angle

Figure 24. Full-scale AICS schedules.
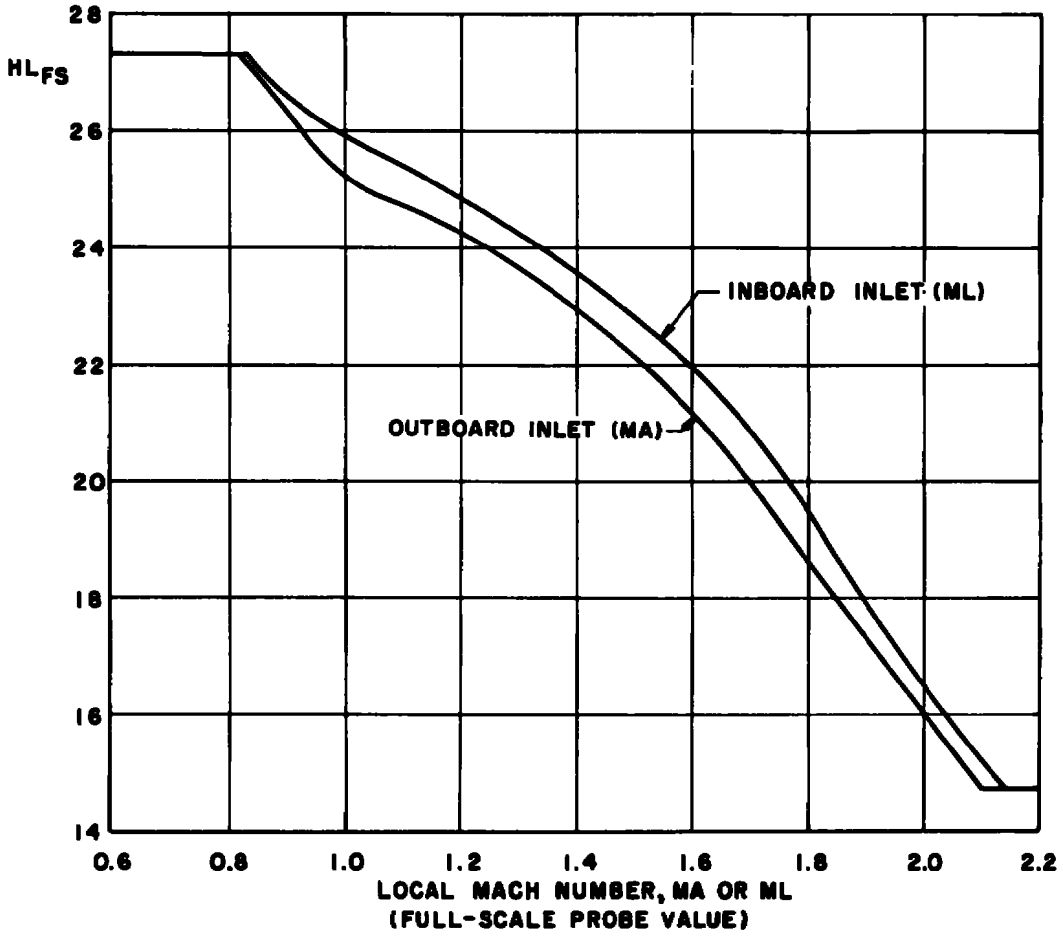
b. Lip height
Figure 24. Continued.
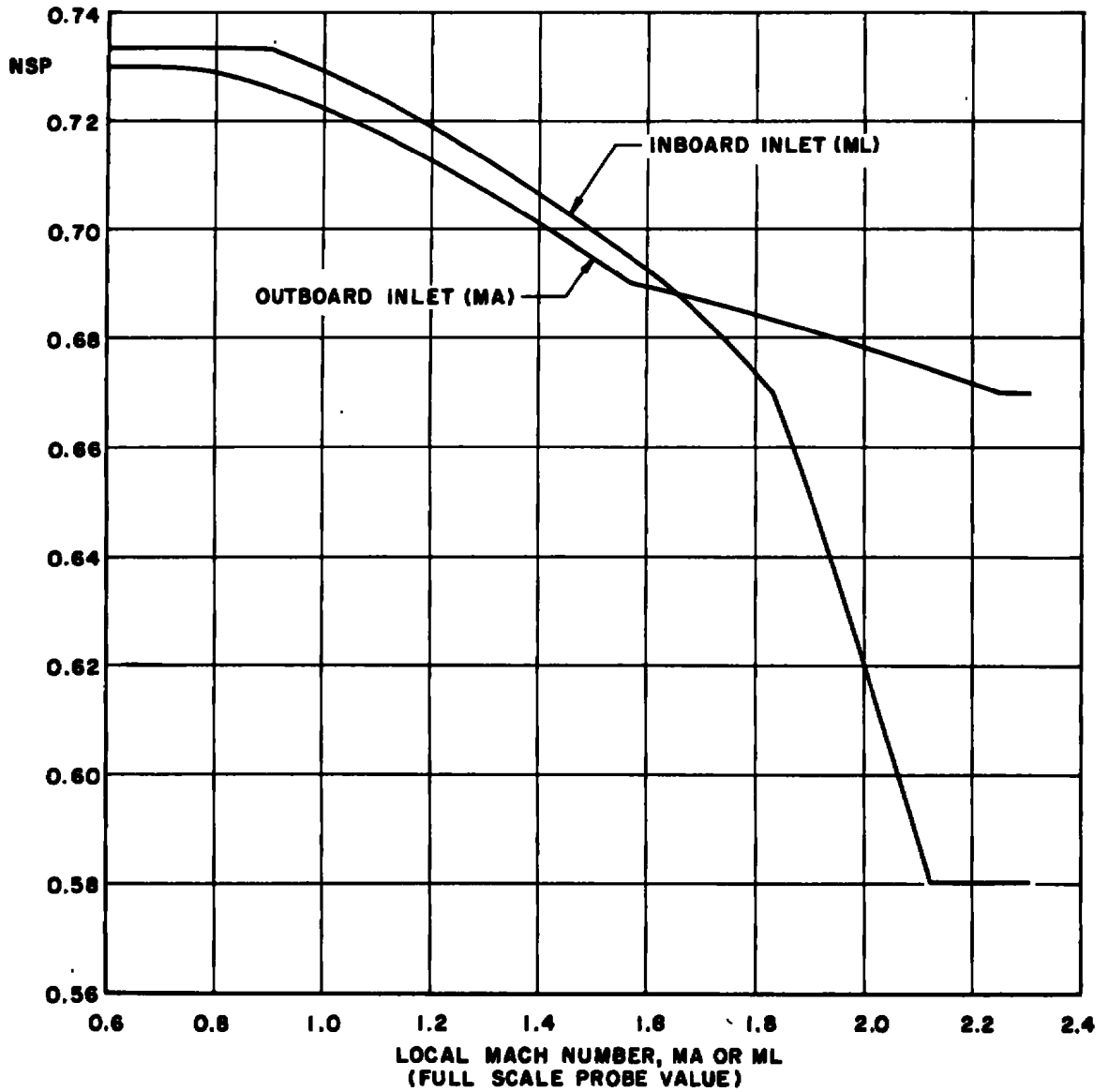
c. Normal shock parameter
Figure 24. Concluded.
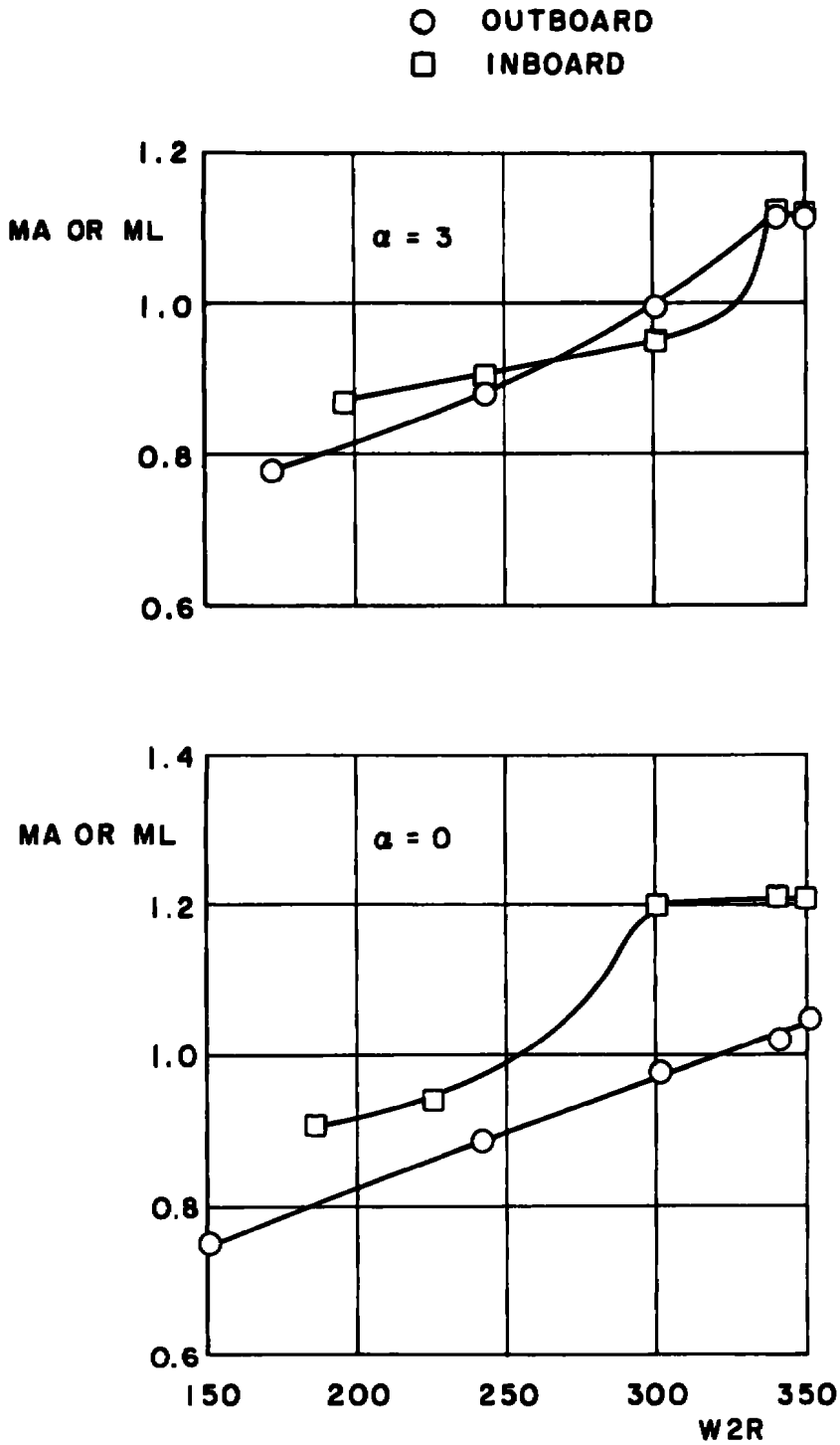
Figure 25. Effects of airflow on sensed local Mach numbers at
MO = 1.40, ψ = 0.

SYMBOL	α	ψ	RB	ML	GEOMETRY	
☐	2.5	0	7.4	5.45	SUBSONIC	2172
△	2.5	0	15.0	3.46	MISPOSITIONED	2170
◎	2.5	0	14.0	3.36	MO = 2.2 CRUISE	2084
◇	2.5	0	18.0	2.95	MAX. SUPERSONIC	2168

FLAGGED SYM-STABILITY LIMIT

— — — INTERMEDIATE POWER AIRFLOW, 36K ft
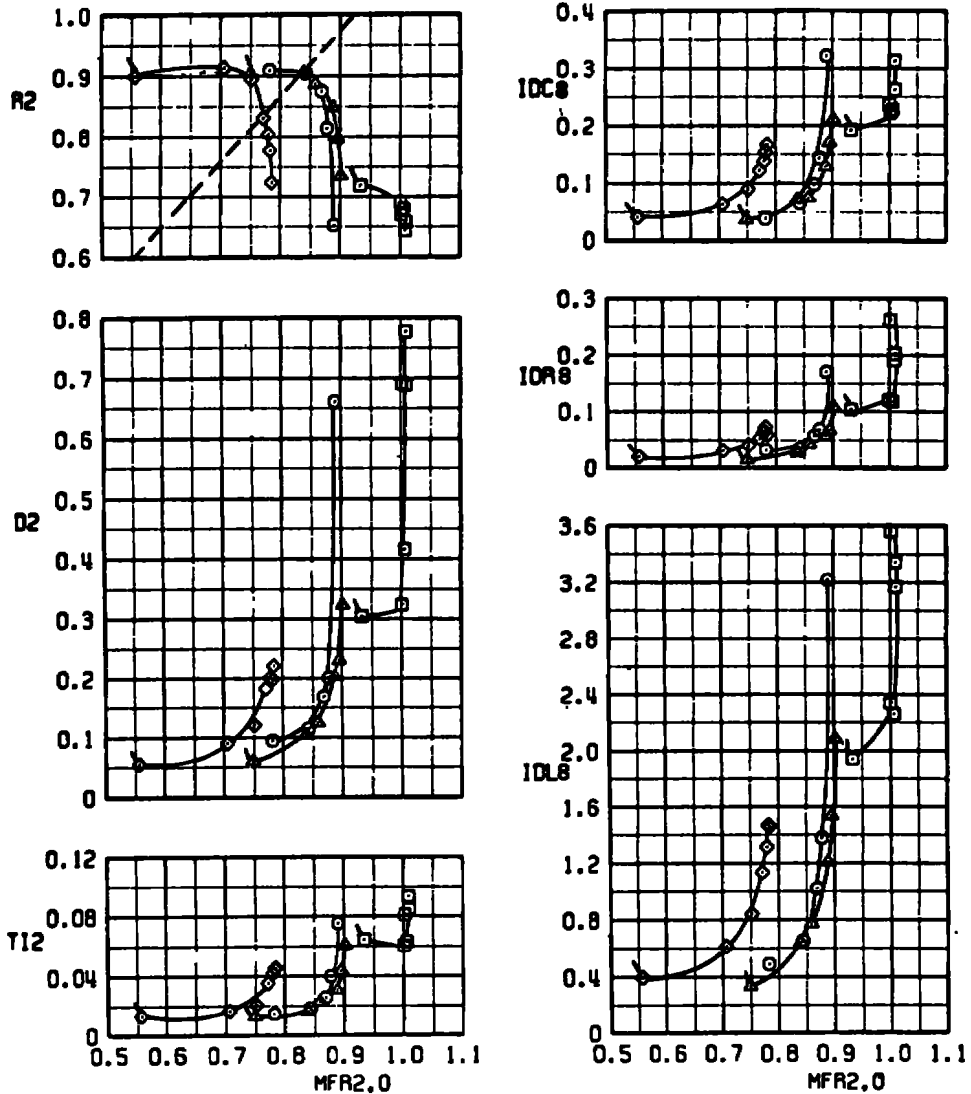
a.   MO = 2.2, outboard

Figure 26.   Inlet performance effects of extreme ramp geometry.

SYMBOL	∝	ψ	RB	HL	GEOMETRY	
▫	2.5	0	7.1	5.46	SUBSONIC	2172
△	2.5	0	14.9	3.46	MISPOSITIONED	2170
⊙	2.5	0	13.9	3.36	MO=2.2 CRUISE	2064
◇	2.5	0	18.0	2.94	MAX. SUPERSONIC	2168

FLAGGED SYM - STABILITY LIMIT

— — — INTERMEDIATE POWER AIRFLOW, 36K ft

a. Concluded, inboard
Figure 26. Continued.

84
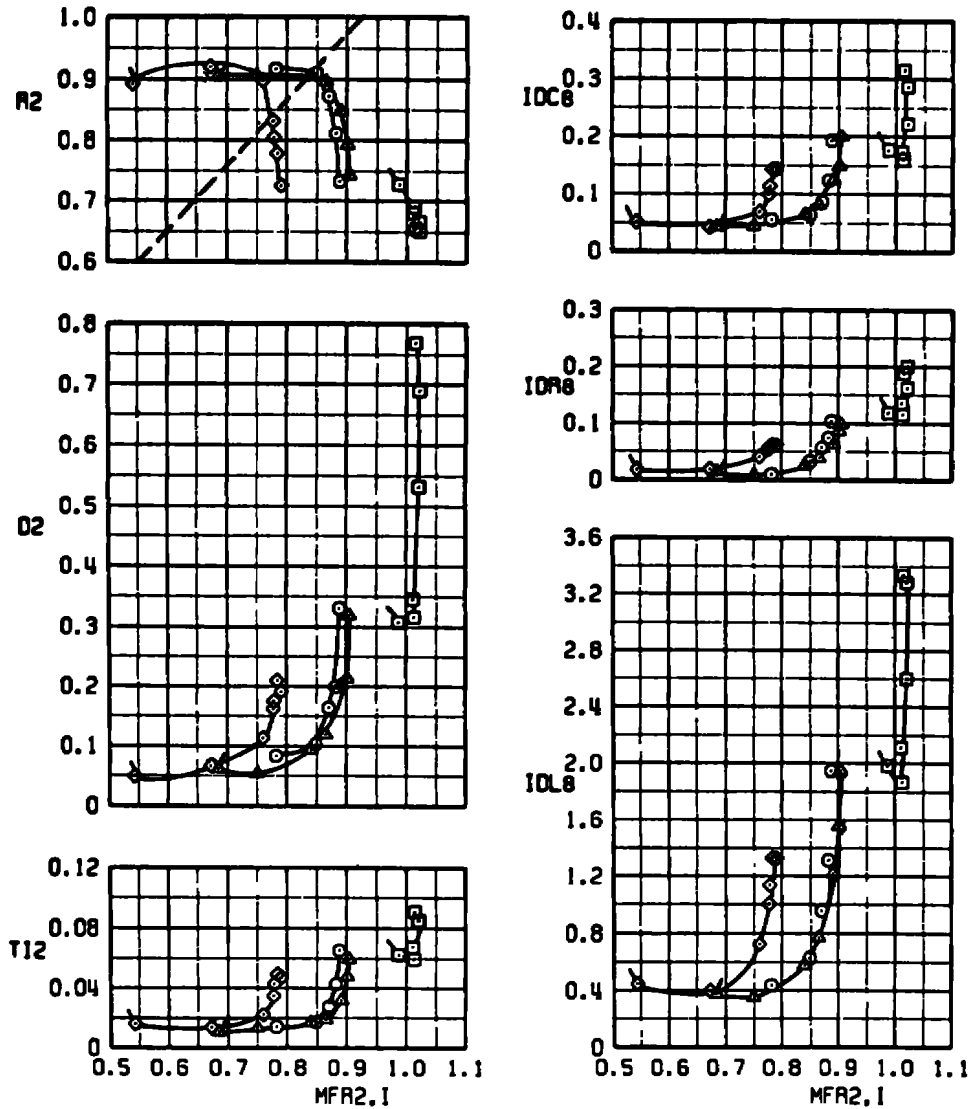
| SYMBOL	α	ψ	RB	HL	GEOMETRY	
□	2.5	0	7.0	5.50	SUBSONIC	2119
⊙	2.5	0	11.4	4.34	MO = 1.8 CRUISE	2118
△	2.5	0	14.0	3.36	MO = 2.2 CRUISE	2122
◇	2.5	0	18.0	2.95	MAX. SUPERSONIC	2121

FLAGGED SYM - STABILITY LIMIT
— — — INTERMEDIATE POWER AIRFLOW, 36K ft
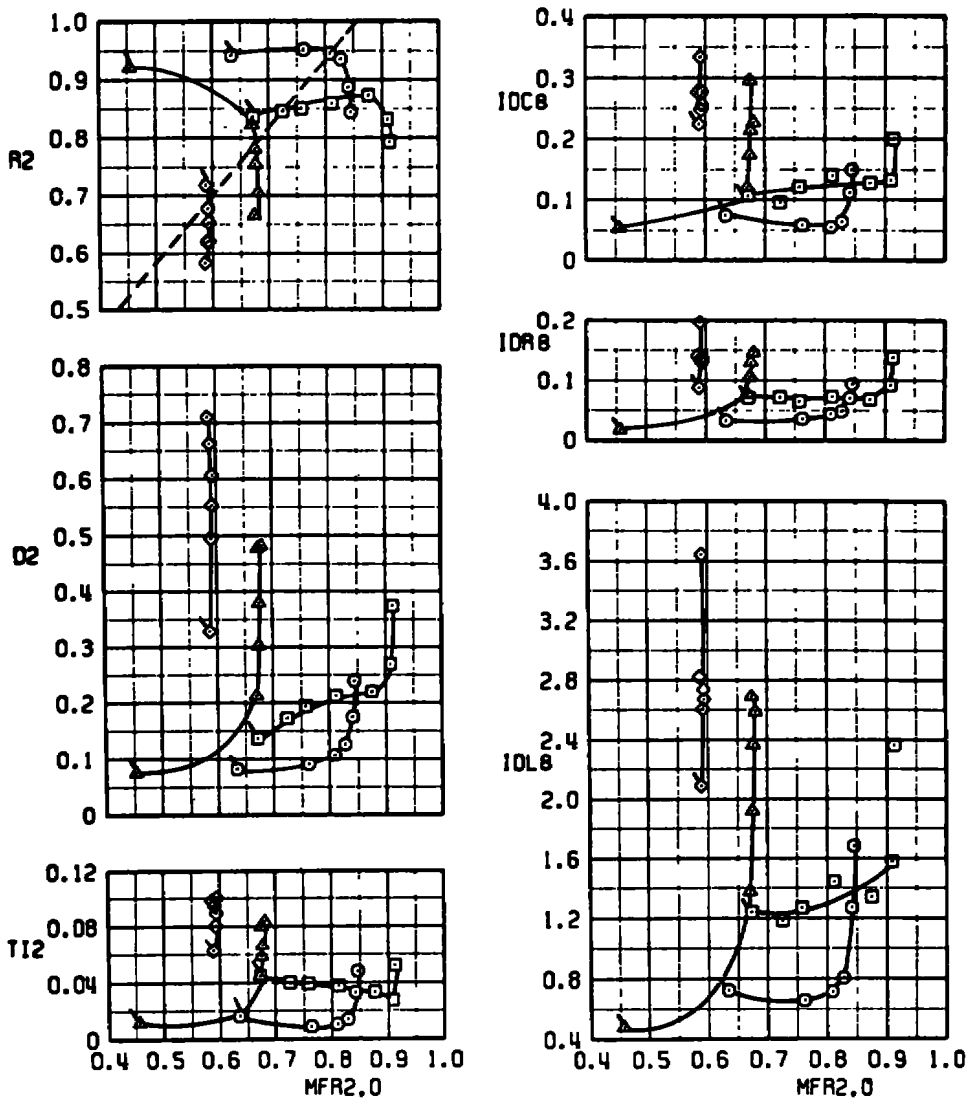
b. MO = 1.8, outboard
Figure 26. Continued.

SYMBOL	α	ψ	RB	ML	GEOMETRY	
□	2.5	0	7.3	5.45	SUBSONIC	2119
⊙	2.5	0	11.4	4.34	MO = 1.8 CRUISE	2118
▲	2.5	0	13.9	3.36	MO = 2.2 CRUISE	2122
◇	2.5	0	18.0	2.94	MAX. SUPERSONIC	2121

FLAGGED SYM STABILITY LIMIT

— — — INTERMEDIATE POWER AIRFLOW, 36K ft

b. Concluded, inboard

Figure 26. Continued.

86

c. MO = 1.4, outboard
Figure 26. Continued.

SYMBOL	α	ψ	RB	ML	GEOMETRY	
⬚	3.0	0.0	7.0	5.46	SUBSONIC	2699
⊙	3.0	0.0	7.0	5.00	MO = 1.4 CRUISE	2617
▲	3.0	0.0	11.0	4.40	MO = 1.75 CRUISE	2614
◇	3.0	0.0	14.0	3.36	MO = 2.2 CRUISE	2615

FLAGGED SYM - STABILITY LIMIT
— — — INTERMEDIATE POWER AIRFLOW, 36K ft
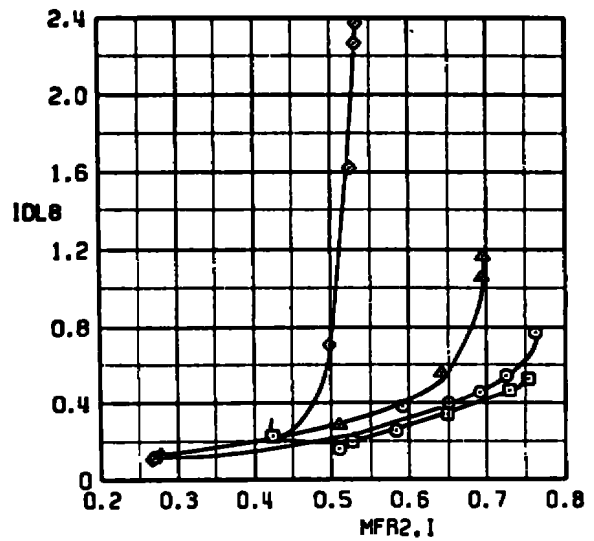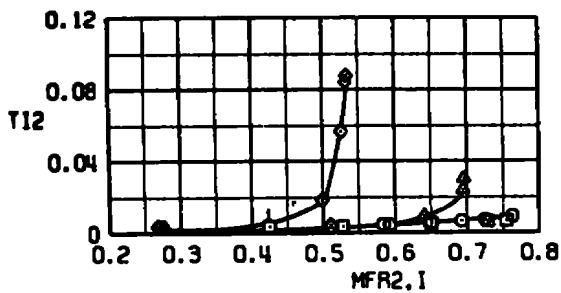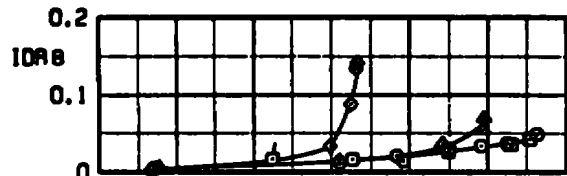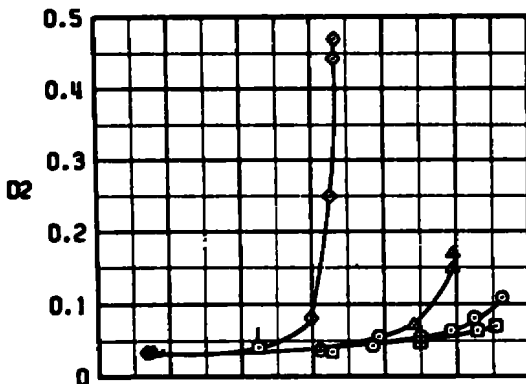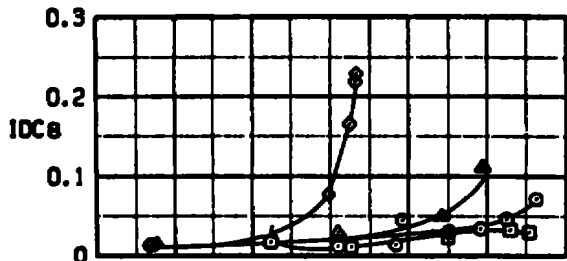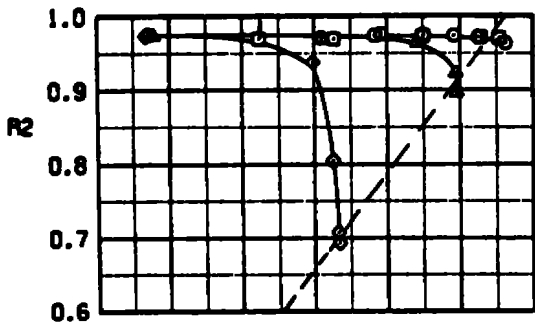
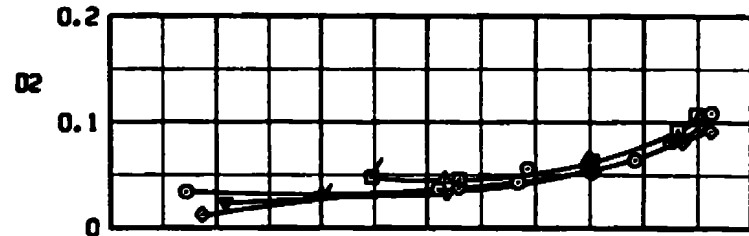c. Concluded, inboard
Figure 26. Concluded.

88

SYMBOL	U	
⊙	SEALED	2084
▣	0	2184
△	5	2185
▽	10	2186
◇	20	2187
⊠	30	2188
⋈	52	2190

FLAGGED SYM - STABILITY LIMIT

— — — INTERMEDIATE POWER, 36K ft
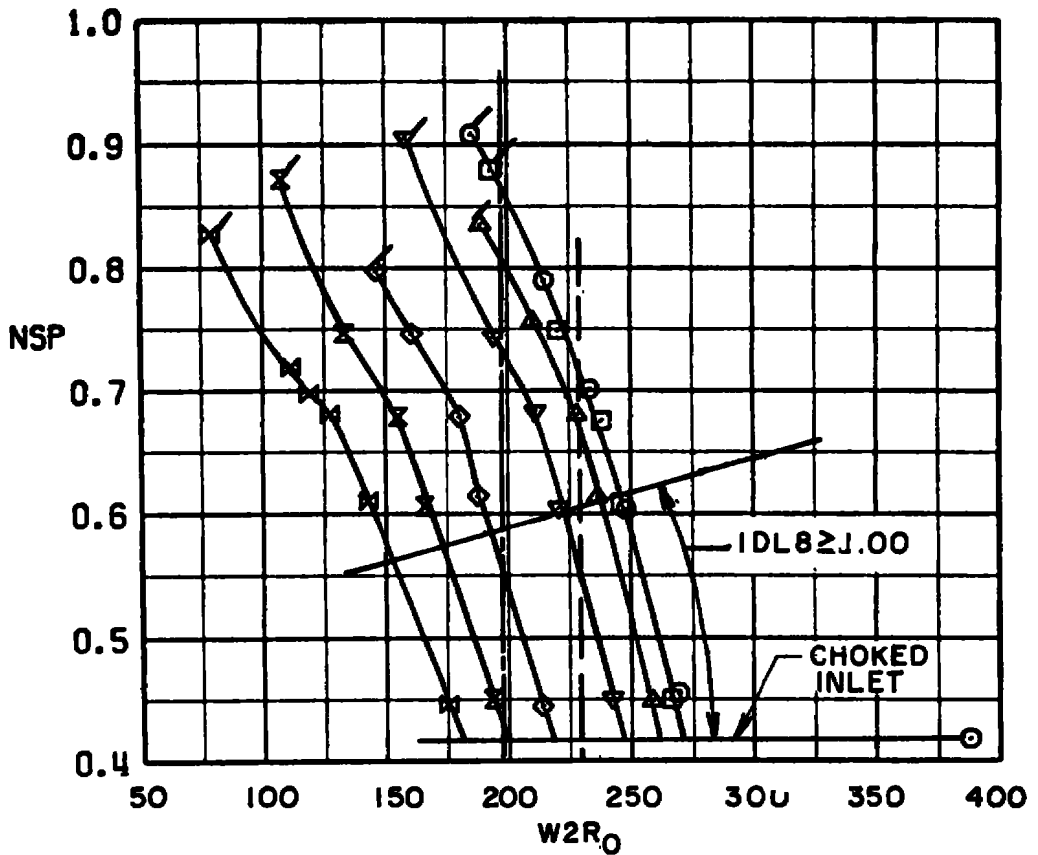
— · — IDLE POWER, 36K ft

a. $M0 = 2.2$, outboard

Figure 27. Bypass door effectiveness at $a = 2.5$ deg, $\psi = 0$.
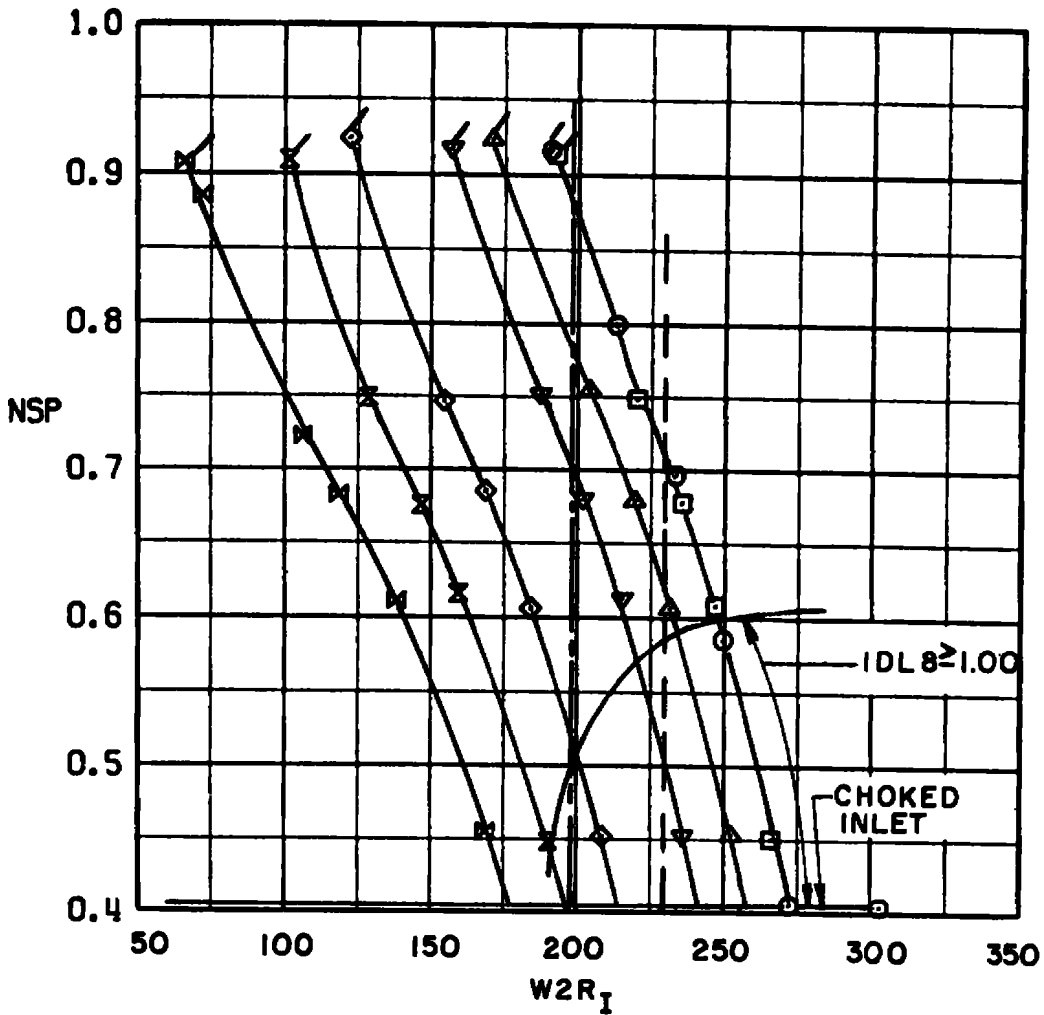
a. Concluded, inboard
Figure 27. Continued.

SYMBOL	U	
⊙	SEALED	2118
⊡	0	2211
△	5	2212
▽	10	2213
◇	20	2214
⊠	30	2215
⋈	50	2217

FLAGGED SYM – STABILITY LIMIT
— — — INTERMEDIATE POWER, 36K ft
— · — IDLE POWER, 36K ft

b. MO = 1.8, outboard
Figure 27. Continued.
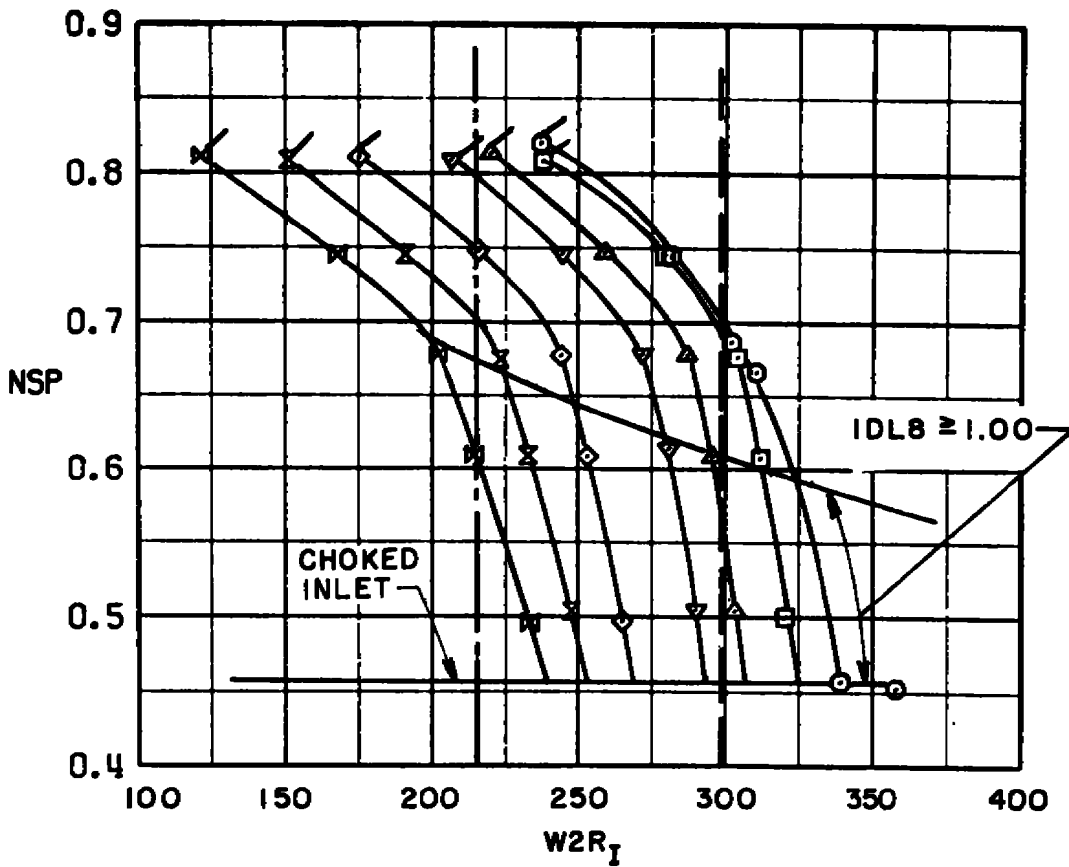
b. Concluded, inboard
Figure 27. Concluded.

SYMBOL	α	ψ	RB	HL	
▫	0.1	0	14.1	3.31	2198
○	2.5	0	14.0	3.36	2194
▲	4.9	0	13.9	3.39	2197
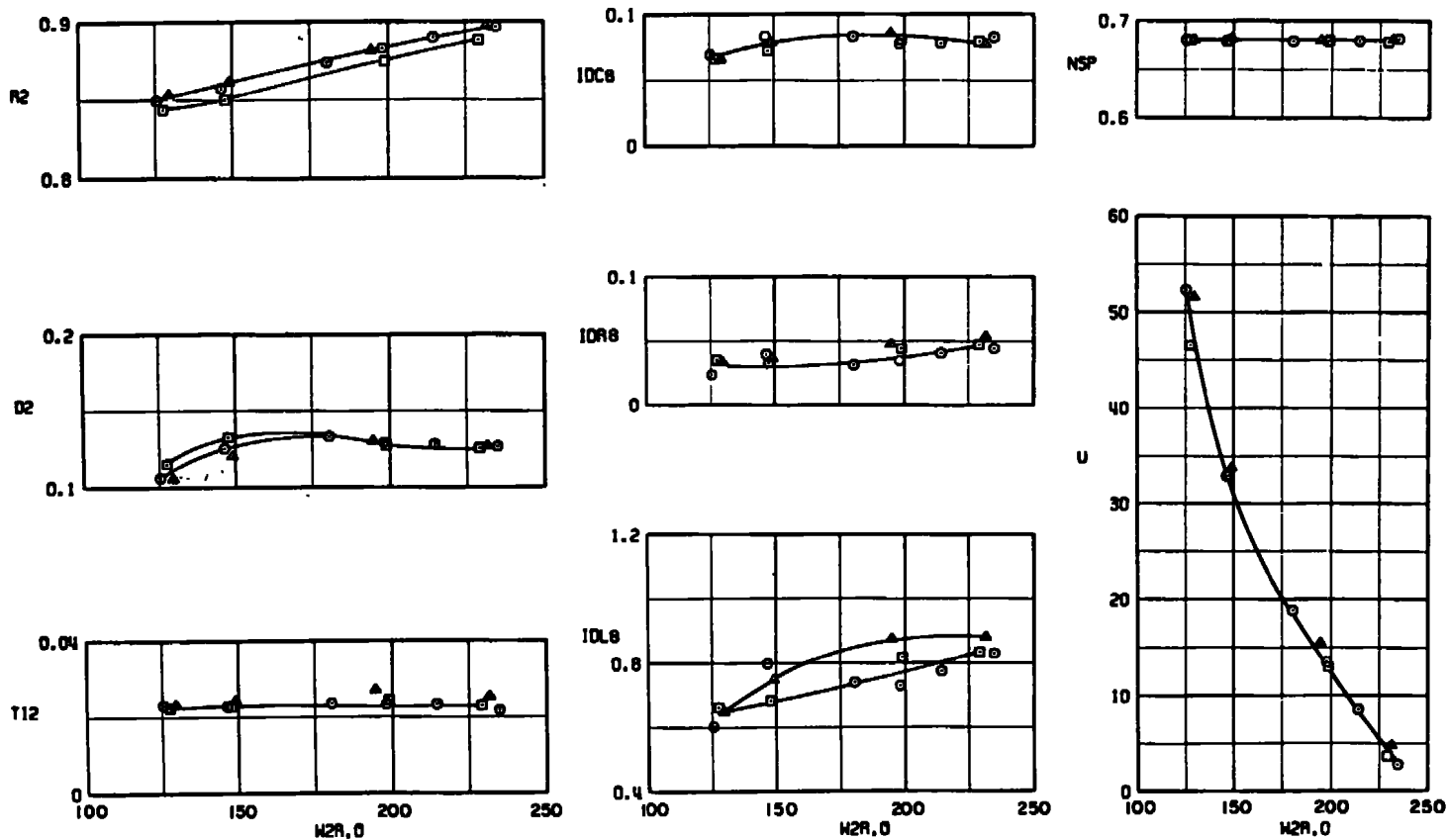
a. M0 = 2.2, outboard

Figure 28. Effects of airflow variations on inlet performance with inlet operated under simulated
AICS control, ψ = 0.
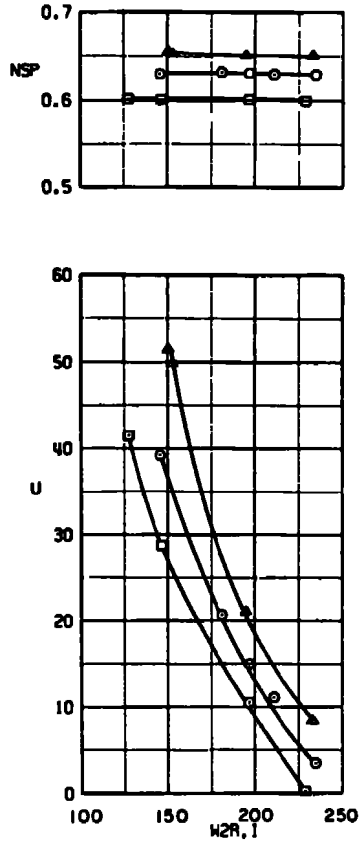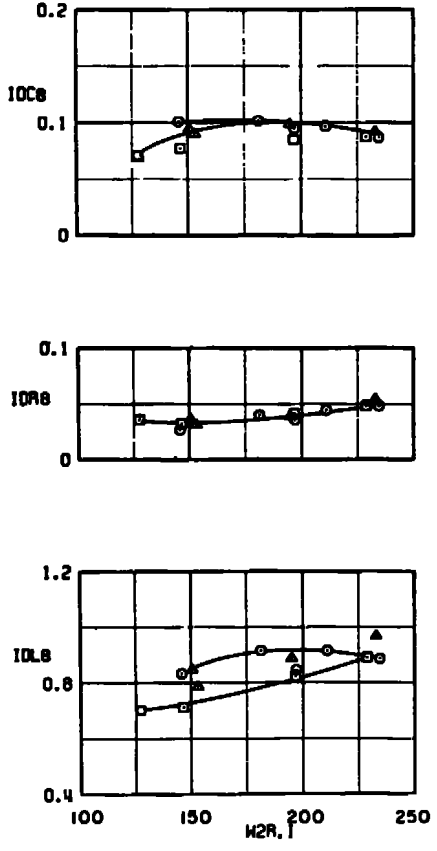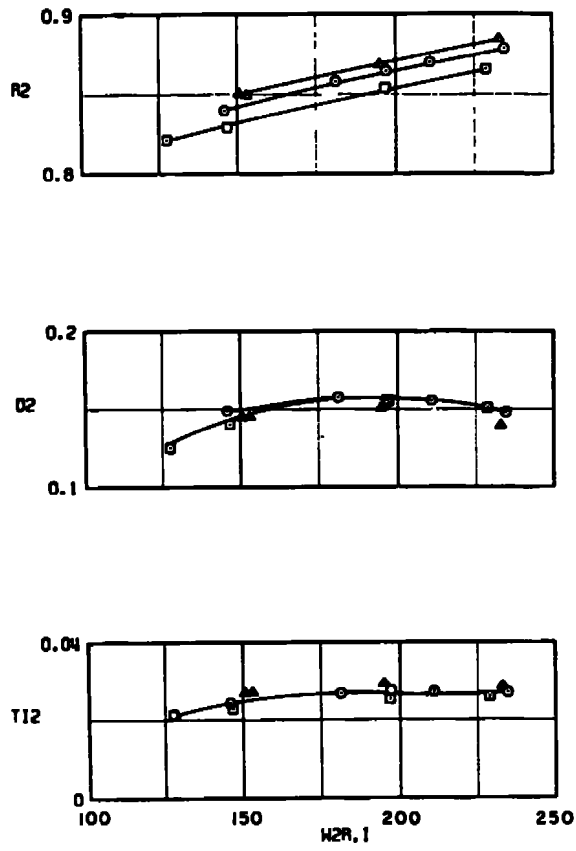
a. Concluded, inboard
Figure 28. Continued.

SYMBOL	α	ψ	RB	RL	
▣	0.1	0	11.6	4.32	2222
◉	2.5	0	11.5	4.34	2219
▲	4.9	0	11.6	4.43	2223
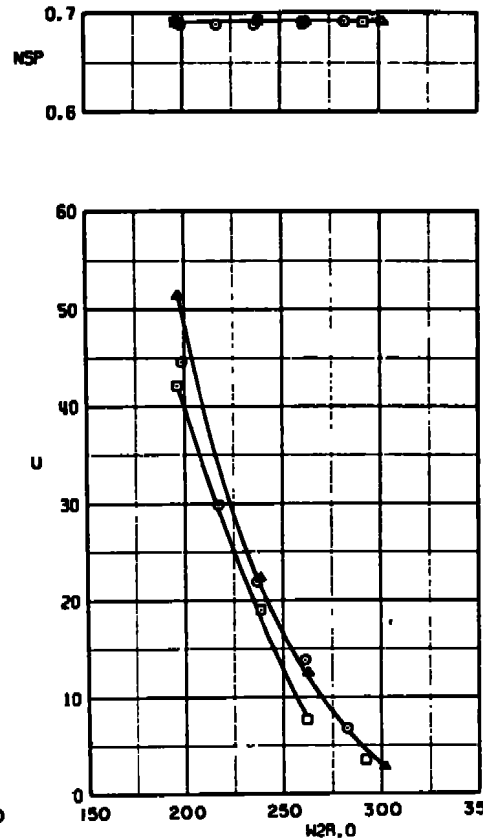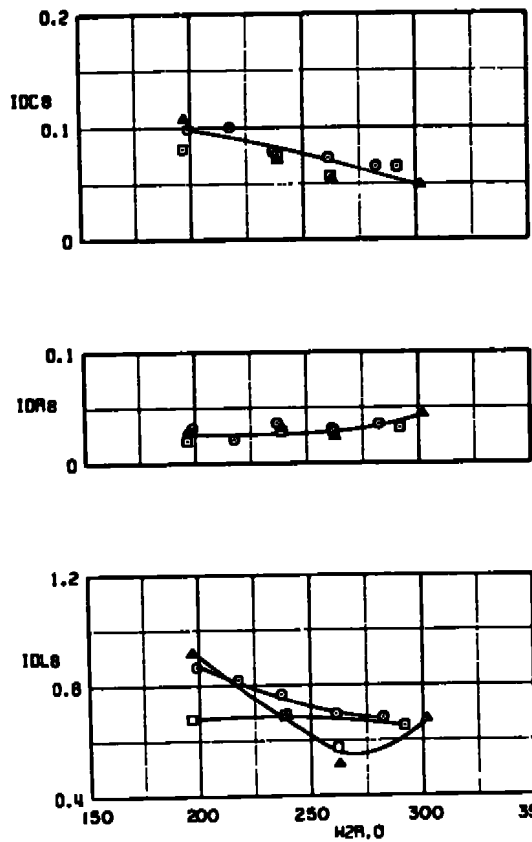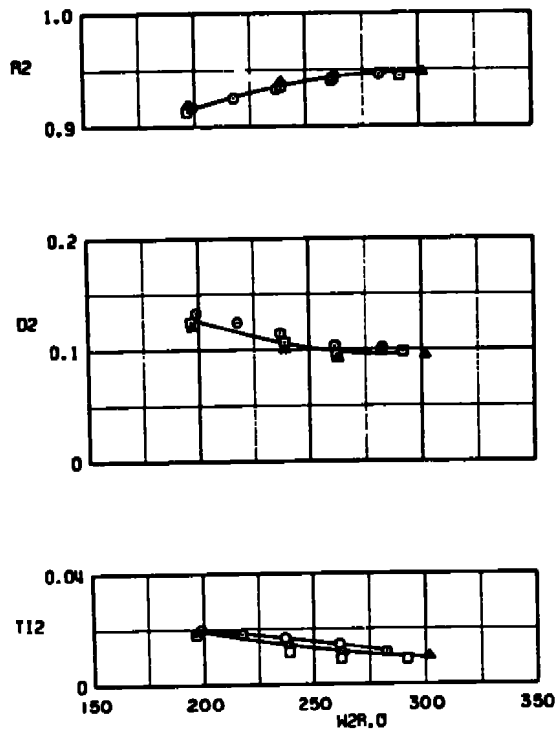
b. M0 = 1.8, outboard
Figure 28. Continued.

SYMBOL	α	Ψ	RB	ML	
□	0.1	0	12.2	4.16	2222
⊙	2.5	0	11.5	4.34	2219
▲	4.9	0	10.5	4.45	2223
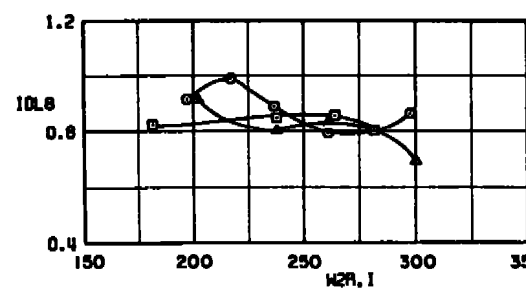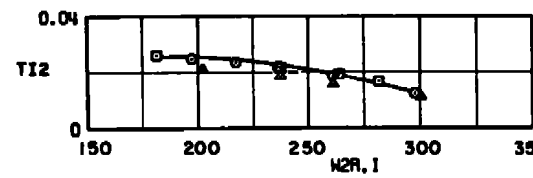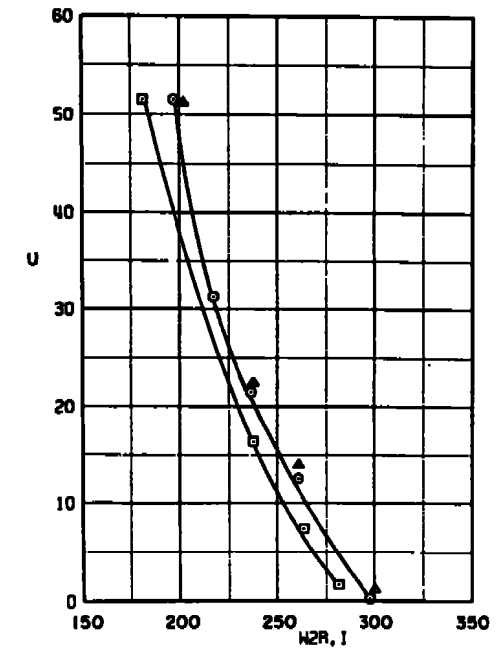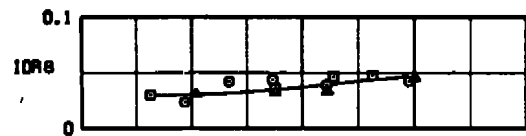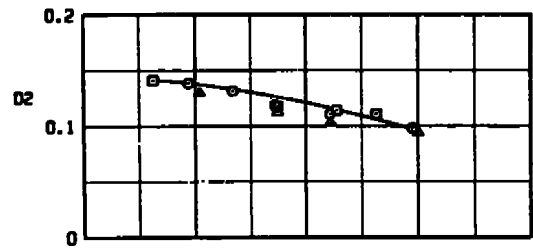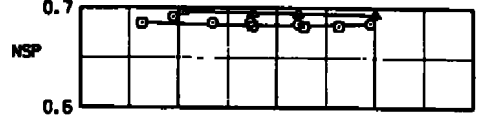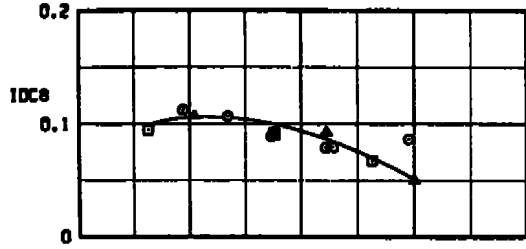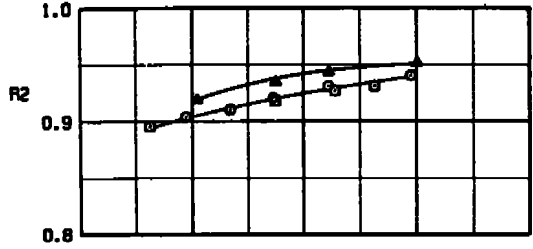
b. Concluded, inboard

Figure 28. Concluded.
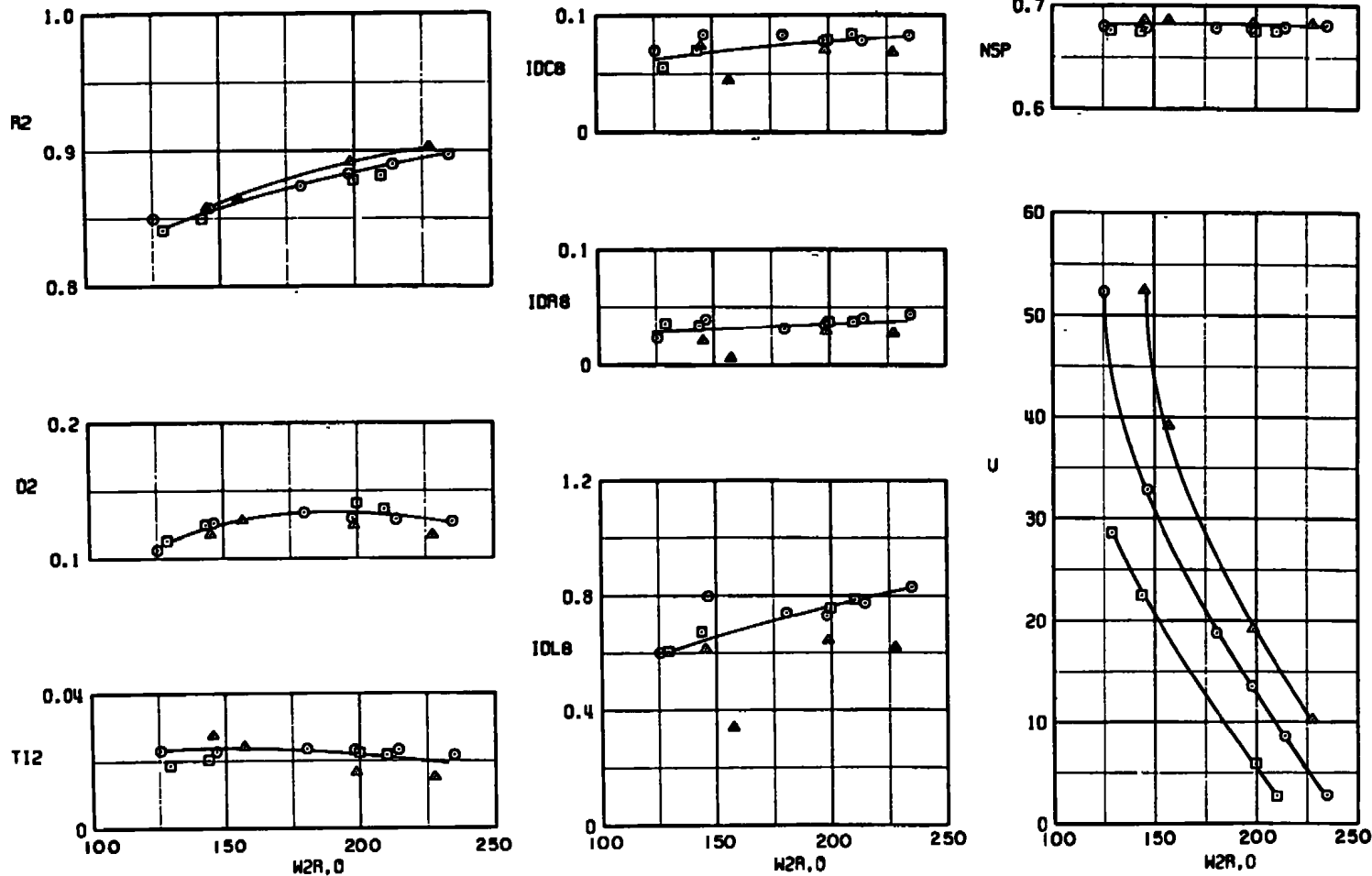
a. M0 = 2.2, outboard

Figure 29. Effects of airflow variations on inlet performance with inlet operated under simulated AICS control, a = 2.5 deg.

SYMBOL	α	ψ	RB	ML	
□	2.5	-3.0	14.0	3.38	2196
⊙	2.5	0	14.0	3.36	2194
▲	2.5	3.0	14.0	3.30	2195
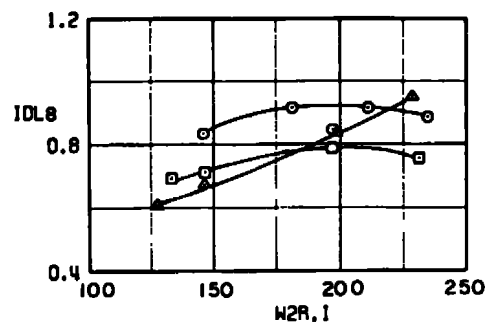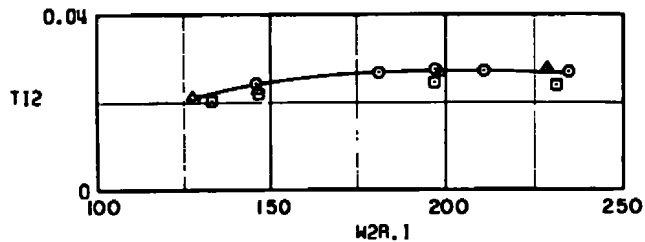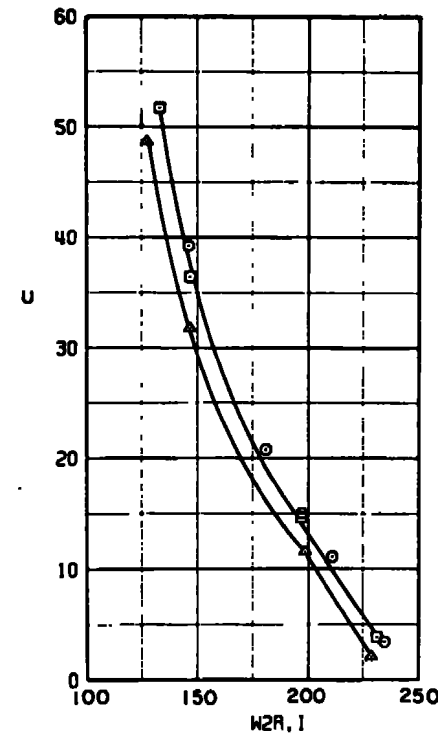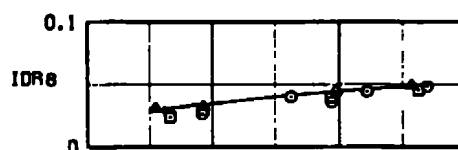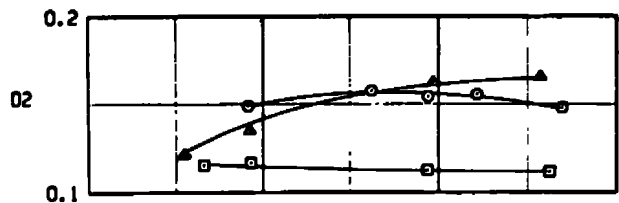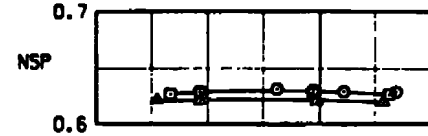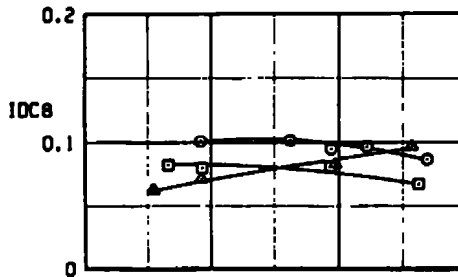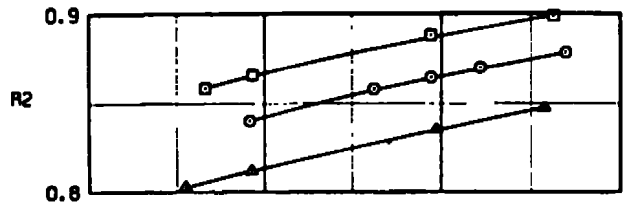
a. Concluded, inboard
Figure 29. Continued.

SYMBOL	∝	ψ	RB	ML	
□	2.5	-3.0	12.6	4.06	2221
⊙	2.5	0	11.5	4.34	2219
▲	2.5	3.0	10.0	4.50	2220
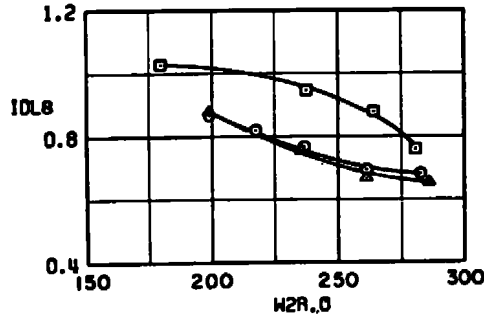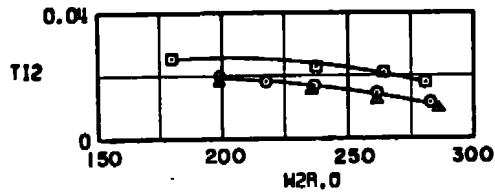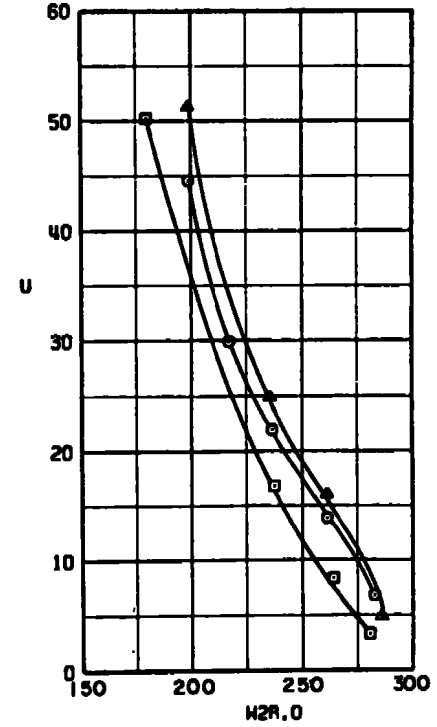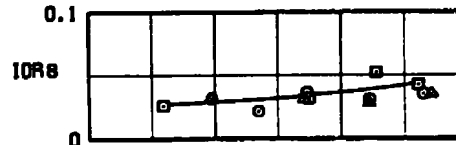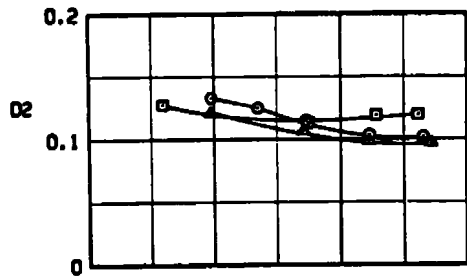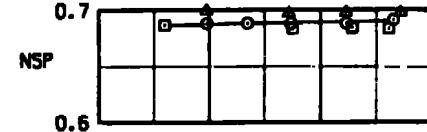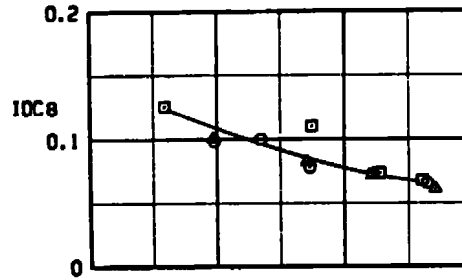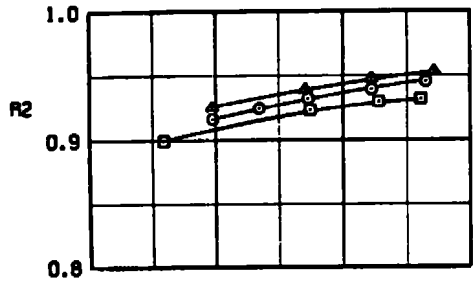
b. M0 = 1.8, outboard

Figure 29. Continued.
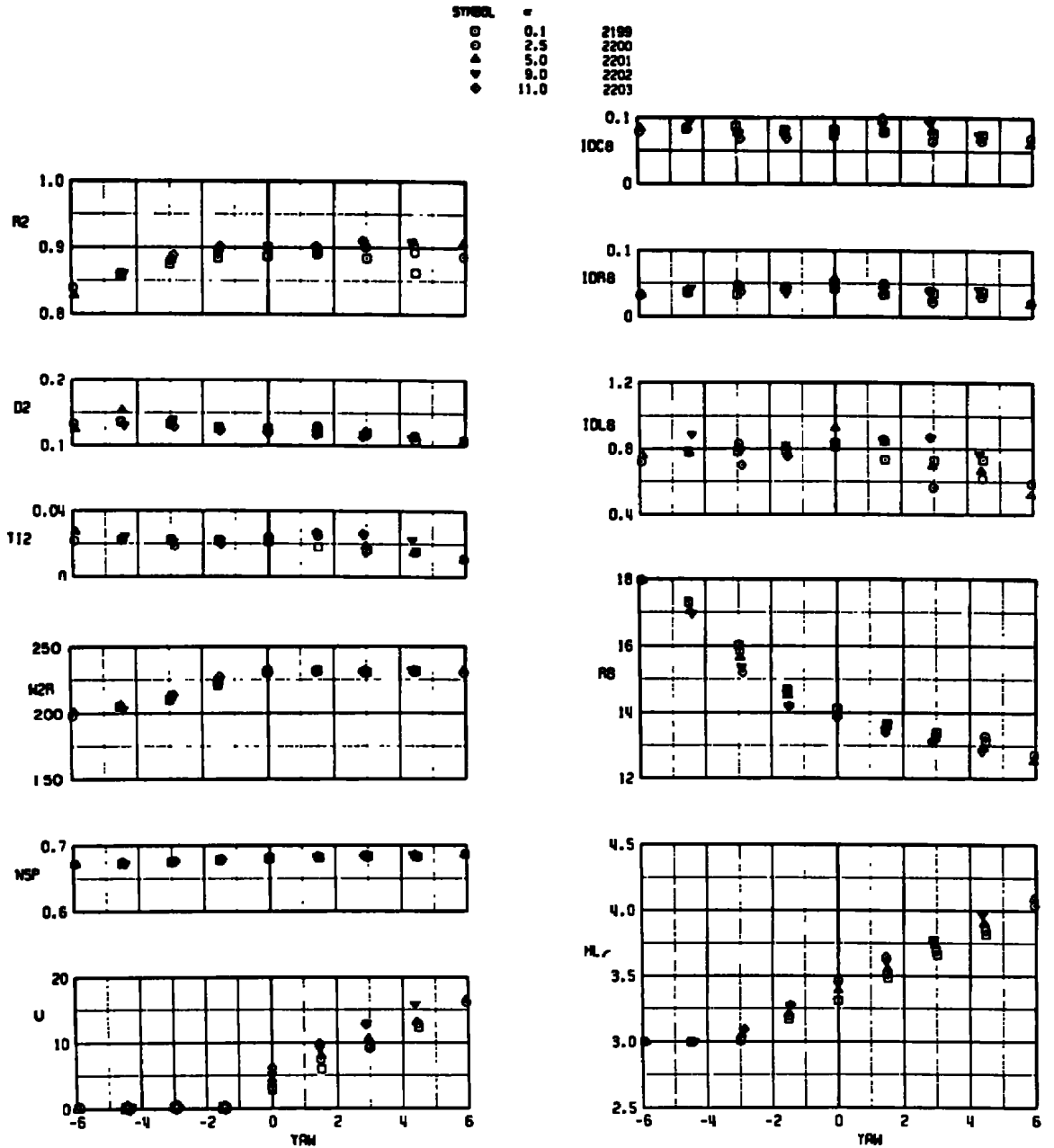
a. M0 = 2.2, outboard

Figure 30. Inlet performance characteristics with inlet operated under simulated AICS control and at engine intermediate airflows.
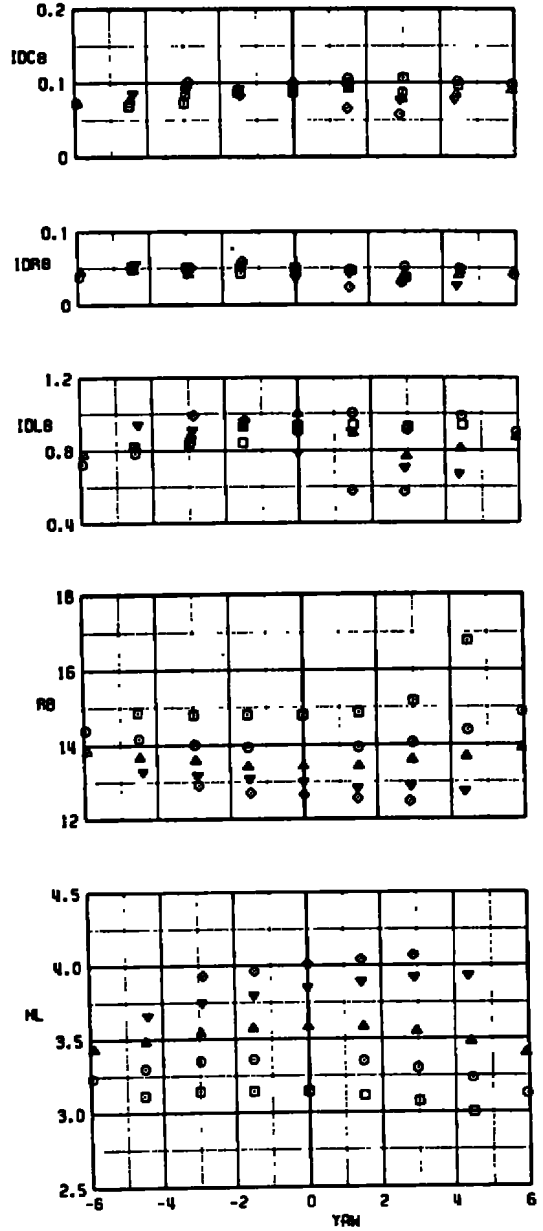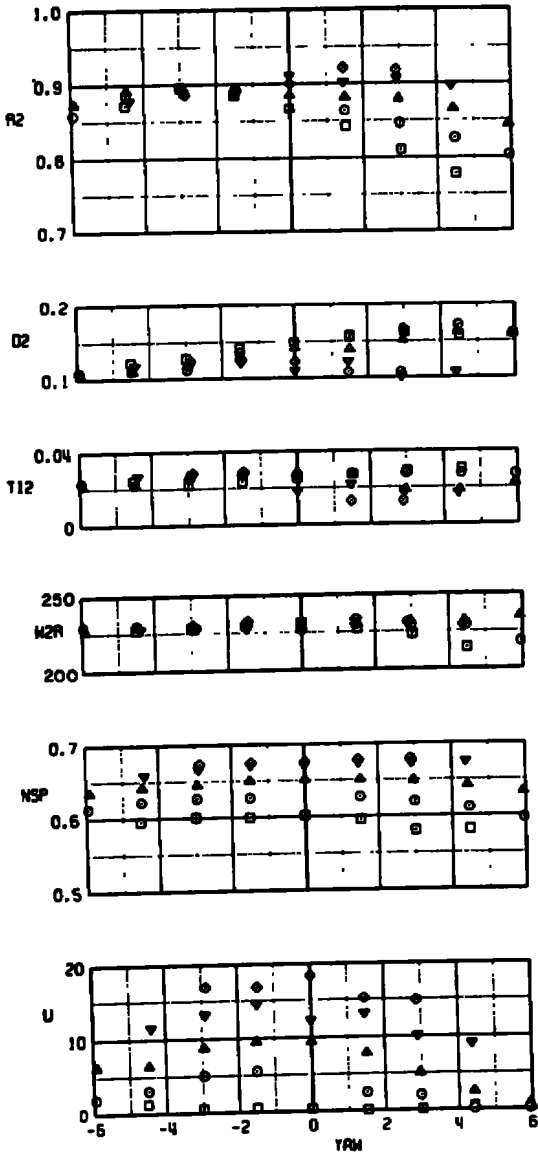
a. Concluded, inboard
Figure 30. Continued.
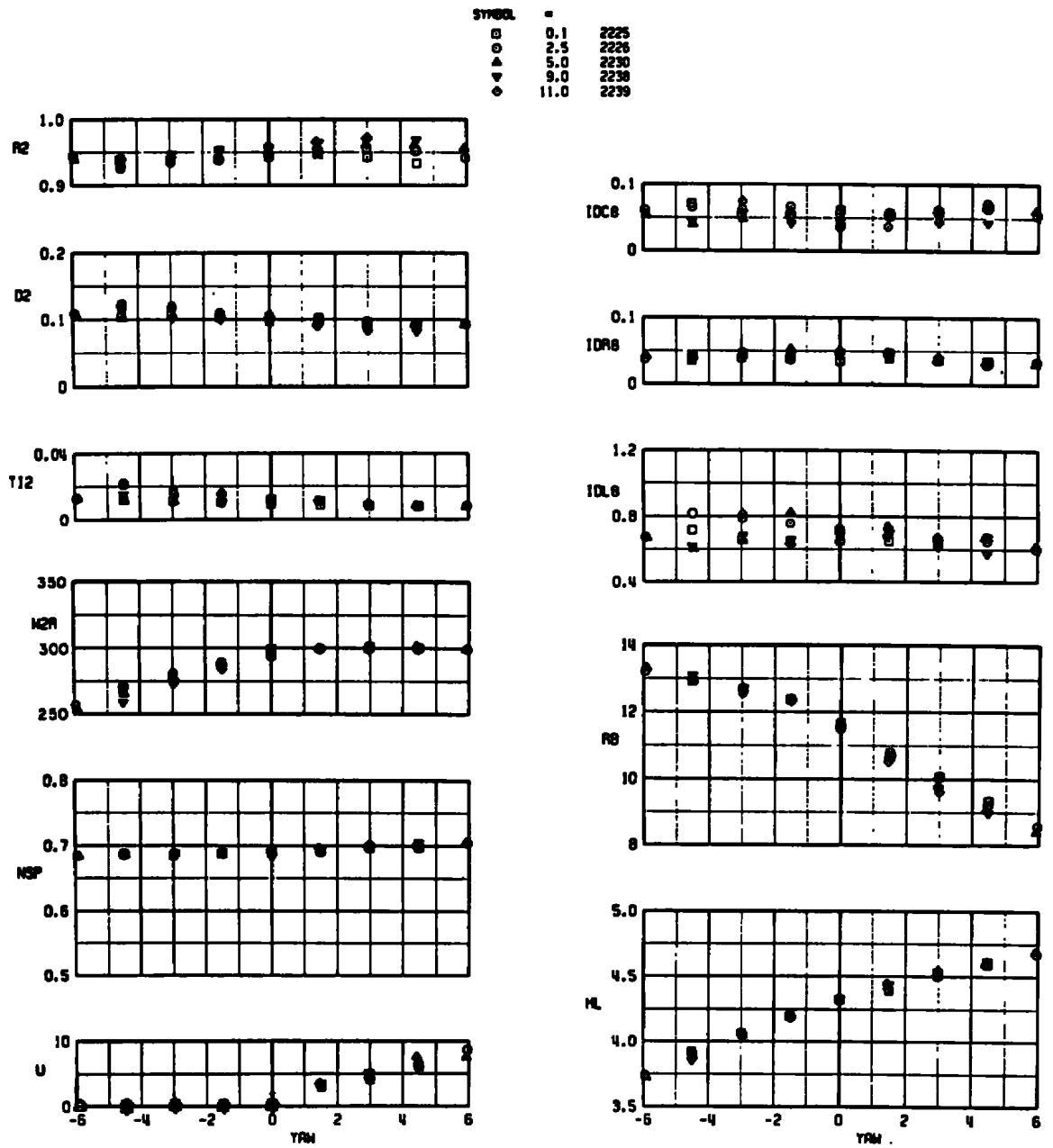
b. M0 = 1.8, outboard
Figure 30. Continued.
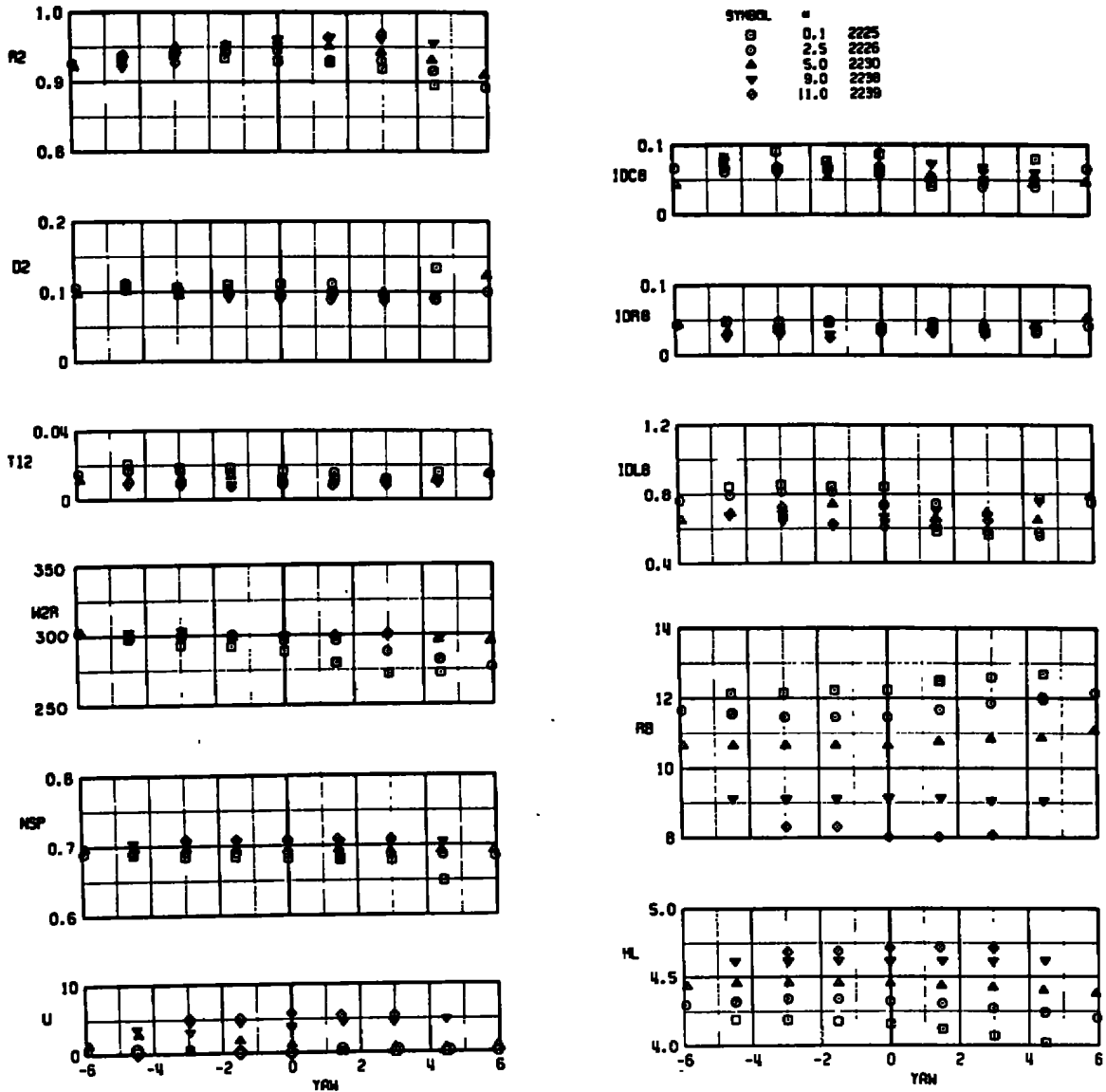
b. Concluded, inboard
Figure 30. Concluded.
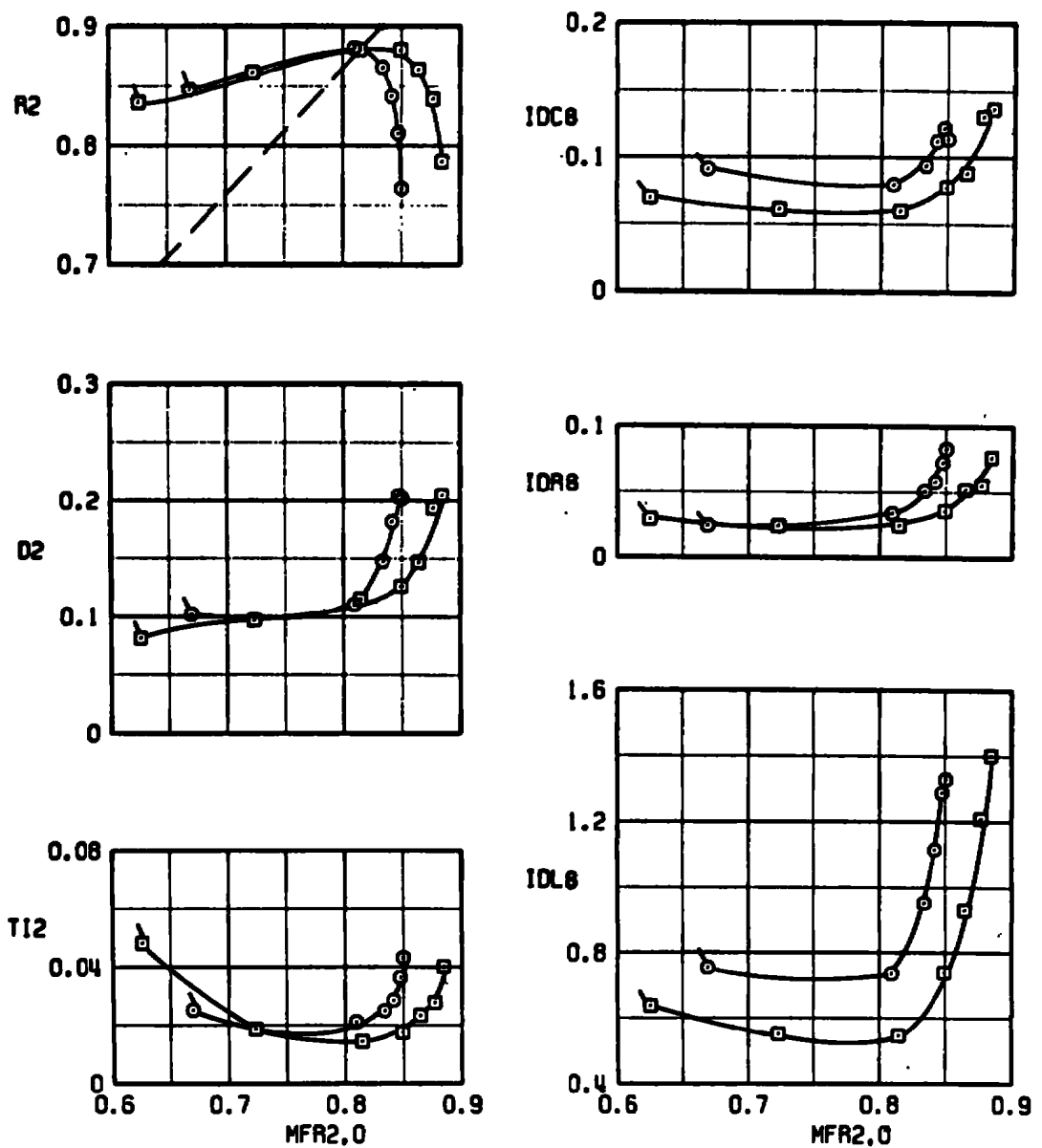
a. a = -2 deg, ψ = 0, outboard

Figure 31. Effects of mispositioned inlet geometry on inlet performance at MO = 2.2.
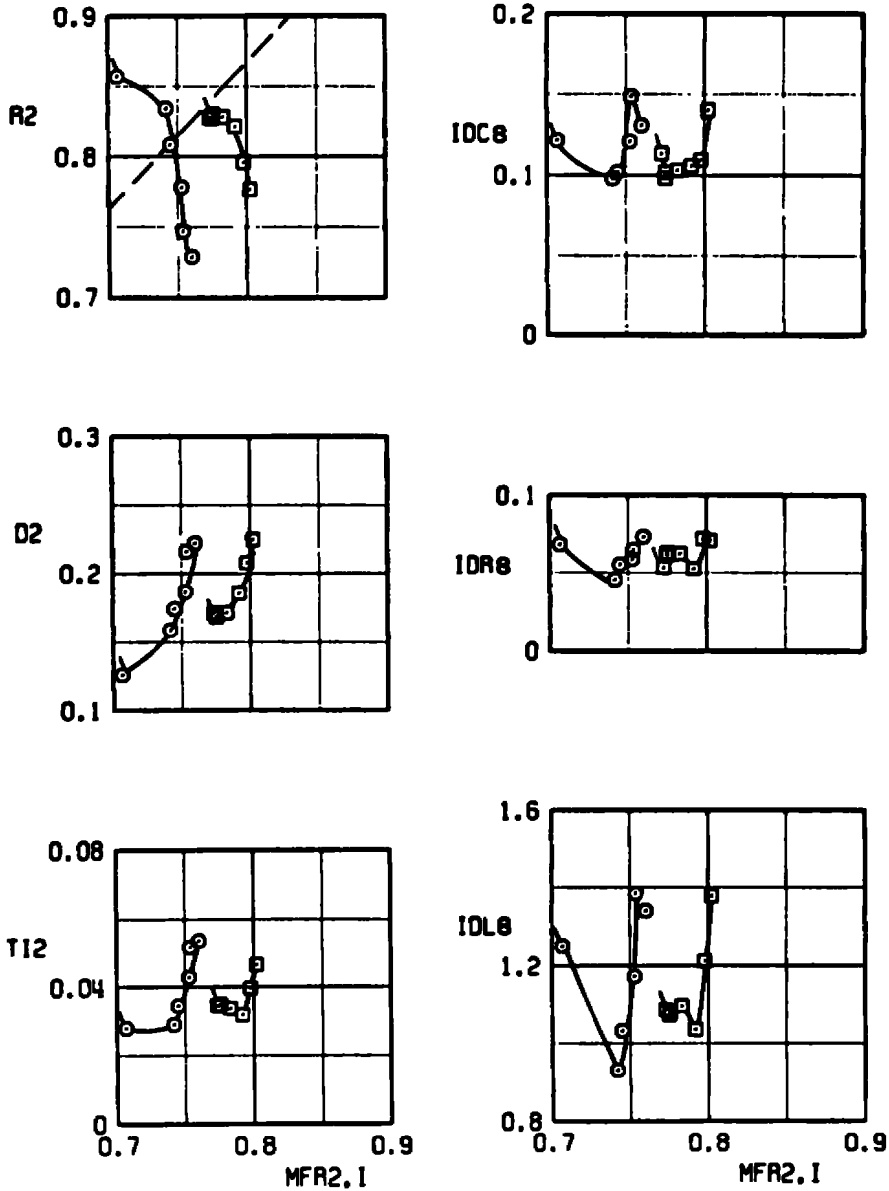
a. Concluded, inboard
Figure 31. Continued.

b. a = 0.1 deg, ψ = 3 deg, outboard
Figure 31. Continued.

b. Concluded, inboard
Figure 31. Continued.

c. a = 2.5 deg, ψ = 4.5 deg, outboard
Figure 31. Continued.

SYMBOL	α	ψ	RB	HL		
⊙	2.5	4.5	14.4	3.23	SCHEDULED	2276
▣	2.5	4.5	16.4	3.03	1-in. FS<SCHEDULED	2286

FLAGGED SYM - STABILITY LIMIT

— — —INTERMEDIATE POWER AIRFLOW, 36K ft

R2

IDC8

D2

IDR8

T12

IDL8

MFR2,I

MFR2,I
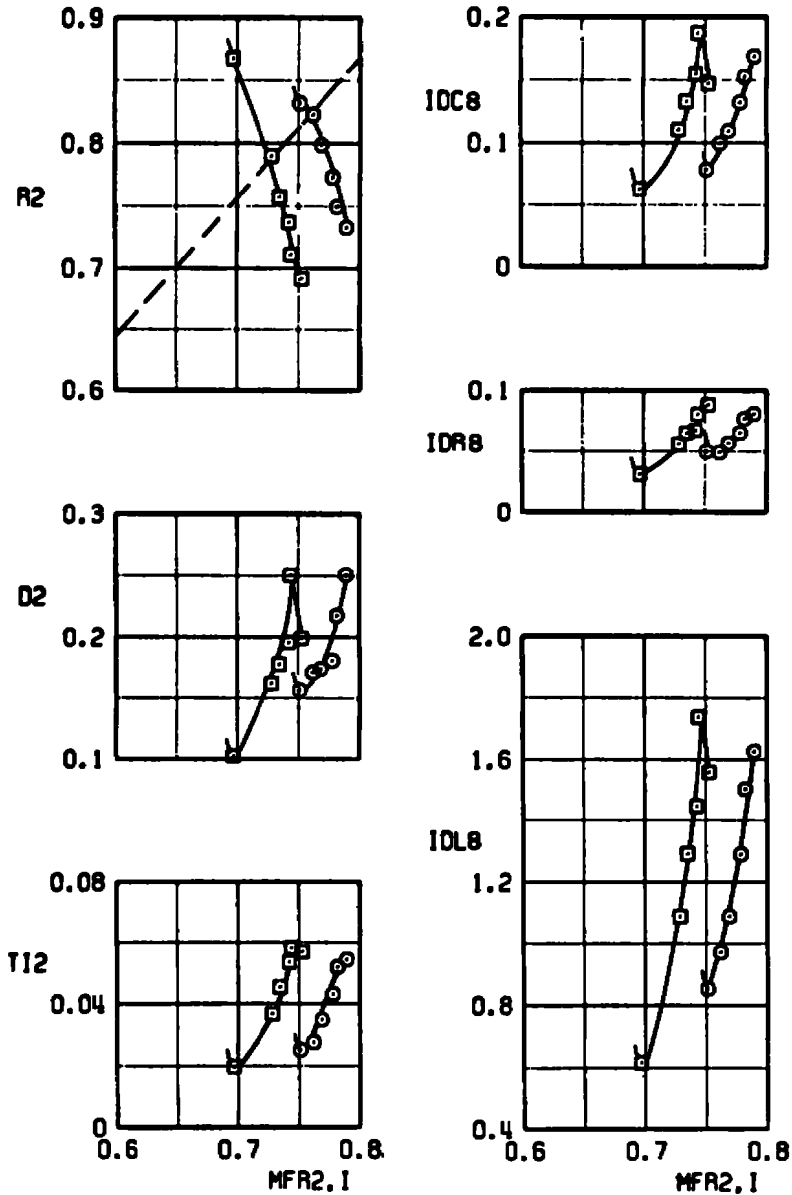
c. Concluded, inboard

Figure 31. Concluded.
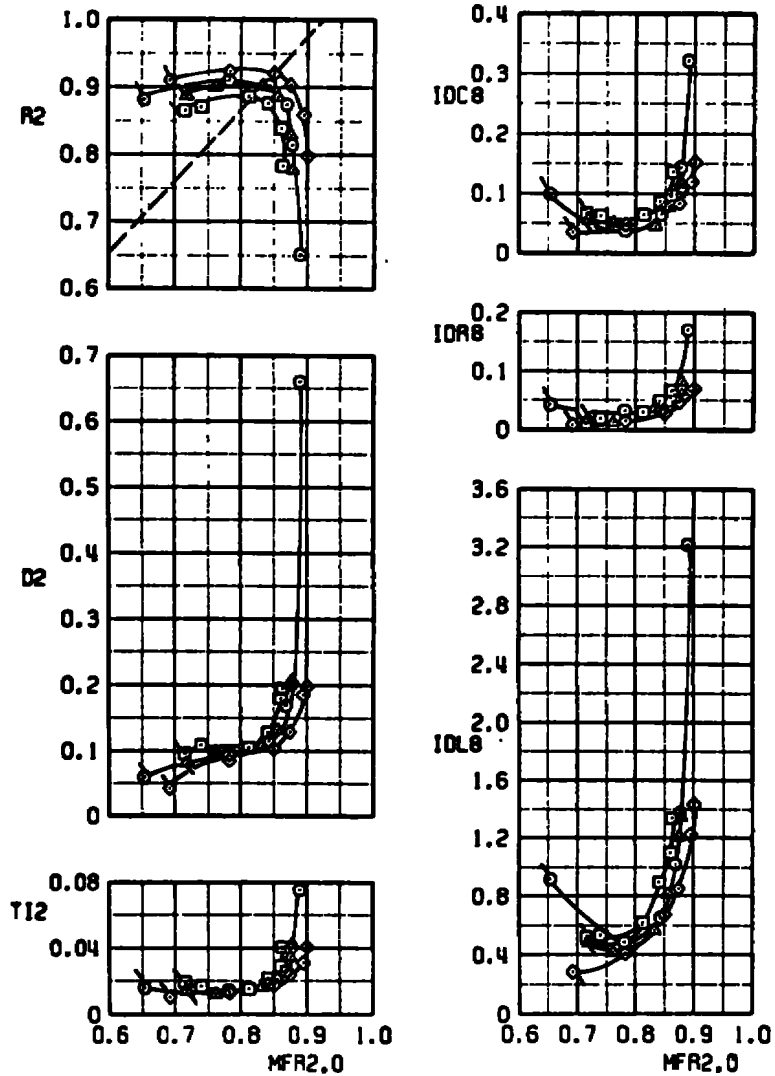
a. a = variable, ψ = variable, outboard

Figure 32. Inlet performance characteristics with MO scheduled geometry at MO = 2.2.
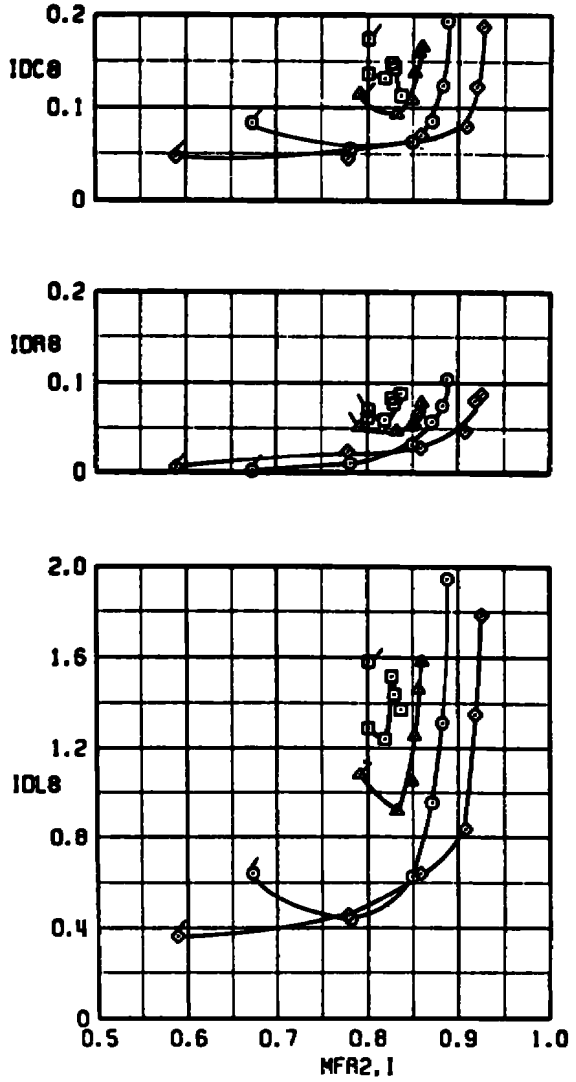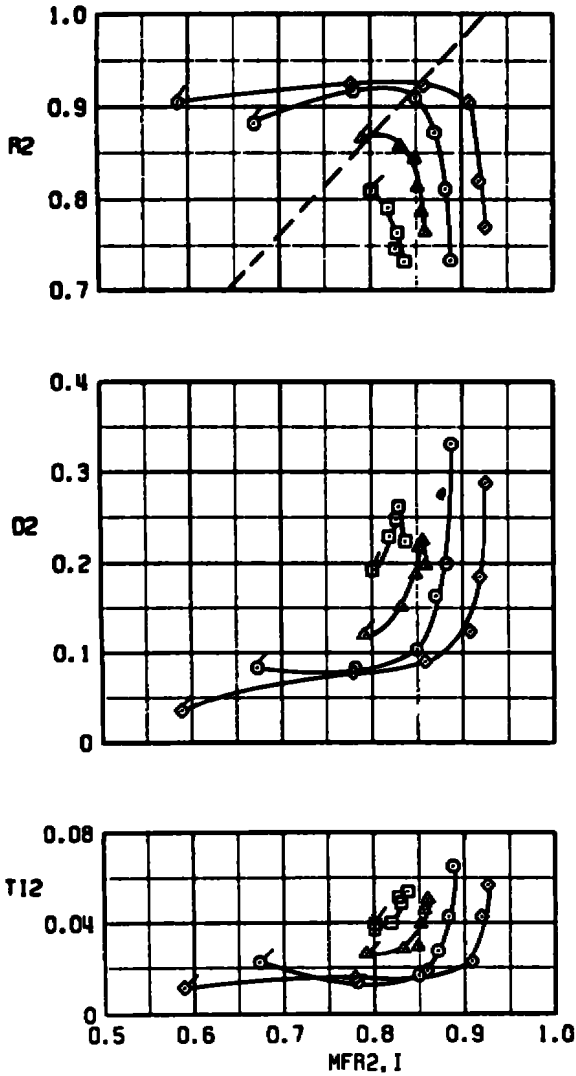
a. Concluded, inboard
Figure 32. Continued.

| SYMBOL	α	ψ	RB	ML	
◻	2.5	-5.8	14.0	3.36	2157
▲	2.5	-2.8	14.0	3.36	2160
◉	2.5	0.0	14.0	3.36	2084
▼	2.5	3.2	14.0	3.36	2161
◇	2.5	5.8	14.0	3.36	2164

FLAGGED SYM - STABILITY LIMIT

― ― ― INTERMEDIATE POWER AIRFLOW, 36K ft
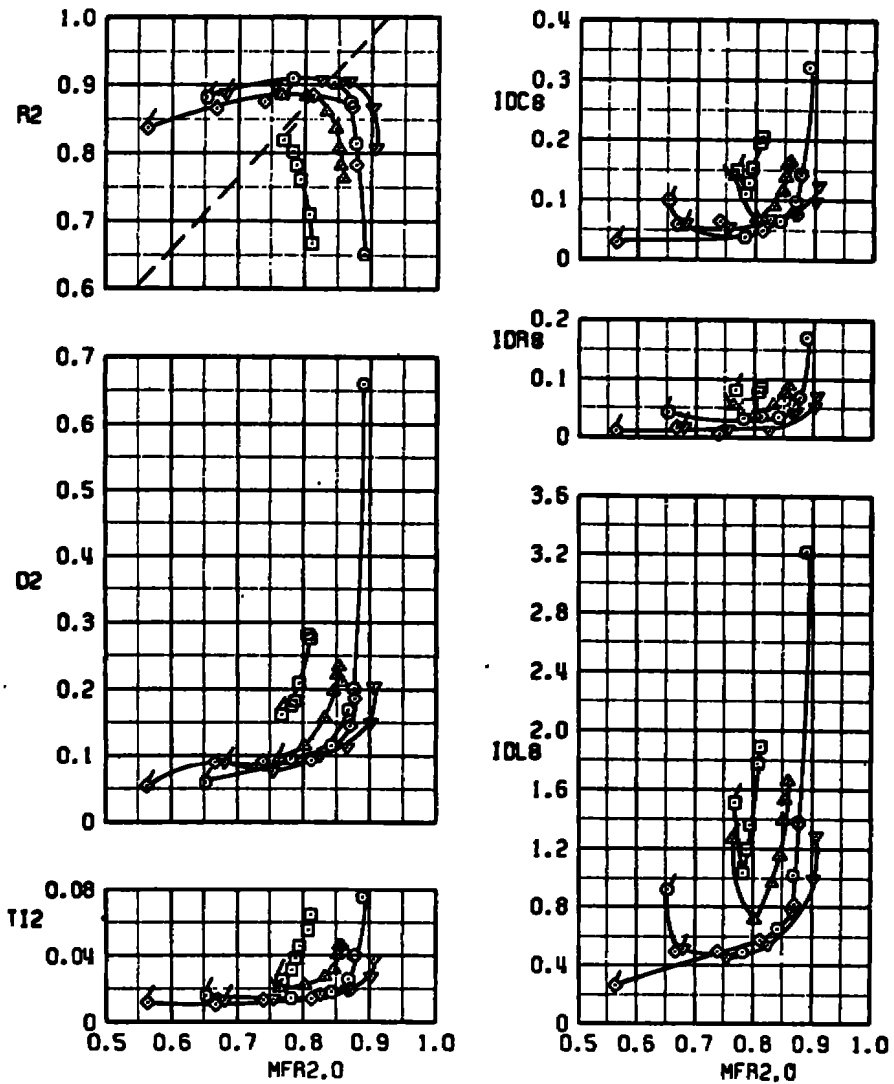
b. a = 2.5 deg, ψ = variable, outboard
Figure 32. Continued.

113

SYMBOL	α	φ	AB	HL	
▢	2.5	-5.8	14.0	3.36	2157
▲	2.5	-2.8	14.0	3.36	2160
◉	2.5	0.0	14.0	3.36	2084
▼	2.5	3.2	14.0	3.36	2161
◈	2.5	5.8	14.0	3.36	2164

FLAGGED SYM - STABILITY LIMIT

— — — INTERMEDIATE POWER AIRFLOW, 36K ft
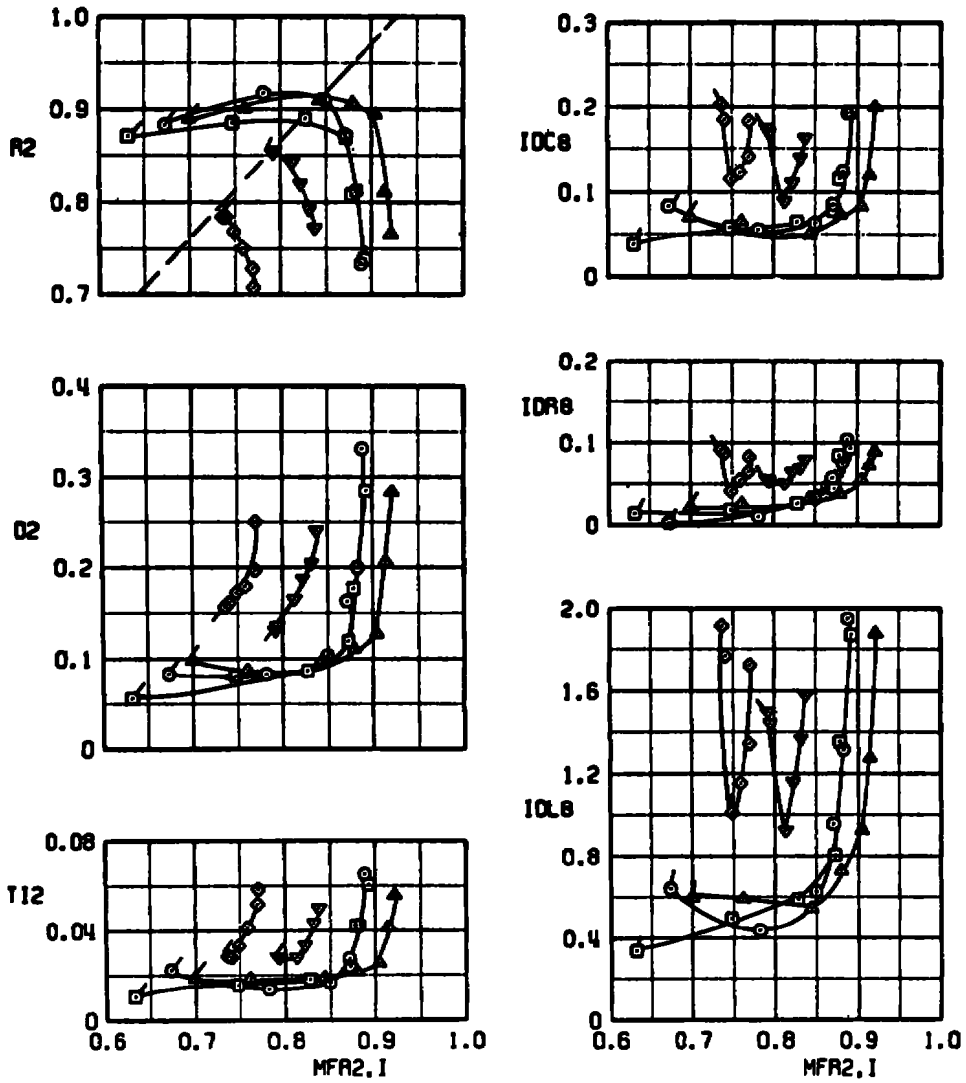
b. Concluded, inboard

Figure 32. Concluded.

114
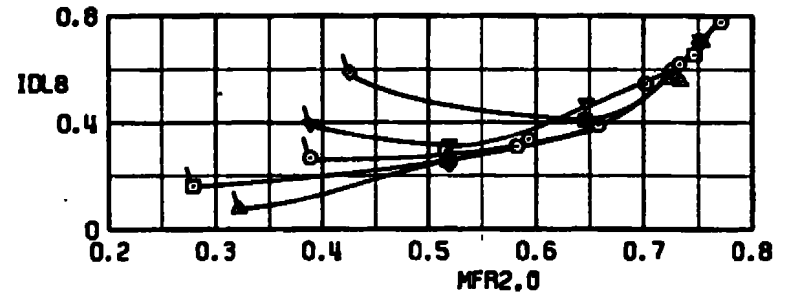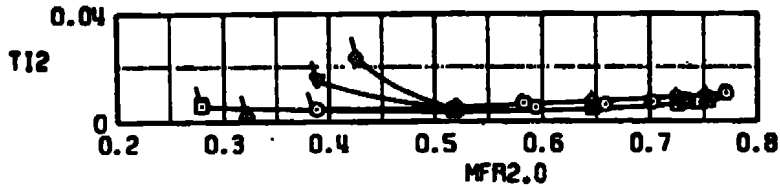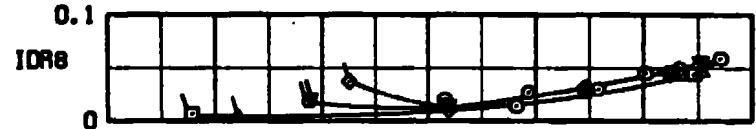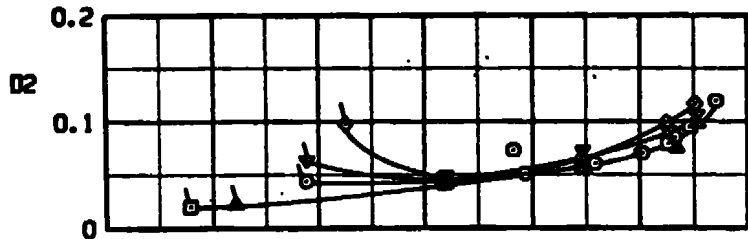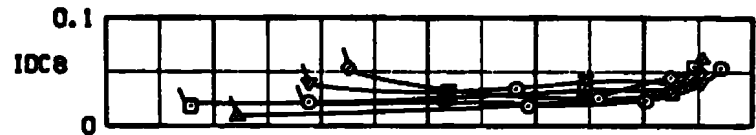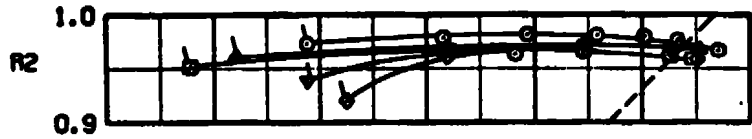
a. M0 = 1.4, a = variable, outboard

Figure 33. Transonic inlet performance characteristics at $\psi = 0$.

SYMBOL	α	ψ	RB	ML	
▢	-2.0	0	7.0	4.87	2694
▲	0.0	0	7.0	4.91	2702
⊙	3.0	0	7.0	5.00	2617
▽	6.0	0	7.0	5.09	2706
◇	9.0	0	7.0	5.19	2709

FLAGGED SYM - STABILITY LIMIT
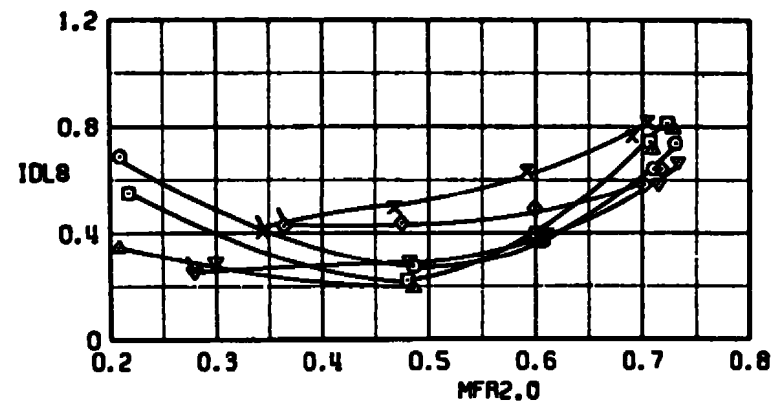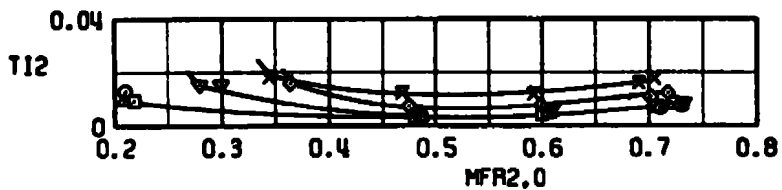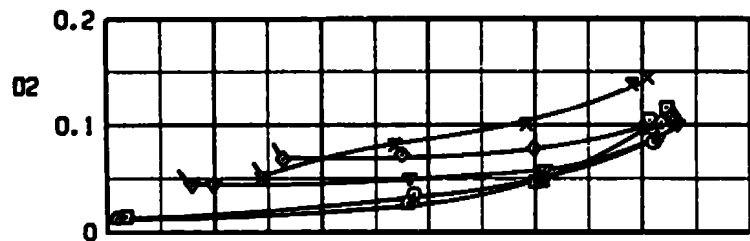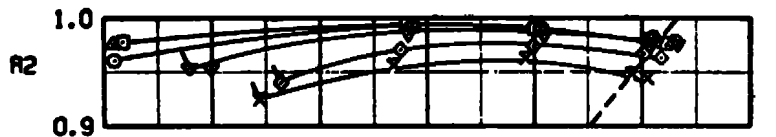
— — —INTERMEDIATE POWER AIRFLOW 36K ft

a. Concluded, inboard

Figure 33. Continued.

b. MO = 0.85, a = variable, outboard

Figure 33. Continued.

b. Concluded, inboard
Figure 33. Concluded.

SYMBOL	α	ψ	RB	ML	
▢	3.0	-4.0	8.2	4.70	2618
▲	3.0	-2.0	7.2	4.87	2619
⊙	3.0	0	7.0	4.91	2617
▽	3.0	2.0	6.9	5.00	2704
◇	3.0	4.0	7.2	5.07	2705

FLAGGED SYM - STABILITY LIMIT

— — —INTERMEDIATE POWER AIRFLOW, 36K ft
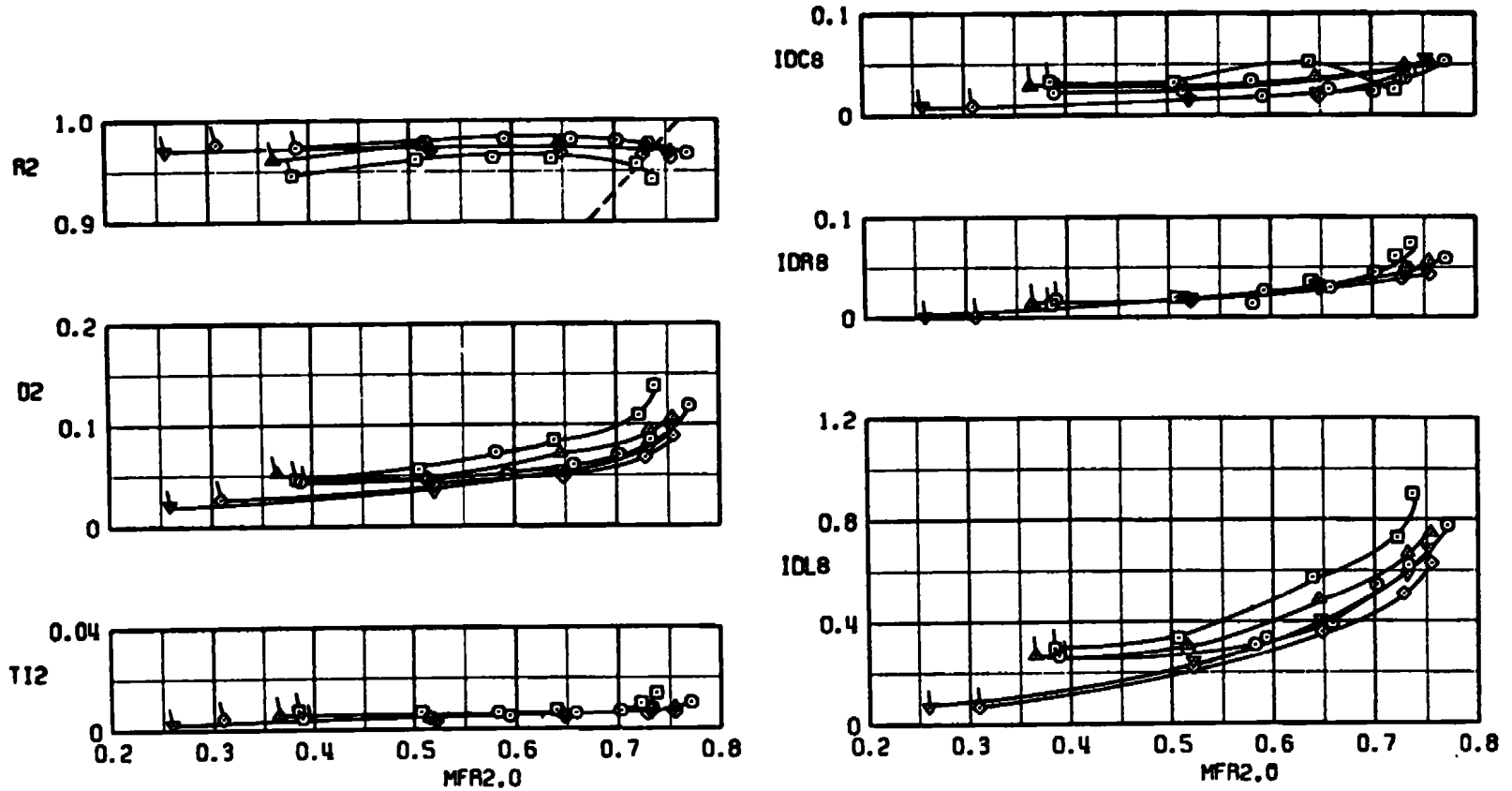
a. M0 = 1.4, ψ = variable, outboard

Figure 34. Transonic inlet performance characteristics at a = 3.0 deg.

SYMBOL	α	ψ	AB	ML	
□	3.0	-4.0	7.0	4.99	2618
▲	3.0	-2.0	7.0	5.03	2619
⊙	3.0	0	7.0	5.00	2617
▼	3.0	2.0	7.0	4.99	2704
◈	3.0	4.0	7.0	4.99	2705

FLAGGED SYM - STABILITY LIMIT

— — —INTERMEDIATE POWER AIRFLOW, 36K ft
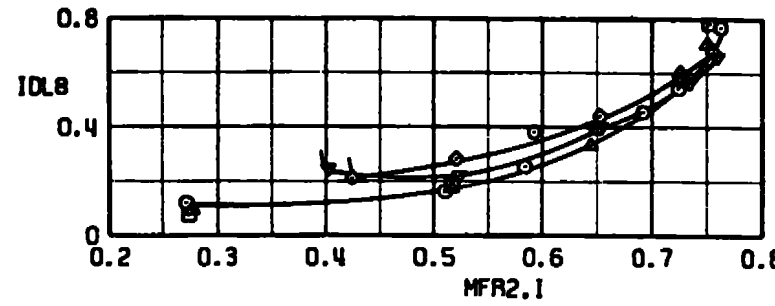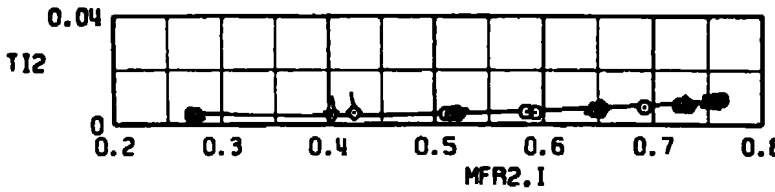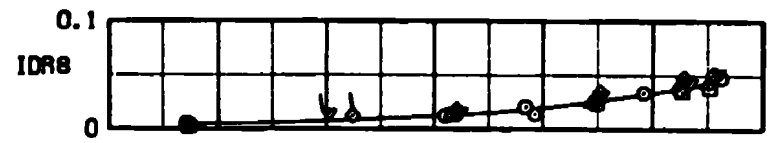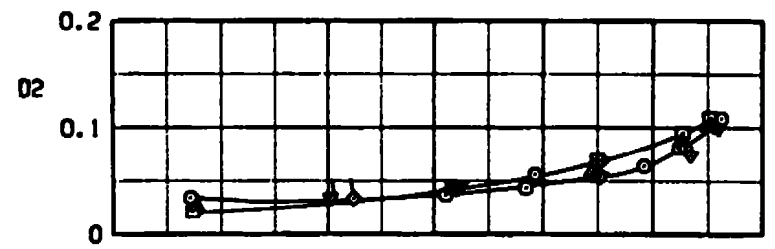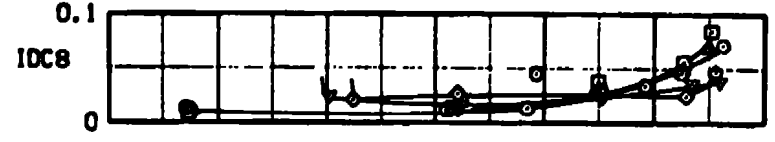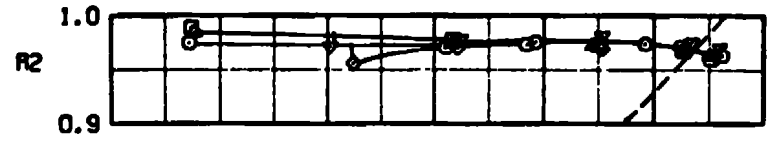
a. Concluded, inboard

Figure 34. Continued.

SYMBOL	α	ψ	RB	HL	
▢	3.1	-5.0	7.0	5.08	2629
▲	3.0	-2.0	7.2	5.46	2630
☉	3.0	0	7.2	5.45	2631
▼	3.0	2.0	7.2	5.45	2632
◈	3.1	5.0	7.2	5.45	2633

FLAGGED SYM - STABILITY LIMIT

— — — INTERMEDIATE POWER AIRFLOW, 36K ft

b. M0 = 0.85, ψ = variable, outboard

Figure 34. Continued.
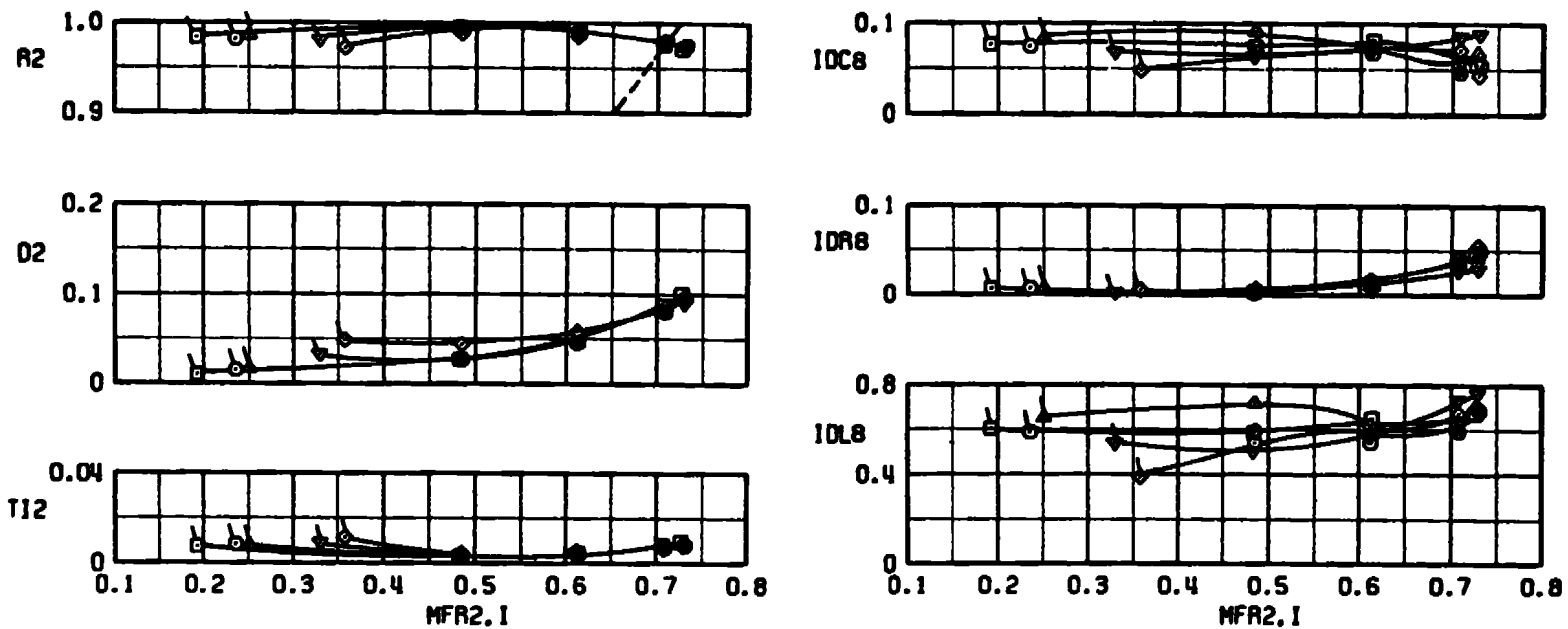
b. Concluded, inboard

Figure 34. Concluded.
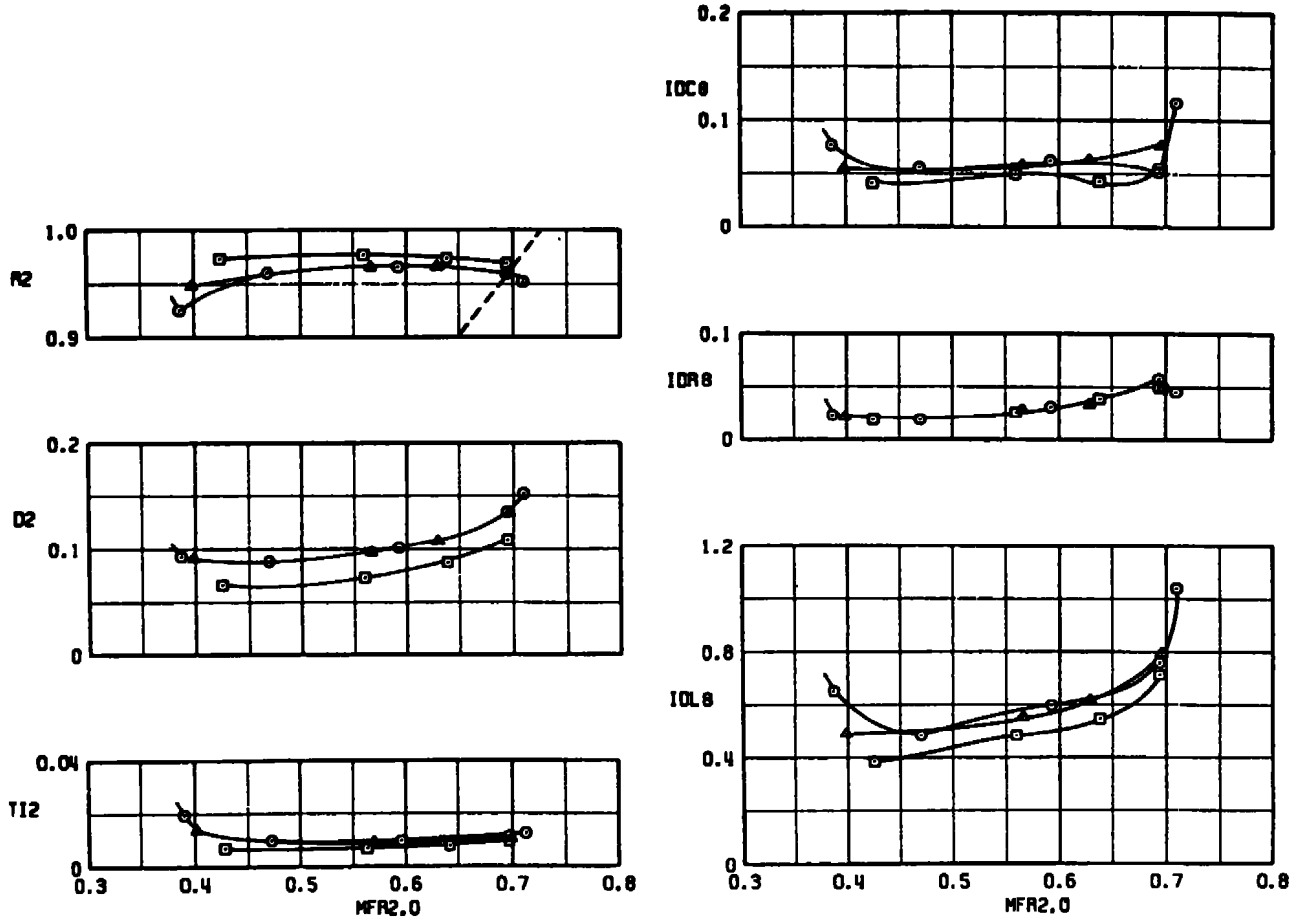
a. ψ = -5 deg, outboard

Figure 35. Effects of opened weapons bay doors and EVS pods at M0 = 0.85.

a. Concluded, inboard
Figure 35. Continued.

SYMBOL	α	ψ	RB	ML		
⊙	3.0	0	7.0	5.46	CLEAN FUSELAGE	2631
⊡	3.0	0	7.0	5.46	WEAPONS BAY DOORS OPEN	2541
▲	3.0	0	7.0	5.46	EVS PODS INSTALLED	2664

FLAGGED SYM STABILITY LIMIT

——— INTERMEDIATE POWER AIRFLOW, 36K ft
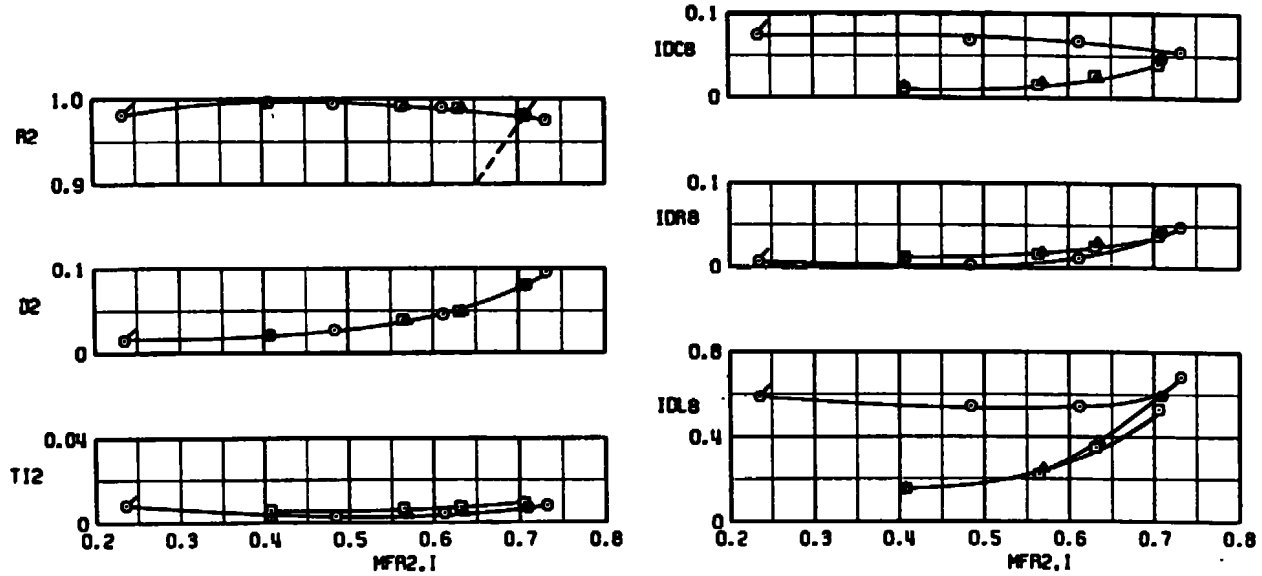
b. $\psi = 0$, outboard
Figure 35. Continued.

AEDC-TR-75-57

SYMBOL	α	ψ	RB	HL		
⊙	3.0	0	7.2	5.45	CLEAN FUSELAGE	2631
⊟	3.0	0	7.1	5.46	WEAPONS BAY DOORS OPEN	2541
▲	3.0	0	7.1	5.46	EVS PODS INSTALLED	2654

FLAGGED SYM - STABILITY LIMIT
— — — INTERMEDIATE POWER AIRFLOW, 36K ft
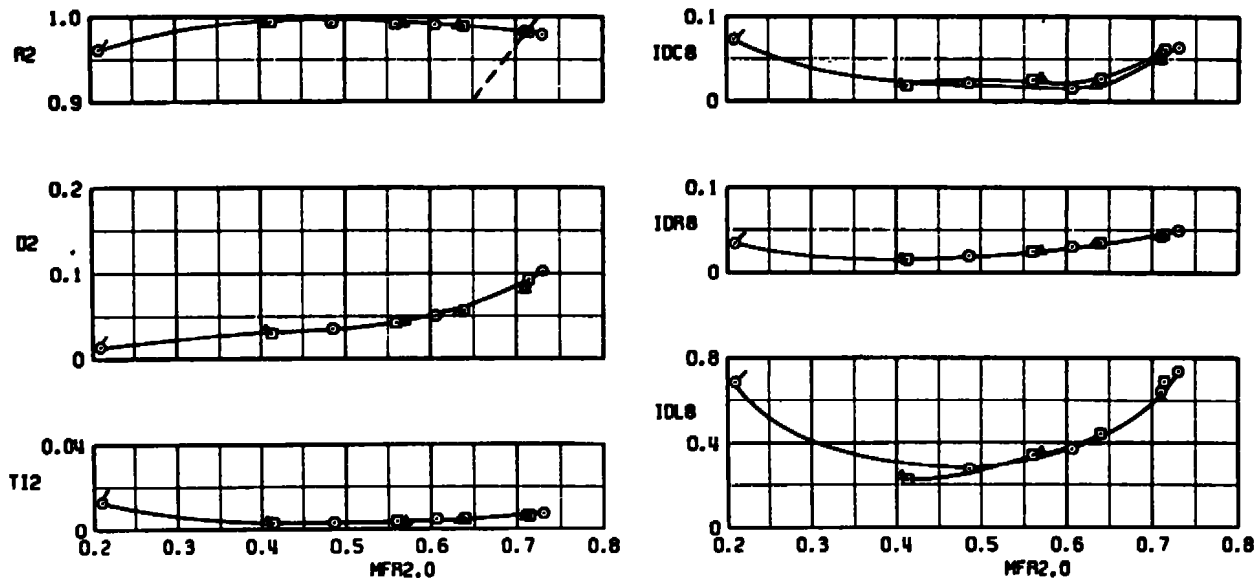
b. Concluded, inboard
Figure 35. Continued.

SYMBOL	α	φ	RB	HL		
⊙	3.1	5.0	7.2	5.45	CLEAN FUSELAGE	2639
▢	3.1	5.0	7.1	5.45	WEAPONS BAY DOORS OPEN	2542

FLAGGED SYM STABILITY LIMIT
———INTERMEDIATE POWER AIRFLOW, 36K ft
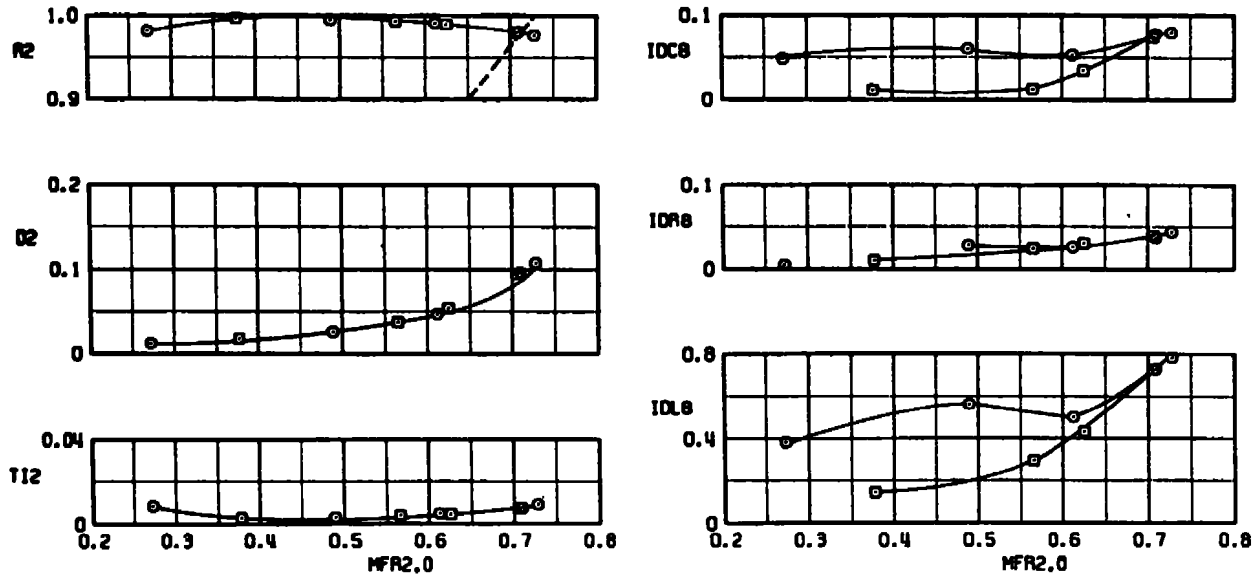
c. ψ = 5 deg, outboard

Figure 35. Continued.

SYMBOL	α	ψ	RB	ML		
⊙	3.1	5.0		5.46	CLEAN FUSELAGE	2633
⊡	3.1	5.0	7.0	5.46	WEAPONS BAY DOORS OPEN	2542

FLAGGED SYM STABILITY LIMIT

——— INTERMEDIATE POWER AIRFLOW, 36K ft
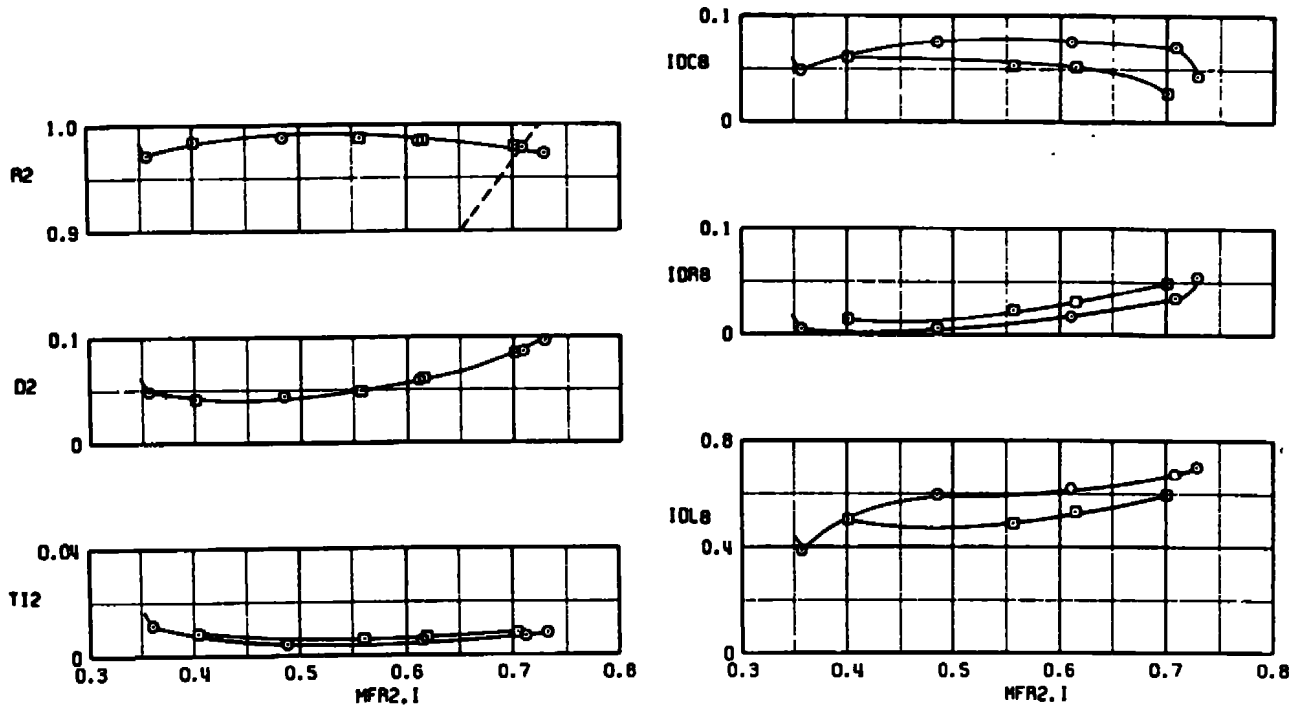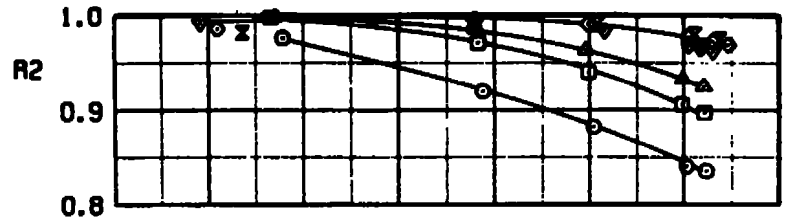
c. Concluded, inboard

Figure 35. Concluded.
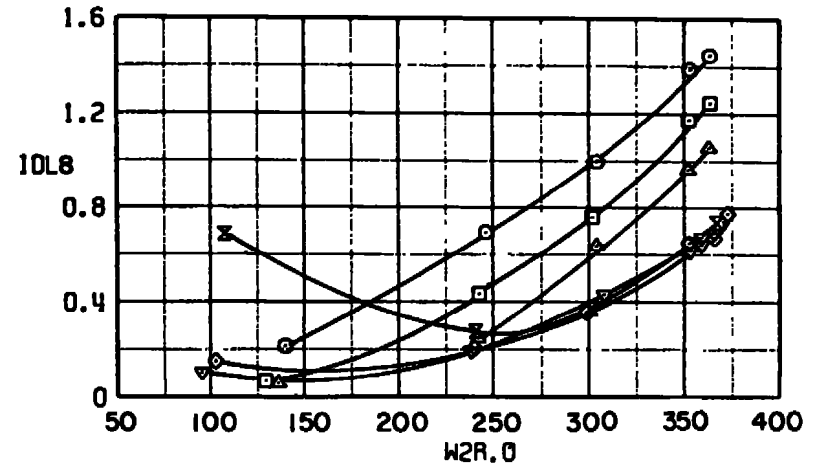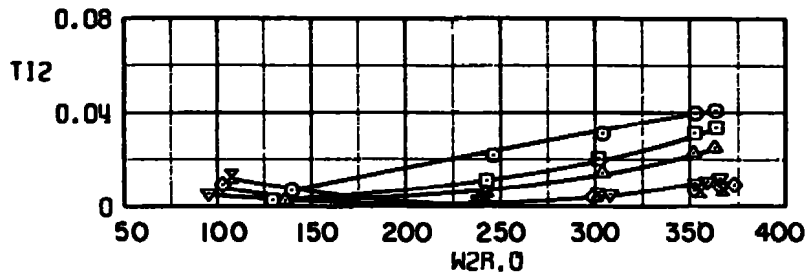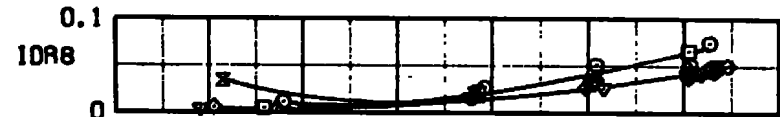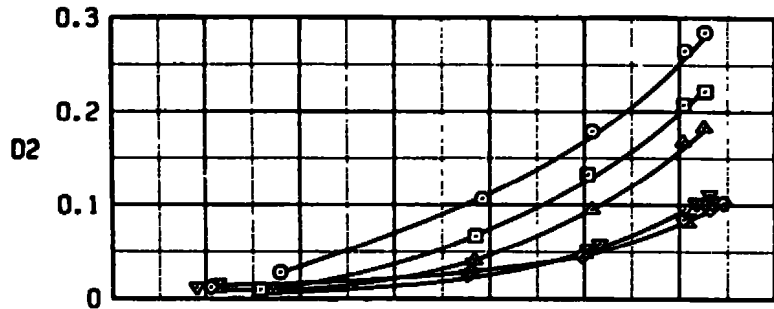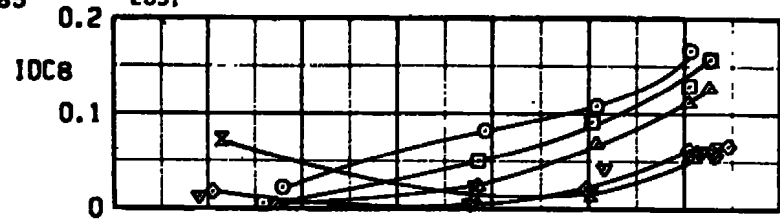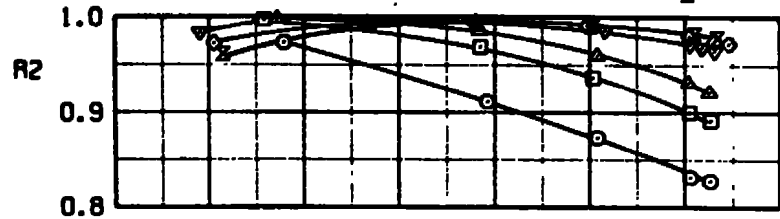
a. Cruise cowl, outboard

Figure 36. Effects of cruise and takeoff cowl lip positions on subsonic inlet performance.

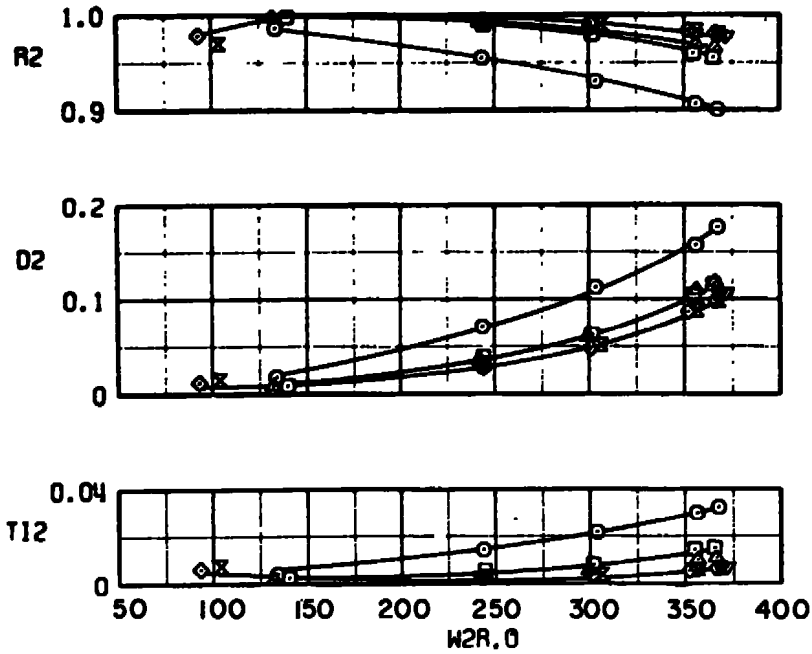| SYMBOL	MO	
⊙	0	2571
⊡	0.20	2575
△	0.30	2580
▽	0.55	2659
◇	0.70	2657
X	0.85	2631

FLAGGED SYM- STABILITY LIMIT

a. Concluded, inboard

Figure 36. Continued.
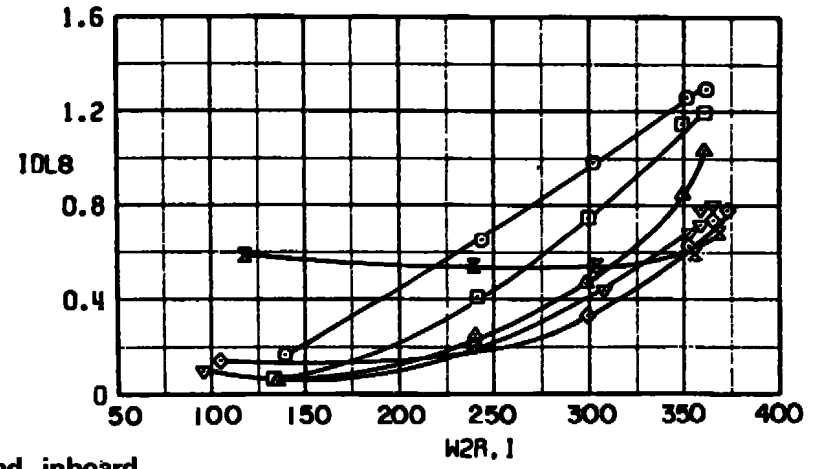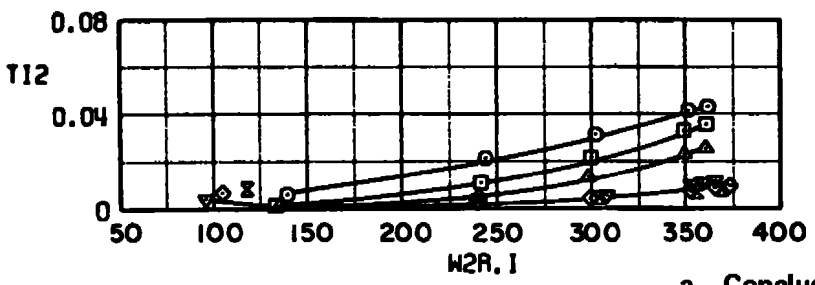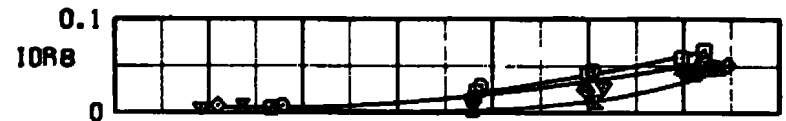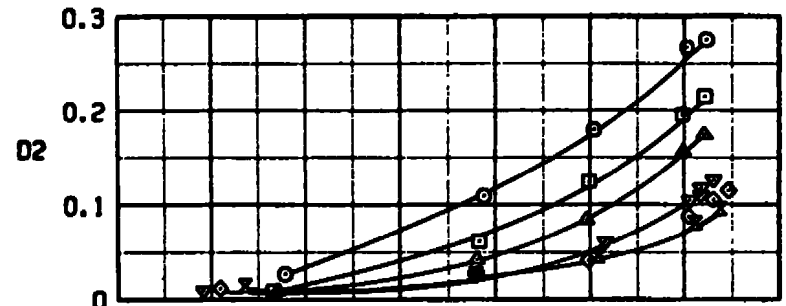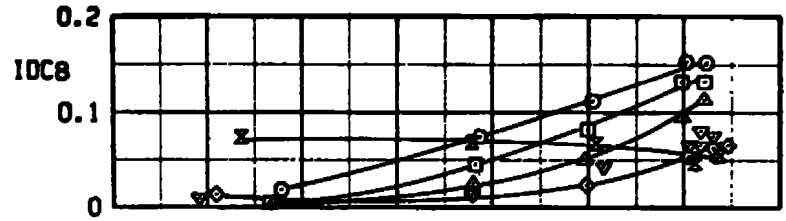
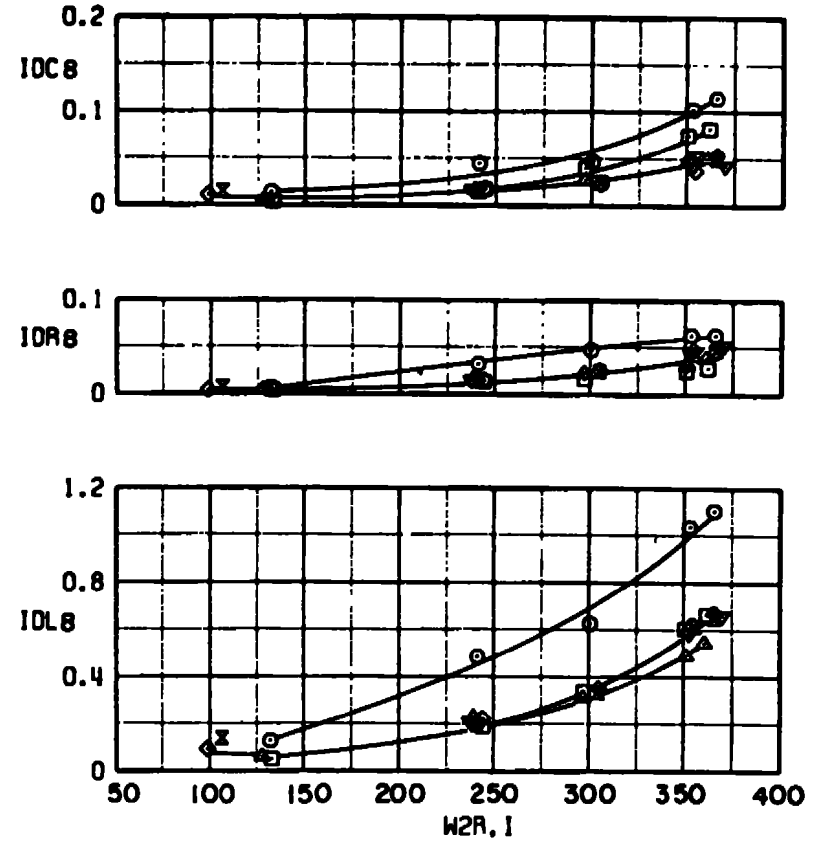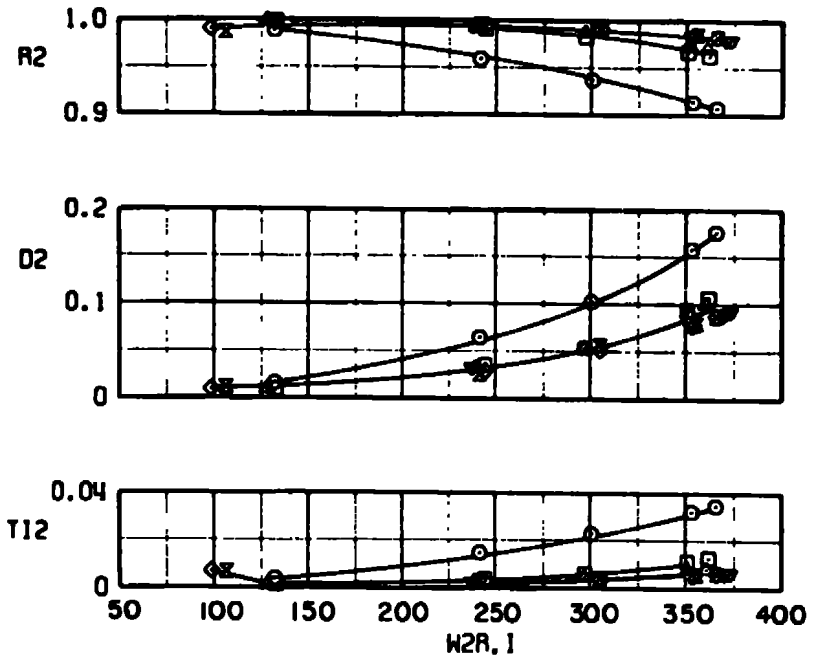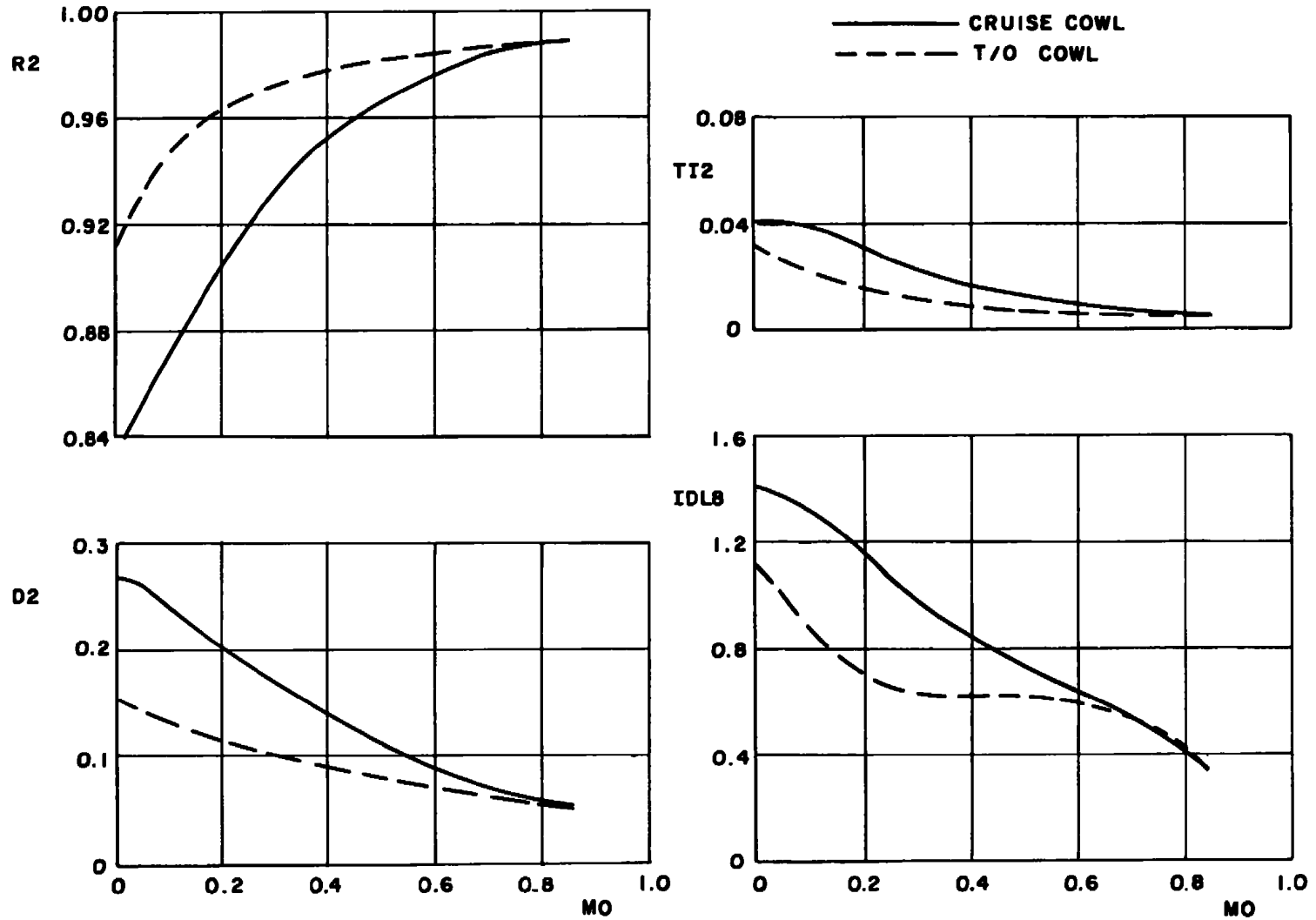b. Takeoff cowl, outboard
Figure 36. Continued.

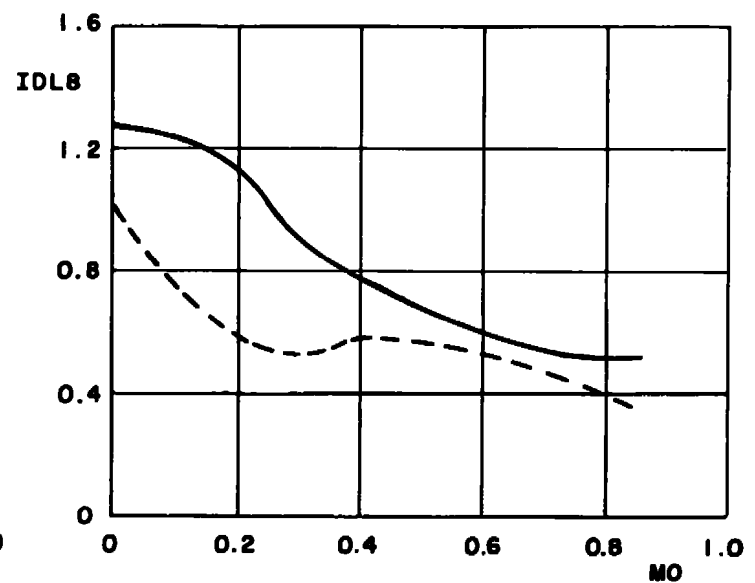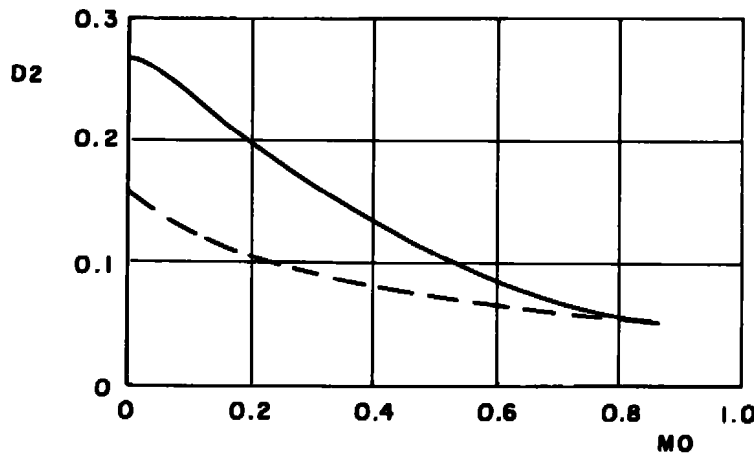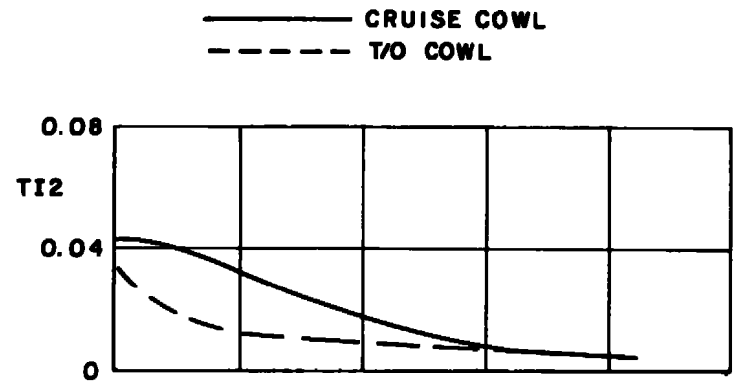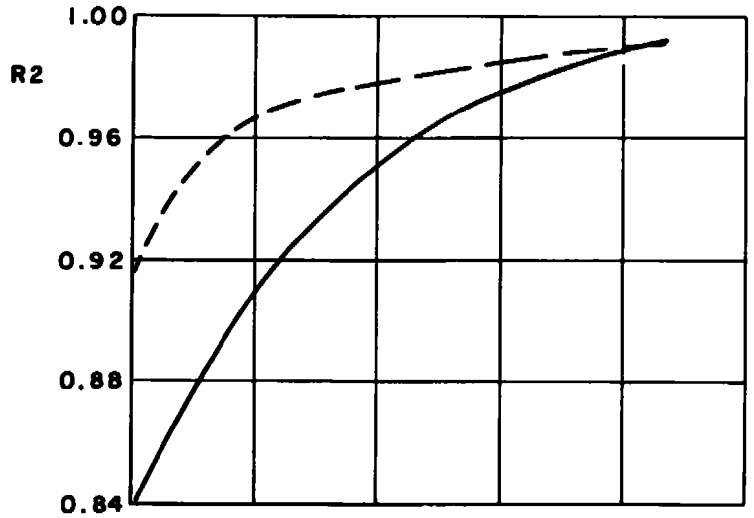| SYMBOL	MO	
⊙	0	2588
▢	0.20	2589
▲	0.30	2593
▼	0.55	2686
◈	0.70	2685
⊠	0.85	2683

b. Concluded, inboard
Figure 36. Concluded.

a. Outboard

Figure 37. Subsonic inlet performance characteristics as a function of Mach number.
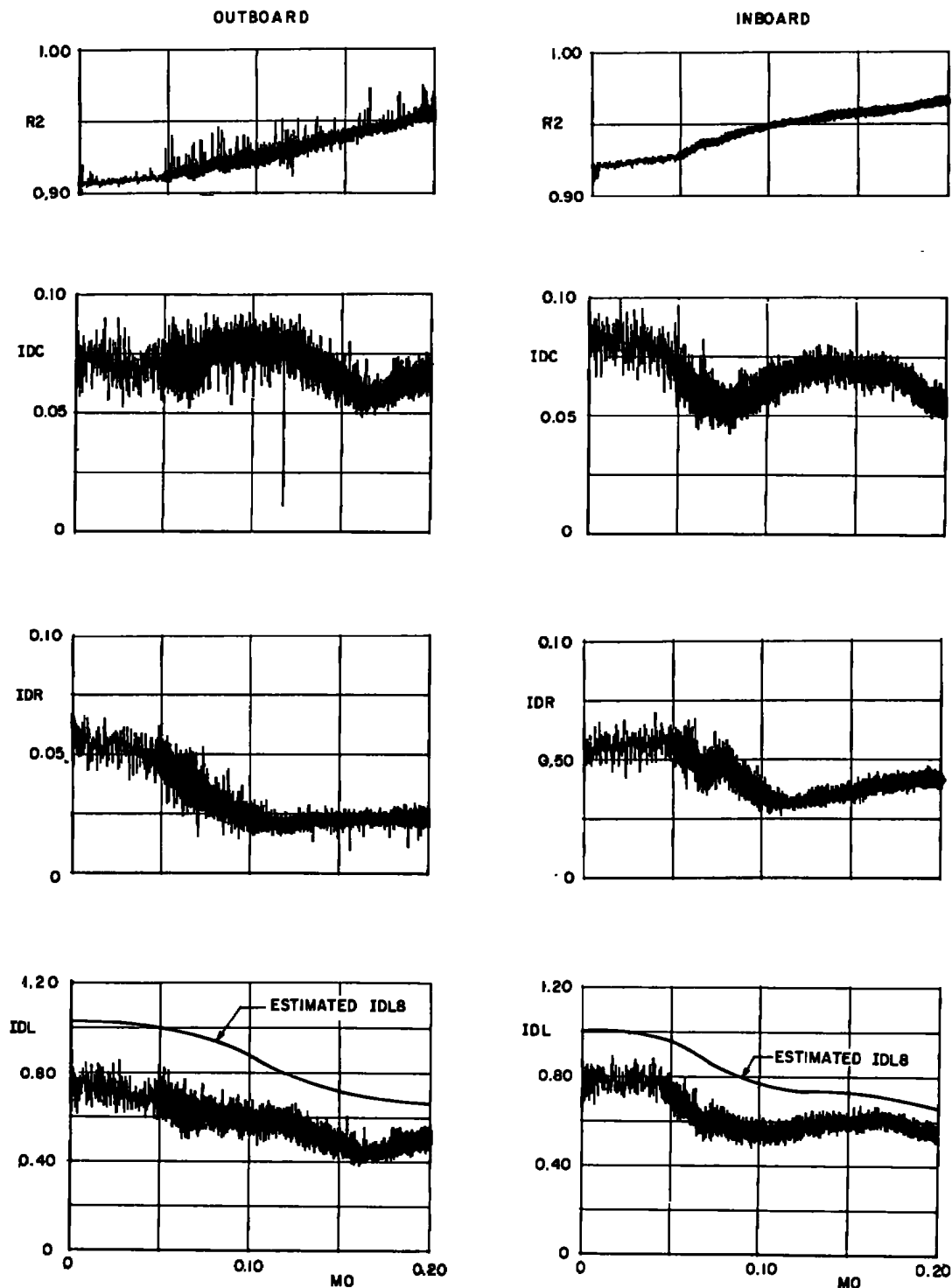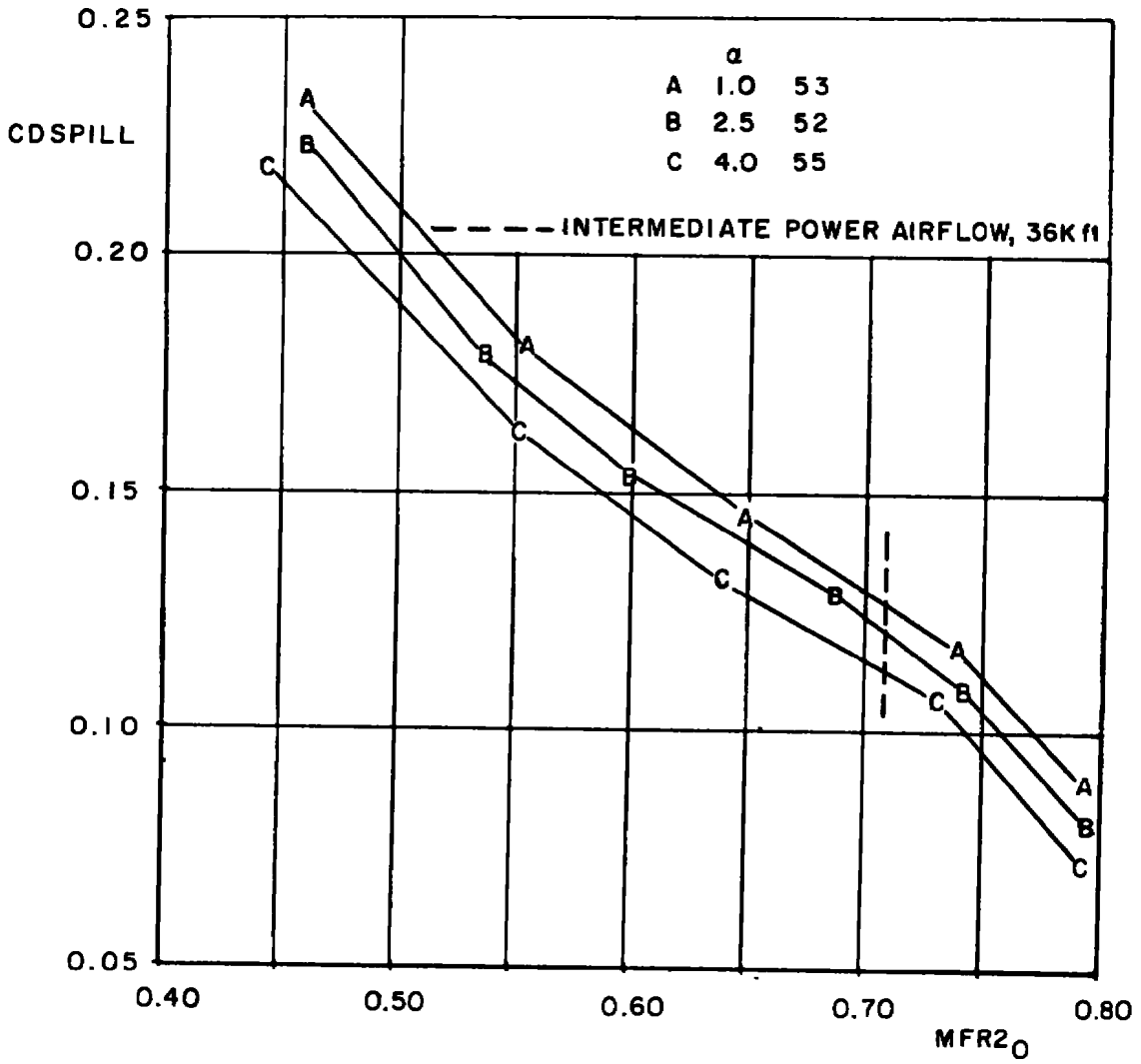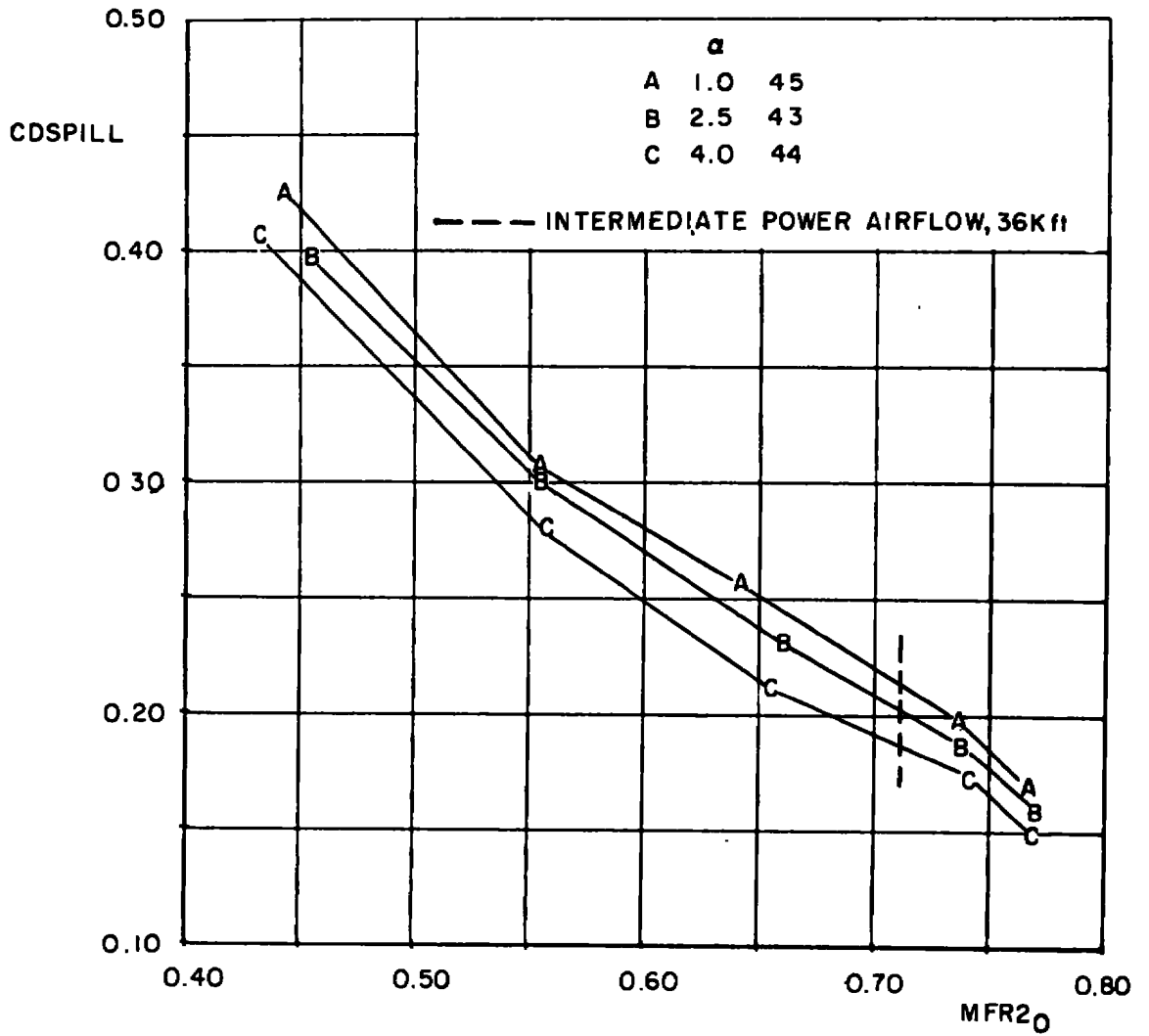
b. Inboard
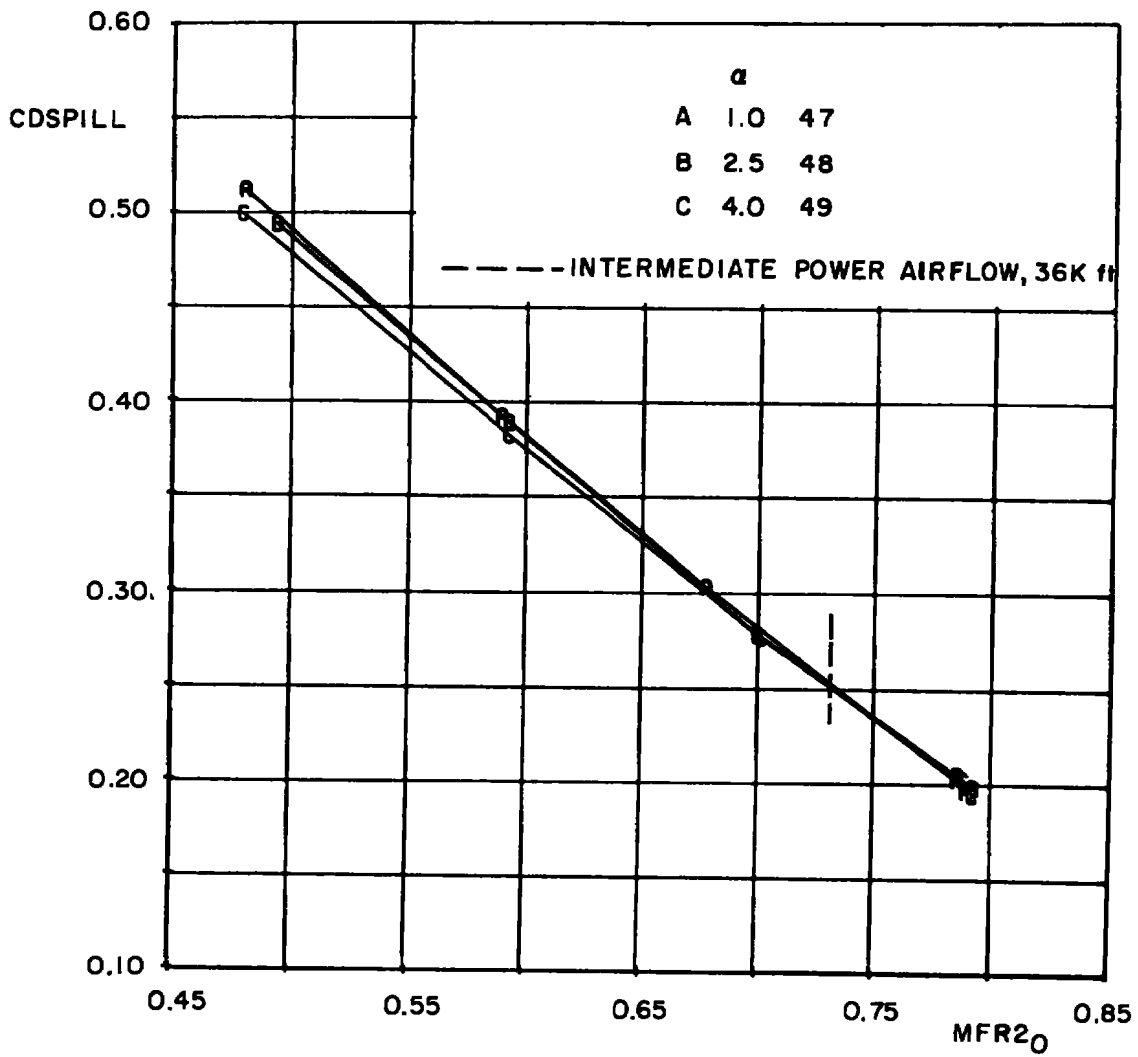Figure 37. Concluded.

Figure 38. Simulated takeoff transient.

a. M0 = 0.85
Figure 39. Inlet spillage drag characteristics.

b. $M0 = 1.20$
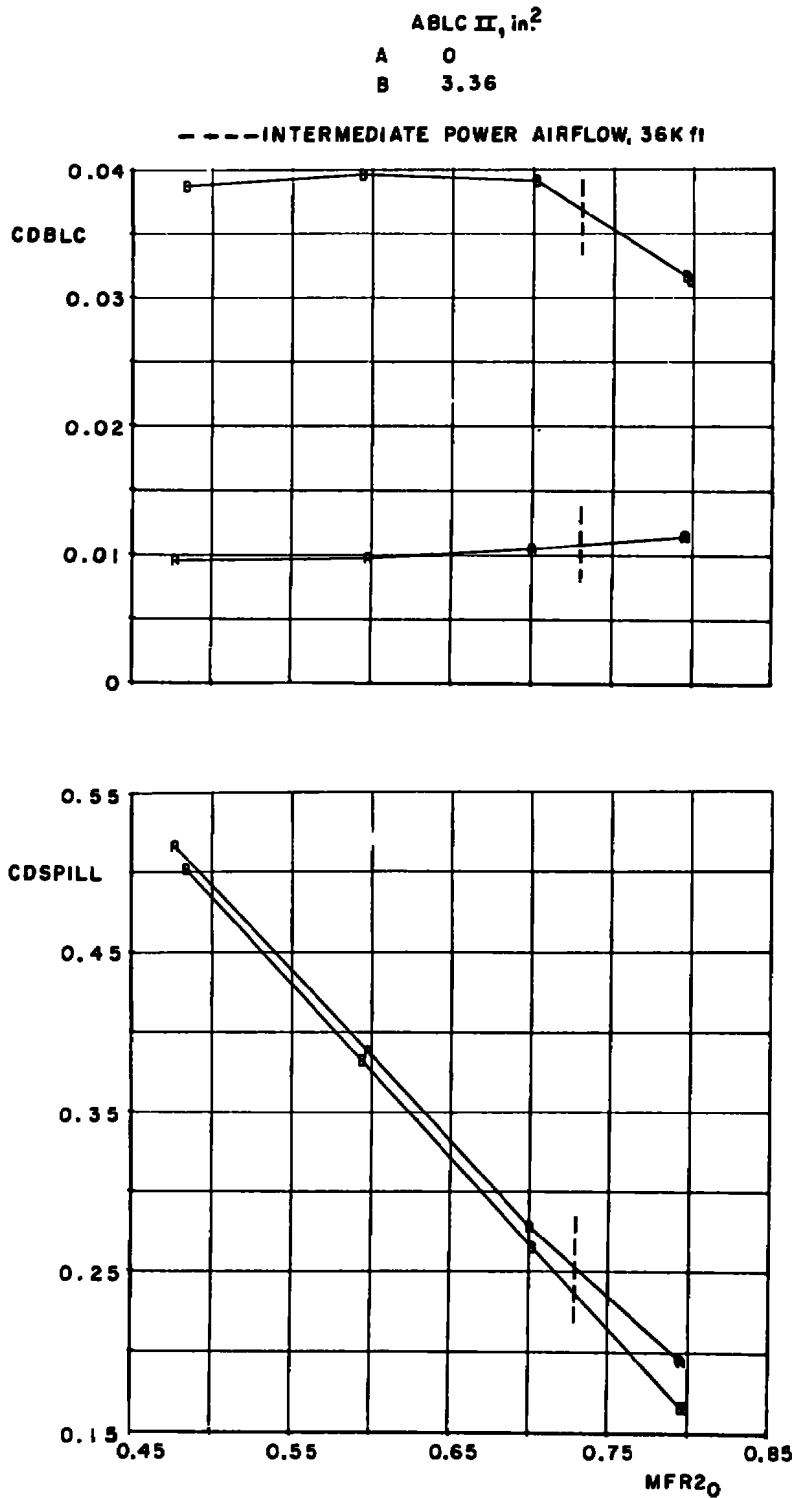Figure 39. Continued.

c. M0 = 1.40
Figure 39. Concluded.

Figure 40. Effects of opened BLCII discharge doors on inlet drag characteristics at M0 = 1.40, a = 2.5 deg.

Table 1. Precision of Measurement

Test Conditions		Estimated Combined Error							
MO	P_{t0}, psfa	ΔMO	Δp_{t0}, psf	ΔT_{t0}, °F	ΔHL, in.	ΔRB, deg	$\Delta\alpha$, deg	ΔU, deg
2.20	1200	0.0157	5.31	5.0	0.015	0.13	0.04	0.60
1.80	950	0.0131	5.18	↓	↓	↓	↓	↓
1.40	1300	0.0047	2.80					
0.85	1850	0.0044	3.35					
0.70	2300	0.0045	3.80					
0.30	2000	0.0061	3.50					
0.20	2000	0.0075	3.50					
0.00	2000	---	3.50					

MO	pt0, psfa	ΔMFR	$\Delta W2R$, lb/sec	$\Delta R2$	$\Delta IDC8$	$\Delta IDR8$	$\Delta IDL8$	$\Delta D2$	ΔMA	ΔML	ΔNSP	$\Delta T12$
2.20	1200	0.008	1.15	0.0046	0.0121	0.0064	0.085	0.0014	0.0396	0.0396	0.0038	0.002
1.80	950	0.007	1.38	0.0057	0.0153	0.0080	0.106	0.0018	0.0214	0.0214	0.0047	↓
1.40	1300	0.004	1.00	0.0025	0.0112	0.0058	0.077	0.0013	0.0080	0.0080	0.0041	
0.85	1850	0.004	0.83	0.0021	0.0078	0.0041	0.055	0.0009	0.0004	0.0004	0.0041	
0.70	2300	0.003	0.75	0.0020	0.0063	0.0034	0.045	0.0008	0.0002	0.0002	0.0042	
0.30	2000	0.008	0.80	0.0021	0.0073	0.0038	0.051	0.0009	---	---	0.0042	
0.20	2000	0.018	0.80	0.0021	0.0073	0.0038	0.051	0.0009	---	---	0.0042	
0.00	2000	---	0.80	0.0021	0.0073	0.0038	0.051	0.0009	---	---	0.0042	

APPENDIX A
EQUATIONS FOR CALCULATING DISTORTION
PARAMETERS: IDC, IDR, AND IDL

Circumferential Distortion on Individual Rings

$$IDC_i = (p_{t2_{ave_i}} - p_{t2_{min_i}})/\bar{p}_{t2}$$

where

$$i = 1 \text{ to } 5 \text{ rings}$$

Hub Distortion

$$IDC_{12} = (IDC_1 + IDC_2)/2$$

Tip Distortion

$$IDC_{45} = (IDC_4 + IDC_5)/2$$

Total Circumferential Distortion

$$IDC = \text{Largest of } IDC_{12} \text{ or } IDC_{45}$$

Radial Distortion on Individual Rings

$$IDR_i = 1.0 - \frac{p_{t2_{ave_i}}}{\bar{p}_{t2}}$$

Total Radial Distortion

$$IDR = \text{Largest of } IDR_1, IDR_2, IDR_4, \text{ or } IDR_5$$

Fan Stall Margin Ratio

$$IDL = b(KCIRC)IDC + (KRAD)IDR$$

where

$$b = \frac{IDR/IDC}{A + B(IDR/IDC)} + C$$

IDL CONSTANTS

(See Ref. 5)

MO	KCIRC	KRAD	Superposition Factor		
			A	B	C
2.2 2.1 2.0	7.69	11.75	-0.56	-0.92	1.0
1.8	7.69	13.33	-0.55	-0.71	1.0
1.4 1.2 0.85	7.69	12.83	-0.52	-0.644	1.0
0.7	7.69	12.92	-0.52	-0.644	1.0
0.55	7.69	12.28	-0.52	-0.644	1.0
0.3 0.2	7.69	11.76	-0.52	-0.643	1.0
0	7.93	12.41	-0.536	-0.951	1.0

APPENDIX B
METHOD OF CALCULATION
FOR INLET SPILLAGE AND BLEED DRAG TERMS

A. Spillage Drag

--------- control volume
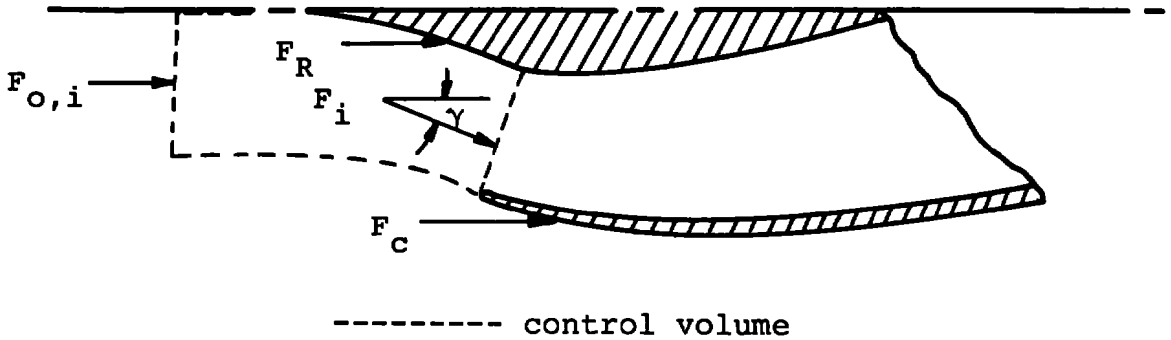
$$CDSPILL = - \frac{F_{o,i}}{(QO)(AC)} + \frac{\cos \alpha}{(QO)(AC)} \left[F_R + F_i \cos \gamma + F_c \right]$$

where

F_c is the cowl axial force to nacelle station 26 as determined by pressure-area integration, lb

F_i is the inlet air momentum, lb

$F_{o,i}$ is the free-stream momentum of the air that enters the inlet, lb

F_R is the ramp axial force as determined by pressure area integration, lbs

QO is the free-stream dynamic pressure, psi

γ is the angle of inclination of the average inlet airflow path from the model x-axis

$\left. \begin{array}{l} AC \\ \alpha \end{array} \right\}$ see Nomenclature

B. Bleed Drag

Lower Sideplate External Surface

door, i   1   2   3   4   1   2   3   4

BLCI Fixed
Exits

BLCII Variable
Exits
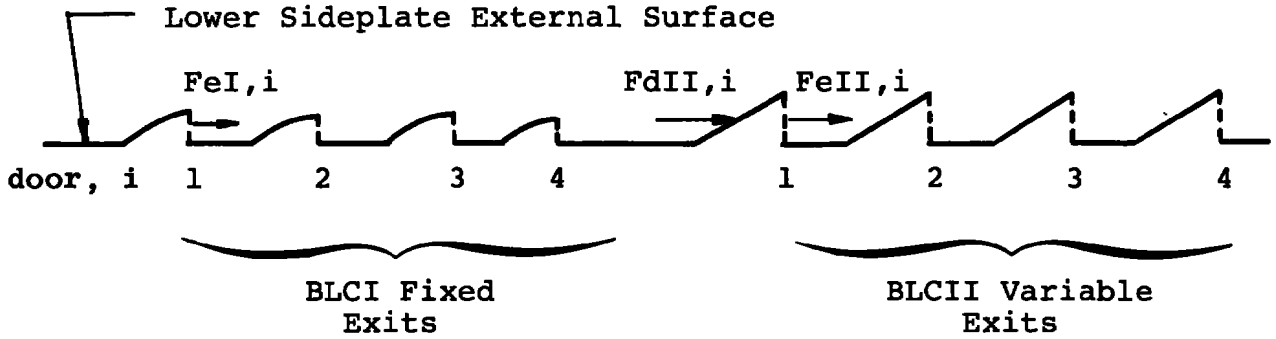
$$CDBLCI = \frac{Fo,I}{(QO)(AC)} - \frac{\cos \alpha}{(QO)(AC)} \sum_{i=1}^{4} FeI,i$$

$$CDBLCII = \frac{Fo,II}{(QO)(AC)} - \frac{\cos \alpha}{(QO)(AC)} \left(\sum_{i=1}^{4} FdII,i + \sum_{i=1}^{4} FeII,i \right)$$

$$CDBLC = CDBLCI + CDBLCII$$

where

FdII is the BLCII exit door external axial
force as determined by pressure-area
integration, lb

FeI or II is the BLCI or II airflow exit
momentum, lb

Fo, I or II is the free-stream momentum of
the BLCI or II airflow, lb

CDBLCI or II is the BLCI or II drag coefficient

QO is the free-stream dynamic pressure, psi

AC
CDBLC } see Nomenclature
a

NOMENCLATURE

ABLCI	Boundary-layer control bleed zone I exit area, in.^{2}
ABLCII	Boundary-layer control bleed zone II exit area, in.^{2}
AC	Inlet capture area, 58.54 in.^{2} (cruise cowl), 74.94 in.^{2} (takeoff cowl)
BLCI	Bleed zone I
BLCII	Bleed zone II
CDBLC	Bleed drag coefficient (see Appendix B)
CDSPILL	Spillage drag coefficient (see Appendix B)
D2	Compressor-face total-pressure distortion $(p_{t2_{max}} - p_{t2_{min}})/\overline{p}_{t2}$
FBL	Fuselage buttock line, in.
FS	Fuselage station, in.
FWL	Fuselage waterline, in.
HL	Inlet lip height, in.
IDC	Instantaneous circumferential total-pressure distortion factor
IDC8	Instantaneous circumferential total-pressure distortion factor at time of occurrence of IDL8
IDL	Instantaneous fan stall margin ratio (Appendix A)
IDL8	Peak value of instantaneous fan stall margin ratio
IDR	Instantaneous radial total-pressure distortion factor
IDR8	Instantaneous radial total-pressure distortion factor at time of occurrence of IDL8
M0	Free-stream Mach number
MA	Outboard inlet first ramp local Mach number

MFR2	Engine-face mass-flow ratio: ratio of compressor-face station mass flow to inlet capture mass flow
ML	Inlet local Mach number exterior to inlet on surface of lower sideplates, used as control sensor for inboard inlet
NBL	Nacelle buttock line, in.
NS	Nacelle station, in.
NSP	Normal shock position parameter: inlet throat static to total-pressure ratio (see Section 3.1)
NWL	Nacelle waterline, in.
p	Static pressure, psfa
p_{BI}	Bleed zone I plenum pressure, psfa
p_{BII}	Bleed zone II plenum pressure, psfa
$\bar{p}_{rms}$	Area-weighted average engine-face foot-mean-square value of total pressure, psfa
p_{t0}	Free-stream total pressure, psfa
p_{t2}	Engine-face total pressure, psfa
$\bar{p}_{t2}$	Area-weighted average engine-face total pressure, psfa
R2	Compressor-face total-pressure recovery: average (area-weighted) compressor-face total pressure ratioed to free-stream total pressure, $\bar{p}_{t2}/p_{t0}$
RA	Inlet first ramp angle (7-deg fixed ramp), deg
RB	Inlet second ramp angle (first movable ramp), deg
RC	Inlet third ramp angle (second movable ramp), deg
RE	Free-stream unit Reynolds number, Re, ft^{-1} x 10^{6}
T_{t0}	Free-stream total temperature, °R

T_{t2} Average compressor-face total temperature, °R

TI2   Turbulence index: average root-mean-square value of total-pressure oscillations at the compressor face normalized by the average compressor-face total pressure, $\bar{p}_{rms}/\bar{p}_{t2}$

U   Bypass door angle, referenced to nacelle surface, deg

W_a Engine fan airflow, lb/sec

W2R   Engine fan airflow corrected to standard sea-level conditions for full-scale vehicle, $W_a\sqrt{\theta T2/\delta T2}$, lb/sec

a Angle of attack, deg

$\delta T2$ $\bar{p}_{t2}/2116$

$\theta T2$ $T_{t2}/519$

ψ, or yaw   Model angle of yaw (angle between the plane of symmetry and the relative wind), nose right is positive, deg

SUBSCRIPTS

I   Inboard inlet

O   Outboard inlet

FS   Full scale

0.2-SC   0.2 scale